Experimental Study of the Growth and Stable Water Isotopes of Ice Formed by Vapour Deposition in Cold Environments

Philippe Brasseur

A thesis submitted to the
Faculty of Graduate and Postdoctoral Studies
in partial fulfillment of the requirements for the degree of
Master of Science in Geography

Department of Geography, Environment and Geomatics
University of Ottawa

Abstract

Ice formed by water vapour deposition has been identified in different terrestrial environments: 1) in the atmosphere; 2) at the ground's surface; 3) in caves; 4) in seasonally frozen ground; and 5) in perennially frozen ground (permafrost). Thus far, ground ice formed by diffusion and deposition of vapour in soils (types 4 and 5) has rarely been studied in a natural setting and remains one of the most poorly described ice types on Earth. This thesis focuses on the dynamics of deposition and sublimation of atmospheric water vapour into permafrost and the isotopic signature (D/H and $^{18}O/^{16}O$) of the emplaced ground ice under different experimental conditions. Ground ice was produced in sediments with different thermo-physical characteristics (glass beads, JSC Mars-1 simulant). After a two-month growth period, the higher porosity sediments (JSC) had more than 7x the gravimetric water content than the lower porosity soil. Ground ice profiles had a distinct concave downwards shape due to the decrease in saturation vapour pressure with depth. Results also indicate that vapour deposited ground ice has a distinct δD-$\delta^{18}O$ composition that plots near regression slope value of 8. Pore water isotopes plot below the global meteoric water line (GMWL) when the source of moisture is directly on top of the sediments. If an air gap is introduced between the source of moisture and the sediments, the pore water isotopes shift above the GMWL due to re-sublimation at the ground surface. Overall, this thesis addressed some fundamental knowledge gaps required to better understand the growth and isotopic evolution of ground ice emplaced by vapour deposition.

Résumé

La glace formée par déposition de vapeur d'eau a été identifiée dans différents environnements terrestres : 1) dans l'atmosphère; 2) à la surface du sol; 3) dans les cavernes; 4) dans le sol gelé de façon saisonnière; et 5) dans le sol gelé en permanence (pergélisol). Jusqu'à présent, la glace de sol formé par diffusion et déposition de vapeur dans les sols (types 4 et 5) a rarement été étudié dans un environnement naturel et est l'un des types de glace le moins connu sur Terre. Cette thèse porte sur la dynamique de déposition et la sublimation de la vapeur d'eau atmosphérique dans le pergélisol ainsi que la signature isotopique (D/H et $^{18}O/^{16}O$) de la glace de sol produite dans différentes conditions expérimentales. La glace de sol a été créée dans des sédiments avec de différentes caractéristiques thermo-physiques (billes de verre, simulant JSC Mars-1). Après une période de croissance de deux mois, les sédiments de porosité plus élevés (JSC) avaient une teneur en eau gravimétrique plus de 7x supérieure que le sol de faible porosité. Les profils de glace de sol avaient une forme concave distincte en raison de la diminution de la pression de vapeur saturante avec la profondeur. Les résultats indiquent également que la vapeur déposée dans les sédiments a une composition δD-$\delta^{18}O$ distincte avec une pente de régression près de 8. Les isotopes de la glace interstitielle sont en dessous de la droite météorique mondiale (DMM) lorsque la source d'humidité est directement au-dessus des sédiments. Si un espace d'air est introduit entre la source d'humidité et les sédiments, les isotopes de la glace interstitielle se déplace au-dessus de la DMM en raison d'une re-sublimation à la surface du sol. Dans l'ensemble, cette thèse porte sur les quelques lacunes fondamentales nécessaires pour mieux comprendre la croissance et l'évolution isotopique de la glace de sol mises en place par déposition.

Acknowledgements

This project wouldn't have been possible without the expertise and support of many people.

I kindly thank my supervisor D. Lacelle for introducing me to polar research during my undergraduate studies and offering me the possibility to pursue my graduate studies with you. It was a pleasure to undertake this challenging project that you had envisioned and I thank you for remaining with me during the ups and downs of this project.

I am grateful to have D.A. Fisher as my co-supervisor. Your expertise on the topic and on modeling helped me greatly in my research. I thank you again for the talks we had at Patty's and for coring with us at Petrie Island.

Thank you to my thesis committee members B. Lauriol and I.D. Clark for your valuable comments and expertise on the topic.

I would like to thank the valuable lab technicians that helped with the engineering of the project and the analysis of my data. Thank you J. Bjornson for ordering the parts and guiding me during troubleshooting. G. St-Jean, thank you for helping us assemble the environmental chamber and for our new furniture addition. S. Murseli, thank you for helping with the pump and cold bath problems. Thank you M. Wilk and I.D. Clark for letting me use your laboratory to process my samples and helping me with my distillation. I gratefully thank W. Abdy and the staff of the G.G. Hatch Laboratory for processing my samples in the fastest time possible.

I would like to acknowledge my subbasement friends and especially thank my officemates C. Lapalme, M. Fontaine and B. Main. You guys made this adventure more enjoyable and I wish you all the best in your future endeavors.

Most importantly, I want to acknowledge the people outside of academia who helped me. I thank my mother and father for encouraging and supporting me in my many years of education. I am forever grateful to my girlfriend and my friends who kept me happy through these years.

This project was supported by NSERC awarded to D. Lacelle.

Table of Contents

List of Figures

List of Tables

List of Acronyms

ARC	Advanced Research Complex
a.s.l.	Above sea level
CLAAPS	CryoLab for Arctic, Antarctic and Planetary Studies
CRREL	Cold Region Research and Engineering Laboratory
GMWL	Global meteoric water line
GWC	Gravimetric water content
LMWL	Local meteoric water line
MAATs	Mean annual air temperatures
MDV	McMurdo Dry Valleys
MSAT	Mean summer air temperature
PCZ	Perennially cryotic zone
SD	Standard deviation
SMOW	Standard mean ocean water
SUZ	Stable upland zone
TDD	Thaw degree-days
VSMOW	Vienna standard mean ocean water

Chapter 1: General Background

Introduction

Water on Earth exists in three phases: gas (water vapour), liquid (water) and solid (ice). The solid phase, ice, appears in most cryotic environments (< 0°C at standard atmospheric pressure) and takes various forms such as: 1) snow, frost, hail, rime in the air; 2) glacier, river/lake ice, ground ice on land; and 3) sea ice in the oceans. The most common process that forms ice occurs when liquid water is cooled below 0°C at standard atmospheric pressure and freezes. Ice can also form directly from water vapour with no liquid phase intervention (deposition), such as the formation of frost. On Earth, all types of ice tend to develop a hexagonal crystalline structure, although cubic crystalline structure can also be encountered (Petrenko and Whitworth, 2002).

Ice formed by water vapour has been identified in five different terrestrial environments: 1) in the atmosphere; 2) at the ground's surface; 3) in caves; 4) in seasonally frozen ground; and 5) in perennially frozen ground (permafrost). Type 1 ice is composed of snow crystals that form in the atmosphere. Type 2 ice is frost that forms on objects above the ground surface; where conditions are favourable (i.e., temperature/pressure below triple point of water and under stable equilibrium). Type 3 ice tends to be found in freezing caves as frost along the cave's walls or ceiling and can over time lead to the build-up of ice plugs (Lauriol et al., 1988). In seasonally frozen grounds (type 4), pipkrakes (needle ice) and pore ice are examples of vapour depositional ice. Although their formation is not fully understood, pipkrakes can grow orthogonally to the soil surface from soil moisture migrating to a freezing front (Branson, 1996; Nel and Boelhouwers, 2014). In permafrost (type 5), vapour deposited ice has been documented only from the cold-dry environment of Antarctica (Lacelle et al., 2013). In this environment, the perennially sub-freezing air and ground surface temperatures ensures that moisture (air or snow-covered ground) migrates and is deposited in colder ground. With the exception of types 1, 2 and 3 vapour deposition ice, vapour diffuse through a soil matrix before being deposited as ice in the ground (i.e. type 4 and type 5). The main difference between type 4 and 5 ice is the direction of vapour flux. For type 4 ice, the vapour generally migrates upward from the soil towards the 0ºC isotherm found near the soil surface; by contrast the vapour migrates downward from the ground's surface and is deposited into the soils along a thermal gradient for type 5 ice. Given the

varied soils properties (porosity, thermal conductivity, salt content), the growth and δD-δ^{18}O evolution of type 4 and 5 ice types are still poorly understood.

Vapour deposited ground ice has only been observed in the perennially cryotic zones of the McMurdo Dry Valleys, Antarctica where no liquid water is present. Thus far, ground ice formed by diffusion and deposition of vapour (types 4 and 5) has rarely been sampled in a natural setting (Bockheim and McLeod, 2008; Kowalewski et al., 2011, Lacelle et al., 2013). As such, most studies focused on reproducing these types of ice in laboratory experiments (Hudson et al., 2007; 2009) or developing numerical models to simulate their growth (Fisher, 2005; Fisher and Lacelle, 2014). The research conducted by Hudson et al. (2007; 2009) have experimentally reproduced pore ice in a 5 cm soil column by diffusion deposition of vapour at Mars temperature (193 to 268K) and pressure (600 Pa). Fisher and Lacelle (2014) derived stable water isotope evolution in ground ice formed from vapour using the REGO vapour diffusion model with poorly constrained isotope fractionation factors for low temperatures (< -30°C). However, to date, no studies experimentally reproduced ground ice formed by vapour diffusion in a soil column, determined the ice content profile and the δD-δ^{18}O composition of vapour deposited ice in cryotic soils under terrestrial conditions.

This thesis focuses on the formation and δD-δ^{18}O evolution of ice in cryotic soils by vapour deposition, one of the most poorly described ice types on Earth. The objectives of the study are to: 1) Determine the ground ice content emplaced via vapour deposition; 2) Determine the δD-δ^{18}O signatures of ground ice formed by deposition of atmospheric vapour in a 12 cm cryotic soil column; and 3) Investigate the effects of magnesium perchlorate, a deliquescent salt, on ground ice content and on δD-δ^{18}O signatures of ground ice. These objectives were reached by conducting two series of experiments in an environmental chamber in which the temperature and humidity were controlled. Ground ice has been reproduced in two different soil matrices: 1) a soda lime glass beads with a homogenous grain size of 0.5 mm; and 2) the Martian soil simulant JSC Mars-1 made of volcanic tephra with a mean grain size of 0.3 mm. In addition to the series of experiments, a frozen beach core from Petrie Island in Ottawa was collected in March 2015 to assess the potential growth of vapour deposition in the seasonally frozen soils. Overall, this thesis addresses fundamental knowledge gaps that are required to better understand the growth and isotopic evolution of ground ice emplaced by vapour deposition.

1.1 Vapour depositional environments

There are five main types of environments in which vapour depositional ice can form: in the atmosphere, at the ground's surface, in caves, in seasonally frozen grounds and in permafrost (Figure 1). The following section describes these environments and the ice types that tend to be found.

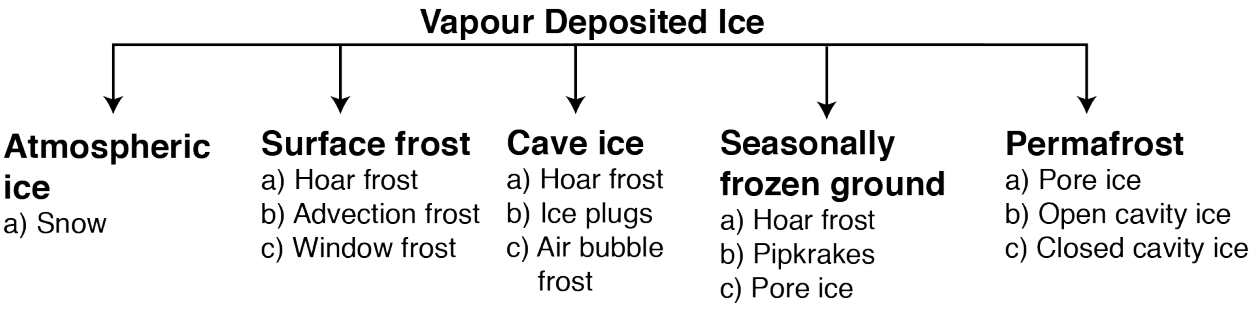

Figure 1. Classification of five vapour depositional environments with their associated ice structures. Type 1: Atmospheric ice, Type 2: Surface frost, Type 3: Cave ice, Type 4: Seasonally frozen ground and Type 5: Permafrost.

1.1.1 Atmosphere

Many types of vapour deposited ice exist in the atmosphere, including snow, frost, rime, hail. Snow can form in clouds when atmospheric moisture reaches saturation and becomes supercooled. Small particles made of dust can act as a nucleation points and initiate the growth of ice crystals. Crystals grow in size as more vapour is transferred onto their facets until they are heavy enough to fall. Snow can take many complex forms that depend on vapour saturation and air temperature (Lock, 1990). The dominant structures of snow can be seen in Figure 2. The primary ice structures made by vapour deposition are stellar, dentrites, columns, plates and needle (Magono and Lee, 1966). Other structures such as graupel, rime and ice pellets (hail) are formed when condensed vapour (liquid water) in the clouds hit snow particles and freezes. These are therefore not directly made by vapour deposition and have a rounded or tear shape (Lock, 1990).

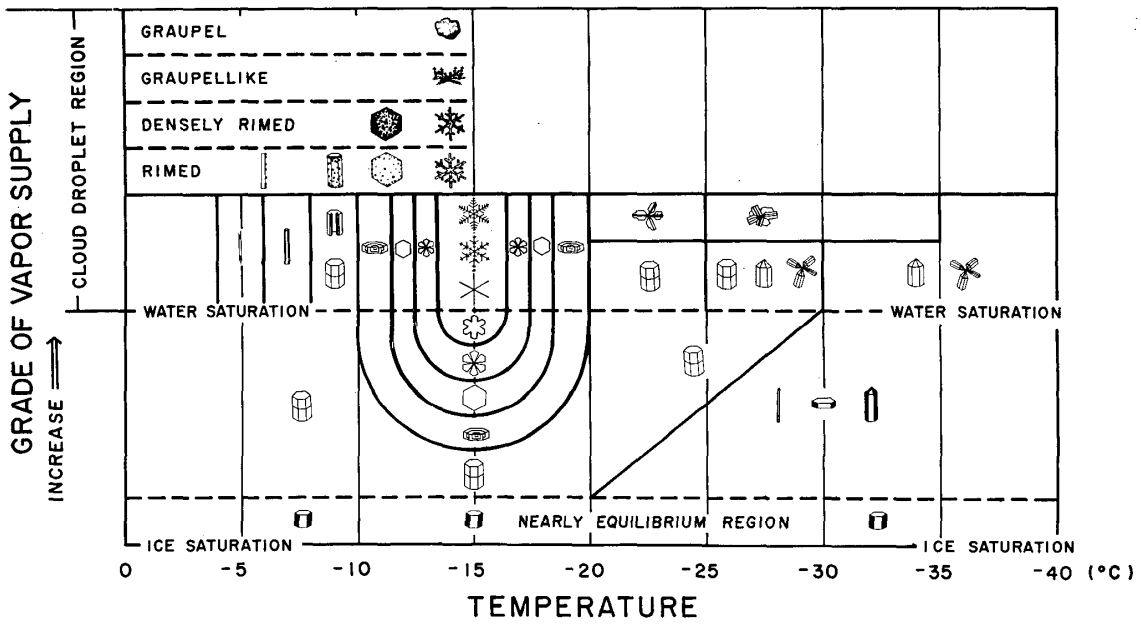

Figure 2. Types of snow crystals classified by temperature and vapour supply (Magono and Lee, 1966)

When snow accumulation exceeds sublimation it can form a snowpack. Over time, a perennial snowpack will metamorphose into firn, which leads to an increase in its grain packing, reduction of porosity and recrystallization. Snow becomes rounder over time due to compaction and sublimation of the crystals. Ice sublimates preferentially at the extremities of the snowflake where vapour pressure is highest and deposit in the hollows (low vapour pressure), making the crystal rounder over times (McClung and Schaerer, 2006). This process can take several 100 years for snow to transform into ice. Snow (100 - 300 kg/m^3) first changes into firn (400 - 800 kg/m^3), then to Névé (700 - 830 kg/m^3) and then to ice (917 kg/m^3) (Petrenko and Whitworth, 1999).

Temperature gradients in small snowpack can be quite large. Typically, the temperature at the base of snowpack is warmer due to geothermal heating and temperature will decrease towards the surface with the top 20-40 cm of the snowpack affected by diurnal temperature variations (McClung and Schaerer, 2006). Vapour can move within the snowpack due to variations in temperature and associated vapour pressure. Vapour pressure is highest near the bottom of the snowpack since this area is warmer and lowest near the surface of the snowpack. If the thermal gradient in the snowpack is < 10°C/m the snow crystals will become rounded through a

destructive metamorphism process. If the thermal gradient is > 10°C/m, the vapour pressure gradient is strong enough to produce large faceted crystal named depth hoars (McClung and Schaerer, 2006). Therefore, cold winter air and thin snowpacks create high vapour pressure gradients capable of producing layers of frost hoars near the bottom of the snowpack where humidity is greatest. Depending on the time of day, ice will form a facet in opposing directions. During the day vapour migrates into the snowpack since it is colder than air and during night vapour migrates out of the snowpack towards the cooler air (Birkeland, et al., 1998). Large frost hoar crystals are more fragile than snowflakes and create areas of weakness capable of producing avalanches.

Hoar frost can also grow on top of the snowpacks, they are formed on moist nights when long-wave radiation cools the snowpack below the dew point. Crystals growth on the surface of the snowpack and form a weaker layer if covered by subsequent storms which can increase the chances of avalanches (McClung and Schaerer, 2006).

1.1.2 Ground surface

When objects on or above the ground surface are cooled below 0°C at standard atmospheric pressure, supercooled water vapour can be deposited on its surface. Water vapour is deposited on the freezing surface if the temperature and pressure are below the triple point of water and under stable equilibrium (Lock, 1990). Moisture will more easily accumulate in isolated areas such as cracks and depressions since these are vapour traps. Cracks offer calmer areas with higher humidity where moisture can enter and crystalize. Additional moisture attaches itself on the objet to evenly coat it with ice crystals. Depending on the conditions, ice can take various structures such as hoar frost, advection frost and window frost (Petrenko and Whitmore, 2002).

a) Hoar frost also know as radiation frost is composed of small white ice crystals that grows rapidly when temperatures on a surface are below 0°C, winds are minimal and humidity is high. Crystals come in various shapes that depend on temperature and vapour saturation. The most common forms of hoar frost are plates (0 to -4°C), needles (-4 to -7°C) and dendrites (-12 to -16°C) that form in vapour saturated environments (Hobbs, 1974). Larger ice crystals, typically of a few cm in size, are called hopper structures. These structures crystalize when the air is ~3% under saturation, wind speed is minimal and temperatures below -10°C. If temperatures are

between -10 and -22°C hollow dish-shaped hexagonal plates will form and if temperatures are below -22°C a hollow prismatic column will crystalize (Figure 3).

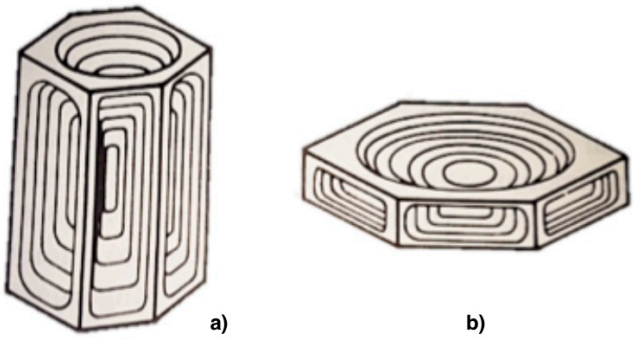

Figure 3. Hopper structures of ice crystals: a) hollow prismatic columns and b) dish-shaped hexagonal plate (Mason et al., 1963)

b) Advection frost are small ice spikes formed when the temperature is below 0°C, humidity is low and winds are moderate to strong (Snyder and Melo-Abreu, 2005). Vapour accumulates on a surface and grows against the direction of the dominant winds. This type of frost usually occurs on cloudy days with no temperature inversions in the atmosphere. On agriculture land, this type of frost is very destructive and can damage crops, especially fruit trees (Snyder and Melo-Abreu, 2005).

c) Window frost has been described in great detail by Bentley in 1907 and is still to this date the only complete surface frost classification. This type of frost appears on flat surfaces such as windows that are several degrees below freezing in calm nearly windless environments. Relative humidity for window frost to form needs to be below 95% or else dew will form on the window. When vapour deposits on flat surfaces it can take many shapes depending on the relative humidity and the temperature. Bentley (1907) identified two main groups of window frost: frost occurring in scratches or striations on surface and frost that grows independently on regions without surface flaws. In total, 11 structures of window frost are found in his classification. The most common structure is called “branch like”, type WBB, that resemble ferns or trees (Figure 4). This type of window frost forms mostly on freezing windows of unheated rooms when the outside temperature is between 0 to -15°C and relative humidity between 55 to 70%.

The other types of window ice are described as linear crystals (WLA), filamentous (WFC), meandering (WMD), stelliform (WSE), lamellar (WLF), columnar (WCG), open (WOH), tooth-shaped (WTI), fibroid (WFJ) and granular (WGK).

Figure 4. Car covered by branch like frost patterns on the windscreen and fibroid patterns on the hood and roof (Lawrie, 2012)

1.1.3 Caves

Caves with temperatures below 0°C may contain many types of ice. Most of the ice features in caves are formed by freezing of liquid water, for example ice stalagmites. However, caves are environments that also favour the formation of ice by vapour deposition due to their high relative humidity and low mixing of the air. These environments create an opportunity for moisture to condense and freeze to form unique ice structures. Vapour deposited ice has been documented in various caves such as Caverne de l'Ours near Ottawa, Ontario (Lacelle et al., 2004), in Bear Cave in northern Yukon (Lauriol et al., 1988), Grande Caverne Glacée and Caverne '85 in northern Yukon (Lauriol and Clark, 1993) and in Castleguard Cave, Alberta (Harris, 1979). The cave itself can either be in seasonally frozen grounds such as Caverne de l'Ours or in areas with continuous permafrost such as Grande Caverne Glacée and Caverne '85.

Super-cooled water vapour crystalizes when it come in contact with a freezing surface. Cave ice features formed by vapour deposition are often found near cave openings (Lacelle et al., 2004) and on the ceilings in the caves (Lauriol and Bertrand, 2014) where temperatures decrease below 0°C.

There are three main types of ice made by vapour deposition in caves: hoar frost, ice plugs also known as massive ice blockages and air bubble frost.

a) Hoar frost is composed of ice crystals formed when air moisture condenses and freezes on the walls of the cave (Figure 5). They are typically found on the deeper sections of the cave where temperatures are lower (Lauriol and Clark, 1993). These frost crystals have a distinct hexagonal shape. Crystals typically show a growth striation and are in a humid area of the cave (Lauriol et al., 1988). Hexagonal crystals can be further divided into three groups: cups, needles and dendrites. Cup shaped crystals appear in calm environmental of the caves where temperatures are near -5°C (Lauriol and Bertrand, 2014). If humidity is near saturation they will grow in length and when humidity is below saturation they will grow along their secondary axes up to a maximum height of a few cm. Needles are an elongated form of cups that have grown following the major axis. They are found in cave environments with temperatures below -10°C and where humidity is high (> 98%). These elongated ice crystals are always found in groups of more than one and can grow to ~10 cm in length. Dendrites occur when the air is colder than -15°C and grow only near the exits of the caves where the air is cold and humid (Lauriol and Bertrand, 2014). These ice crystals have a fern like structure with a central ridge supporting branches of ice.

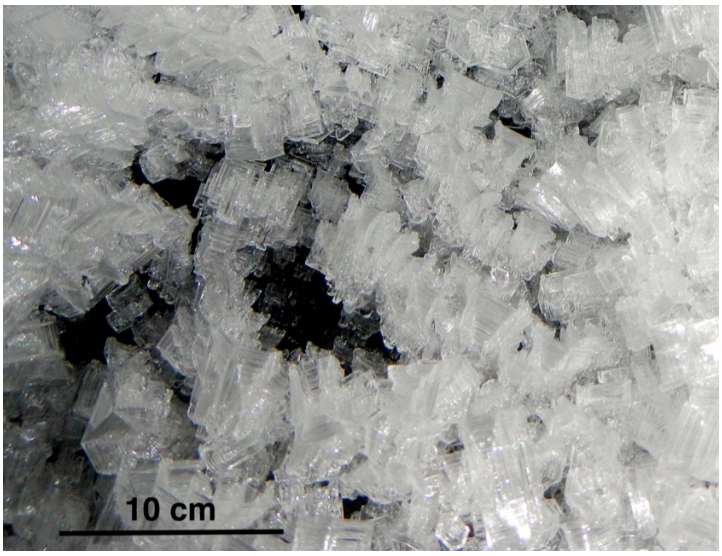

Figure 5. Hoar frost of 1 - 3 cm in length in Larsbreen glacier cave, Svalbard, Norway

b) Ice plugs/massive ice blockage are ice that blocks a passage that would be accessible if ice were not present (Figure 6). These features form when the bottom and top of the cave walls meet fill an opening (Lauriol and Clark, 1993). These ice plugs are made due to moist air entering the cave in summer and depositing onto the ice mass. In winter, the ice plugs sublimates and looses some of their mass. Stable isotopes of ice in caves are enriched in deuterium due to the warm humid air and plot above the local meteoric water line (Lacelle et al., 2004).

Figure 6. Massive ice blockage in Grande Caverne Glacée, northern Yukon (Lauriol and Clark, 1993)

c) Air bubble frost occurs in caves when a body of water start to freeze from the top down. Gas in water originates from decomposed organic materials made in majority of methane (Lauriol and Bertrand, 2014). Theses gases escape towards the surface due to their difference in density can be trapped by newly formed ice at the surface. Air bubbles contain some water vapour that becomes oversaturated due to the decrease in temperature and frost crystals start to develop (Lauriol and Bertrand, 2014). These small crystals of only about a mm contours the shape of the bubble and gives a white appearance to the air bubbles trapped in ice. The size of the bubbles depends on the progression of the freezing front into the water. Larger air bubbles with a wider diameter will form when the ice freezes slowly.

1.1.4 Seasonally frozen grounds

Seasonally frozen ground is the near-surface soil layer in temperate regions that freezes in winter and thaws in summer. These soils have the potential to develop seasonal ice formed by vapour deposition such as hoar frost, pipkrakes and pore ice.

a) Hoar frost can aggregate itself on cold objects such as grass and pebbles through diffusion and form crystals of pure ice. They can take various hexagonal shapes but usually grow to smaller size due to windy conditions. See earlier section for the various types of hoar frost and more description.

b) Pipkrakes are small ice needles that grow slightly under or at the surface of soils. This ice formation often has sediments inclusions in their needle ice structures (Figure 7). Pipkrake formation is limited to seasonally frozen grounds and often occurs during the fall freeze back when soils are saturated with moisture (Nel and Boelhouwers, 2014; Mackay and Mathews, 1974). Pipkrakes can develop in the near surface soil layer when the soil surface experiences radiative cooling during the night. Water and vapour condenses to form a few cm long needle shaped ice near the surface of the soil composed in majority of silts and sands size particles. They grow at a rate varying between 1 to 16 mm/h and can grow up to a few cm (Branson et al., 1996). Their formation has been studied but there are still many unanswered questions.

Figure 7. Needle ice formed in fine-grained soil in Chiltern Hills, UK during two nights of frost (Gibbs, 2014)

The crucial conditions to create pipkrakes are the following: (1) a recently thawed soil is supercooled at/or ~1 cm below the surface, (2) the soil has sufficient moisture to move to the freezing front and (3) the freezing front is stable (Branson et al., 1996).

If the freezing front moves deeper into the soil, sediment inclusions in the ice may occur, otherwise the produced ice will be sediment-free (Figure 8). Over time, pipkrakes are able to slowly displace sediments by creep from an area by freezing and melting of these features (Branson et al., 1996). Earlier studies by Lawler (1993) demonstrated that soil from a river bank in South Wales (UK) had been eroded by pipkrakes. Lawler's study attributed 32% to 43% of the total bank erosion to creep by pipkrakes.

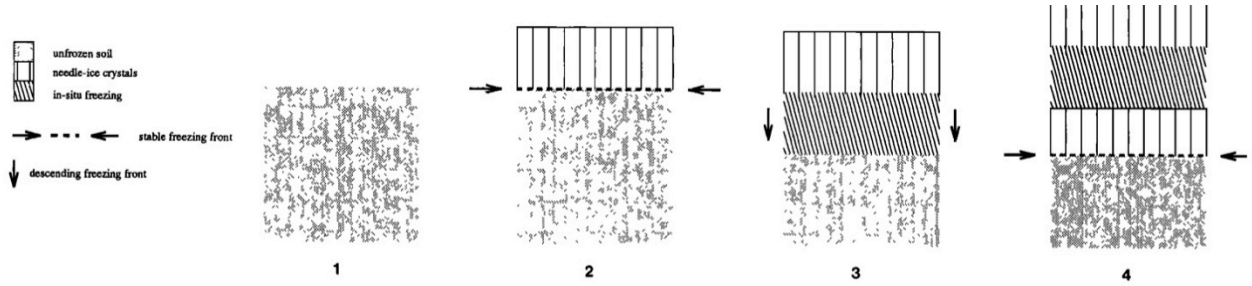

Figure 8. Sediment inclusion during pipkrake growth (Branson et al., 1996)

c) Pore ice can form when moisture in the soil column migrates to the freezing front. This process is similar to permafrost environments discussed in the next section but the soil completely thaws in the summer and doesn't aggrade to a far depth. Pore ice in seasonally frozen soil tends to be restricted to sandy soils where vapour diffusion is more efficient. Areas such as beaches environment could possibly form vapour deposited pore ice in the first 30 cm of soil given its low moisture content. See Chapter 4 of this thesis for more detail.

1.1.5 Permafrost

Permafrost is soil that remains at or below 0ºC for more than two consecutive years (French, 1996). In most permafrost environments, the near-surface soil layer (the active layer) thaws in summer and freezes in winter and this layer often contains liquid water. In the few terrestrial regions where an active layer does not develop, ground ice formed by vapour diffusion and deposition can be observed, such as in the perennially cryotic zone in the upper McMurdo Dry Valleys (MDV) of Antarctica (Lacelle et al., 2013; Lacelle et al., 2015).

The upper MDV has mean annual air temperatures (MAATs) < -23°C, mean summer air temperatures < -10°C and the sum of thaw degree-days (TDD) is < 5 degrees/year (Doran et al., 2002). Precipitation in the upper MDV is very low with snow accumulation < 10 mm/yr of snow water equivalent (Fountain et al., 2009). However, the region can be separated into two groups

based on ground surface temperatures. Places where hourly soil surface reach above 0°C during the day for a few hours due to radiative heating are classified as a non-seasonally cryotic zone, it occupies 84% of the upper MDV (Lacelle et al., 2015). The soils in this zone contain evidence of liquid water such as wetting of the uppermost 20 cm, frozen ponds and sand flows. Other areas in upper MDV are shaded and have hourly ground surface temperatures that remain below 0°C throughout the year (Lacelle et al., 2015). These places fall in the perennially cryotic zone (PCZ) and soils do not contain liquid water; ground ice is formed by vapour diffusion and deposition (Lacelle et al., 2013; Fisher and Lacelle, 2014). In the PCZ, the upper soil layer (0 to > 80 cm) is dry (< 3% water content) and the interface between the dry soil and ice-bearing permafrost is the ice table (Mellon and Jakosky, 1993).

Ground ice formed by vapour deposition in permafrost is different than those formed in seasonally frozen grounds since the direction of the vapour flux is downward from the ground surface (Figure 9). In seasonally frozen grounds, the vapour flux is upward, towards the 0ºC isotherm and leads to the formation of ice near the surface.

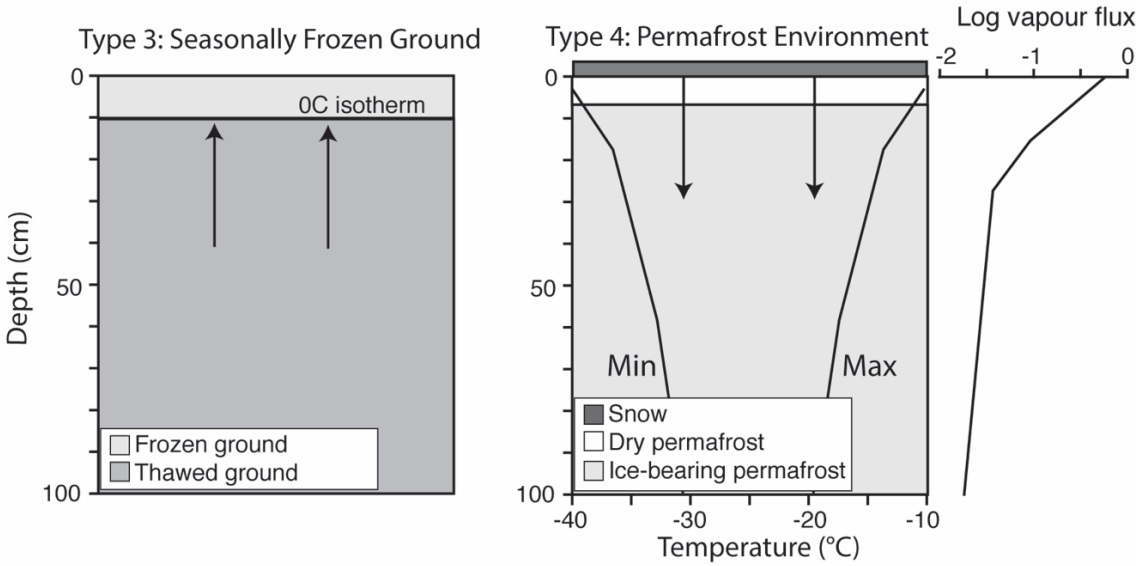

Figure 9. Sketch comparing ice growth between Type 4: Seasonally Frozen Ground and Type 5: Permafrost. Arrows indicate direction of vapour flux

Mackay (1972) proposed a classification of ground ice types in permafrost. Out of the 10 types, only 1 was for ice formed from by water vapour and it includes pore ice, open cavity ice and closed cavity ice.

a) Pore ice occurs when water vapour enters and fill pore spaces in the soil. For this to happen, very dry and cold temperatures need to be obtained. On Earth, we find pore ice in cold dry regions such as in the upper McMurdo Dry Valleys of Antarctica (Lacelle et al., 2013). See next section for a full explanation on the processes.

b) Open cavity ice is made by a moisture derived process during which ice sublimates and is transported into a crack in the soil. Cracks in permafrost are formed when temperatures suddenly drop and soil contracts. Melt water and precipitations can enter these types of ice but vapour can also fill open crakes in soils such as an ice wedge (Mackay, 1972).

c) Closed cavity ice are made in large gas pockets enclosed permafrost and can have large (~20 cm) ice crystal that grow in this enclosed space (Mackay, 1972).

1.2 Vapour diffusion and deposition in soils

Ground ice formed by vapour diffusion and deposition in cold regions results in large part from temperature and vapour pressure gradients in the soil column. Vapour will migrate from a source (e.g. snowpack) into an underlying porous soil depending on its thermal and moisture gradient. This section explains the governing processes controlling the transport of vapour and deposition of water vapour in soils.

1.2.1 Vapour transport and diffusion in soils

Vapour is transported through diffusion and advection due to differences in concentration, temperature and pressure (Reid et al., 1987). Diffusion occurs when there are differences in concentration, temperature or pressure (Reid et al., 1987). Diffusion in soils can be classified under four main types: concentration diffusion, advection, thermodiffusion and barodiffusion. The most dominant type of diffusion in soils is concentration diffusion and is the process in which the experiments were conducted. Vapour in low concentration areas receives moisture from high concentration areas due to equilibration of the system. The gradient can be positive, negative or null. If a gradient exist there will be a net flux of water molecules down the gradient, which would result on a net growth or depletion of the subsurface ice. The scales at which diffusion occurs depend on the concentration gradient and the diffusive properties of the soil.

In permafrost, diffusion can occur in two directions: 1) downward from the ground surface and into the soil; and 2) upward along the geothermal gradient if it remains below vapour saturation (Hudson, 2008). Vertical sections of the soils will interact differently with the incoming water vapour (Figure 10). Water vapor from the atmosphere will migrate through a layer of dry soil and deposit below the ice table depth where more ice aggrades than sublimates. The thin layer of ice-free sediments above the ice table protects the subsurface ice-bearing permafrost from thermal changes. If the ice is exposed, it will tend to equilibrate faster with the atmosphere and this will lead to thinning of the ice table through sublimation. Vapour flux decreases as it migrates in depth and can be inverted (vapour moves towards the atmosphere) during winter (colder air temperatures than the soil). The wavy arrows indicate the net vapour flux movement in or out of the soil, but never both at once (Hudson, 2008). Water vapour can easily enter the near-surface loose porous sediments from the surface and into the permafrost. At the ice table depth of permafrost, water vapour has more difficulty moving downward due to decreasing soil pore space.

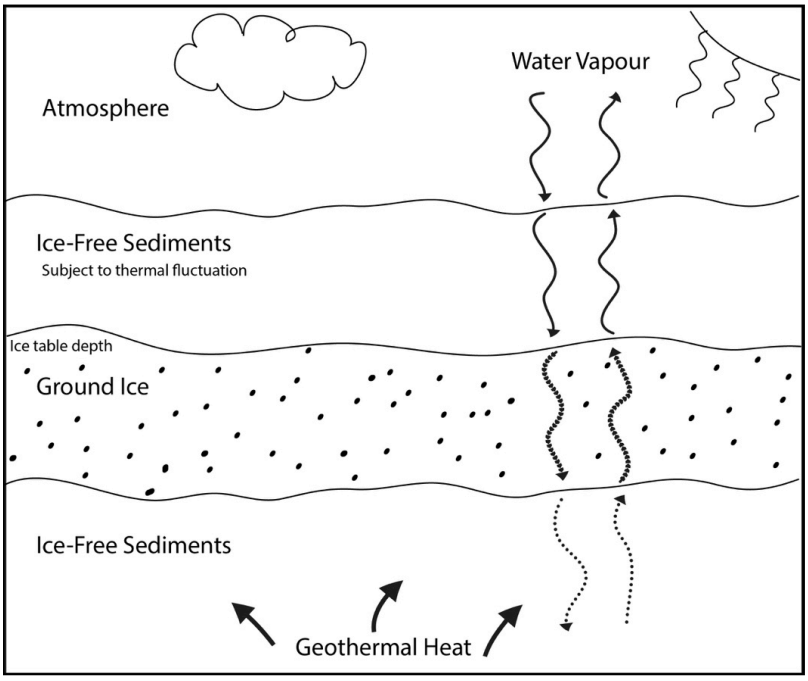

Figure 10. Schematic of vapour exchange interaction between ground ice and the atmosphere, moderated by an intervening layer of porous ice-free soil. The wavy arrows indicate the the net vapour flux movement in or out of the soil. The vapour flux decreases as it migrates in depth due to decreasing soil pore space. (Hudson, 2008)

The rate of vapour transport is governed by the diffusion coefficient. The coefficient of diffusion is the product of the mean velocity and mean free path (Hudson, 2008). The molecule, H_2O in this case, propagates in a fluid (the atmosphere). The rate at which vapour can travel depends on the size of the molecule and the density of the fluid. Diffusion can be classified under two main regimes: Fickian or Knudsen.

Fickian regime: High pressure dominated by molecule-to-molecule collisions thus it is under a Fickian diffusion regime that can be expressed by two laws. Fick's first law (Equation 1) of diffusion stipulates in a constant concentration flux is directly proportional to the steepness of the gradient and Fick's second law says that concentration changes over time. In addition to Fick's first law there is Graham law that impacts the diffusion; it states that small molecules with small masses will diffuse faster than larger molecules.

$$[1]\ \mathrm{J} = -\mathrm{D}\frac{dC}{dx}$$ (Ho and Webb, 2006)

where J is the mass flux (mol/cm^2.s), D is the diffusion coefficient in cm^2/sec, dC is the change in concentration (mol/cm$^{3)}$ and dx is the change in distance (cm).

Knudsen regime: This vapour diffusion regime occurs in small pores and low pressure will create more collisions between the walls of the pores due to their proximity. This means that the presence of other gases has no longer an effect on the transport and flux on the species of interest. The smaller the pore size, the more chances wall-to-wall collisions occur.

The speed at which the diffusion occurs in porous soils depends on the diffusion coefficients (D_e) expressed in m^2/year using this equation:

$$[2]\ D_e = \frac{D_{ab}D_{ka}}{D_{ab}+D_{ka}}$$ (Ho and Webb, 2006)

where D_{ab} is the simple molecular diffusivity of water vapour in the atmosphere (630 m^2/year) and D_{ka} is the Knudsen diffusivity, which in normal terrestrial soils is orders of magnitude smaller than D_{ab}.

1.2.2 Growth of ice by vapour diffusion and deposition

To grow ground ice by vapour deposition, soil temperatures must be below the frost-point of atmospheric water vapour. Vapour first deposits in the upper portion of the soil and migrate further into the soil through diffusion. Ice will first form in the porous medium along the grain contact point and expands into the pore space (Hudson, 2008). The ice may continue to grow and progress further in the soil column until all available pore space is filled. An equilibrium will form at a certain depth were downward diffusion doesn't occur due to the geothermal gradient (depth of zero thermal amplitude).

The rates of diffusion at which the pores are filled depend on the mean annual air temperature and its amplitude, humidity, viscosity of air, permeability of the dry soil column and the open porosity (Fisher, 2005). The diffusion will be refrained by the mean free path of the H_2O molecules in the atmosphere and the pore radius of the soil material (Kuzmin, 2005). Water-vapour densities changes at depth as a function of the divergence or convergence of water-vapour flux. Mass conservation in a purely diffusive soil is given by the following equation:

$$[3] \quad f\frac{\partial \varrho_v}{\partial t} = \partial \frac{(fD_e \partial \varrho_v/\partial z)}{\partial z} \text{ (Fisher et al., In review)}$$

where z is the vertical coordinate (0 at the ground surface and positive downward), t is time in years, f is the open porosity of the soil, ϱ_v is the vapour density of water vapour in the pores and D_e is the effective diffusivity of water vapour in the soil.

Pore space can be increased in soils due to thermal stress. Small cracks can appear in frozen soils and create more space for ice to form due to air temperature fluctuations. Lacelle et al. (2013) found up to 85% excess ice (ice that exceeds the total pore volume of a soil) in perennially cryotic soils in the MDV, Antarctica. Thermal contraction-expansion of the cryotic soils create voids were moisture can enter and crystalize.

1.2.3 Barriers to diffusion

Diffusion needs to have open pore space for water vapour to move in the soil. Windblown dust can fill pores and limit the effectiveness of the diffusion. Another limitation to the accretion of ground ice is the pore mineral ice growth (Hudson, 2009). As ice form inside a pore space and it will progressively reduce diffusion leading to reduced water vapour flux.

Tortuosity and connectedness of the pores have a large influence on diffusivity and water vapour flux. Tortuosity refers to the convoluted nature of the porous pathways in which diffusion occurs (Hudson, 2008). The lower the tortuosity, the better pore connectivity and the further water vapour can reach into the ground.

1.2.4 Effects of deliquescent salts on vapour transport

Deliquescent salts are substances that attract water vapour from the air until they dissolve in the absorbed water and form a solution (Espinosa et al., 2008). These salts have the ability to increase vapour pressure and diffusion rate in soils. The presence of magnesium perchlorate ($Mg(ClO_4)_2$), a strong deliquescent salt, in soils has been measured between 31 to 630 μg/kg in University Valley, Antarctica (Kounaves et al., 2010) but the effects of this salts on water vapour transport and stable water isotopes in soils hasn't yet been studied. Perchlorate ions, ClO_4^-, dissolved in water can significantly lower its eutectic point since ions provide stronger intermolecular bonds. Depending on the concentration of the perchlorate, the eutectic point of water can be reduced to 206K (-67.15°C) and weaken pure ice (Lenferink et al., 2013). Other more common salts such as KCl and NaCl can lower temperature down to -21.2°C (Shumskii, 1964). These salts usually come from weathered bedrock and transported by water. When a brine solution freezes it precipitate a layer of fine white salt dust.

1.3 Stable isotopes of water

1.3.1 Isotope fractionation and the global meteoric water line

Elements on Earth are chemical substances composed of atoms having the same number of protons and neutrons in their nucleus. Isotopes are atoms of the same element that contains different numbers of neutrons in their nucleus. Most elements have at least one stable isotope and for the water molecule, both O and H contain a variety of isotopes. For example, oxygen can be composed of ^{16}O, the most common (99.76 %) and has 8 protons and 8 neutrons but ^{17}O (0.04 %) and ^{18}O (0.20 %) are also found in nature. These are said to be stable isotope since they do not decay into other elements. Hydrogen has 2 stable isotopes (^{1}H and ^{2}H or D) and 1 radioactive isotope, ^{3}H (tritium) with a half-life of 12 years that decays to He.

Isotope concentrations or abundances are measured as the ratio of the heavy to light isotopes, e.g. D/H or $^{18}O/^{16}O$. Gas-source isotope ratio mass spectrometers and off-axis integrated cavity output spectrometers via laser absorption are used to precisely measure the difference in abundance ratio between the sample and a reference gas or sample of known absolute isotopic abundance. Stable isotope data are then expressed as the difference between the sample and the reference, according to the equation (for the example of ^{18}O):

$$[4]\ {}^{18}O/{}^{16}O = \frac{({}^{18}O/{}^{16}O)_{sample} - ({}^{18}O/{}^{16}O)_{reference}}{({}^{18}O/{}^{16}O)_{reference}}$$

Simplified and expressed as parts per thousand or permil (‰) value, this becomes:

$$[5]\ \delta^{18}O = \left(\frac{({}^{18}O/{}^{16}O)_{sample}}{({}^{18}O/{}^{16}O)_{reference}} - 1 \right) \times 1000$$

The most widely used standard is the Vienna Standard Mean Ocean Water (VSMOW), which approximates the bulk isotopic composition of the present-day global ocean reservoir, and hence has δD and $\delta^{18}O$ values both defined to be exactly 0‰. The use of the δ-‰ notation referenced to VSMOW implies that most precipitation and continental waters will have negative values, indicating a lower heavy isotope content compared with the world oceans.

The behaviour of an isotope during physico-chemical reaction is affected by its mass, because atoms with greater mass form slightly stronger hydrogen bonds. Consequently, the heavier isotope is generally enriched in the more condensed phase (i.e. liquid over gaseous, or solid over liquid). In the case of evaporation and condensation of water, that include both ^{18}O and D, liquid water molecules are held together by weak hydrogen bonds whereas water vapour molecules diffuse through air. As there is slightly greater hydrogen bond strength for $H_2{}^{18}O$ vs. $H_2{}^{16}O$ bonds (or $^2H_2{}^{16}O$ vs. $H_2{}^{16}O$), the latter will be more easily broken during phase change. The result is a greater concentration of $H_2{}^{16}O$ in the water vapour and more $H_2{}^{18}O$ in the water (Figure 11). The isotope abundance ratio (e.g. $^{18}O/^{16}O$) does not vary enormously between different samples, and so the fractionation factor, α, generally has a value close to 1 and is expressed with a precision of 4 decimal places. However, isotope fractionation is a

thermodynamic process, and is a function of temperature. For water isotopes, fractionation values increase with lower temperatures (Table 1-4 in Clark and Fritz, 1997).

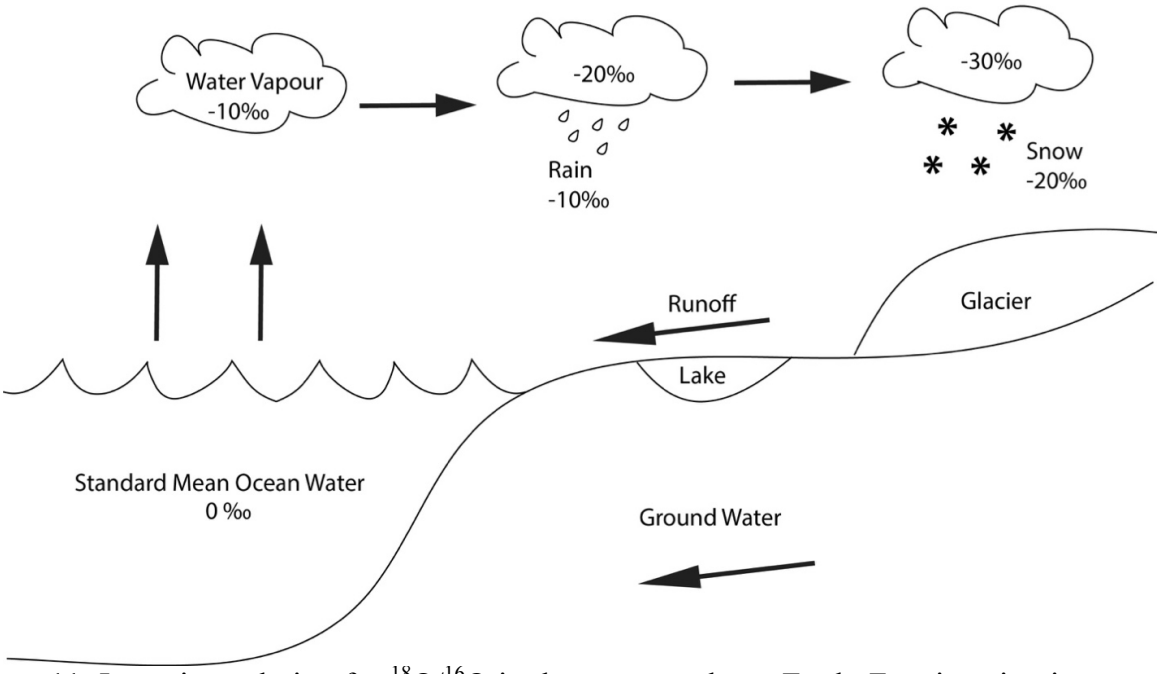

Figure 11. Isotopic evolution for $^{18}O/^{16}O$ in the water cycle on Earth. Fractionation increases as water evaporates from the ocean towards higher latitude due heavier isotopes depletion.

The Global Meteoric Water Line (GMWL) was first used by Craig (1961) to define the relationship between ^{18}O and D of fresh surface water worldwide. The δD and $\delta^{18}O$ isotopes are highly correlated and plot along a slope of 8 (GMWL: $\delta D = 8\ \delta^{18}O + 10$; Craig, 1961). The slope of 8 occurs since it approximates the ratio of equilibrium fractionation factors between water and vapour (Equation 6) for D on ^{18}O (Clark and Fritz, 1997).

$$[6]\quad S_{D-18O} \approx \frac{10^3 \ln(\alpha D_{w-v})}{10^3 \ln(\alpha^{18} O_{w-v})} \approx 8.2 \text{ at } 25°C \text{ (Clark and Fritz, 1997)}$$

where $\alpha_{w\text{-}v}$ is the equilibrium isotope fractionation factor between water and vapour.

1.3.2 Isotope fractionation during equilibrium freezing of water

Typically, the δD and $\delta^{18}O$ composition of meteoric precipitation (and glacial firnified ice) tend to be distributed along a regression slope near that of the global meteoric water line ($\delta D = 8\ \delta^{18}O+10$; Craig 1961). However, during equilibrium freezing of water, the value of the regression slope between D and ^{18}O will be different due to isotope fractionation that occurs

during freezing. During freezing of water, which results in a change in size of the reacting reservoir, isotope fractionation occurs following a Rayleigh-type distillation. The later represents an exponential function that describes isotope fractionation as the reacting reservoir decreases in size; in the case of freezing, the residual water. For ideal distillation to occur, the reacting reservoir must be finite and well mixed and not re-react with the product reservoir (Clark and Fritz, 1997). During freezing, the first ice to form will be enriched in ^{18}O by about 3‰ and about 20‰ in D given by the equilibrium enrichment factors between ice and water (Table 1-5 in Clark and Fritz, 1997). As freezing continues, the isotope composition of the ice formed progressively becomes depleted as the isotope composition of the residual water trends toward lower values.

The observed initial isotopic composition of water affects the isotope composition of the ice during freezing (Jouzel and Souchez, 1982). In a subsequent paper, Souchez and Jouzel (1984) suggest that the influence of the initial isotope composition of water on the ice during freezing can be estimated from the following equation:

$$[7]\ \delta i = \delta_O + (\alpha_{\delta_O}) \cdot \ln f + (\alpha_{\delta_O})$$

where: δi is the isotope composition of the ice, $\alpha_{\delta O} = (\alpha_{i-w} \cdot (\alpha_{i-w} - 1) \cdot (1000 + \delta_O)$, δ_O is the initial isotope composition of water, $\alpha_{i\text{-}w}$ is the equilibrium isotope fractionation factor between water and ice (Table 1) and f is the residual fraction of water during freezing.

The isotope composition of ice during progressive freezing also depends on the freezing rate, boundary layer thickness and isotope diffusion occurring at the ice-water interface (Lacelle, 2011). With this in mind, the isotopic composition of ice can be approximated by Burton's equation (1953) modified by (Lacelle, 2011) for solute segregation:

$$[8]\ \delta i = \delta_O + \ln(\alpha_{FR}) \cdot 1000 \cdot \ln(f) + \ln(\alpha_{FR}) \cdot 1000 \text{ (Lacelle, 2011)}$$

where: δi is the isotope composition of the ice, δ_O is the initial isotope composition of the water, $\alpha_{FR} = \left(\frac{\alpha_{i-w}}{\alpha_{i-w} - (\alpha_{i-w} - 1) e^{\frac{-h \cdot v}{D^*}}} \right)$, $\alpha_{i\text{-}w}$ is the equilibrium isotope fractionation factor between water and ice, h is the thickness of the boundary layer (cm), v is the freezing rate (cm s^{-1}), D* is

the diffusion coefficient in water and *f* is the residual fraction of water during freezing. At 0°C, values for D* and ^{18}O are 1.1x 10^{-5} cm^2s^{-1} and 1.33x 10^{-5} cm^2s^{-1}, respectively.

Combining equations 7 and 8 gives:

$$[9]\ \delta i = \delta_O + ((\ln(\alpha_{FR})\cdot 1000 + \alpha_{\delta O})\cdot \ln(f) + (\ln(\alpha_{FR})\cdot 1000 + \alpha_{\delta O}),$$ (Lacelle, 2011)

Therefore, equation [9] allows us to predict the isotope composition of the ice under equilibrium freezing conditions and for varying initial isotope composition of water, freezing rates and boundary layer thicknesses. The effect of initial composition of water, freezing rate and isotope diffusion at the ice-water interface during equilibrium freezing does not affect the shape of the "classic" Rayleigh fractionation, but it does affect the amplitude of isotopic composition of the ice, with lowest freezing rates showing the greatest spread in δ values (Lacelle, 2011).

During equilibrium freezing of liquid water, the value of the regression slope between δD and $\delta^{18}O$ is different than that of the GMWL ($S_{D\text{-}18O}$ = 8). For example, during equilibrium freezing, the slope of the regression line between D and ^{18}O equals 6.18. This slope, called freezing slope, is lower than the GMWL and represents the ratio between fractionation factor between water and ice for D and ^{18}O:

$$[10]\ S_{D-18O} = \frac{\ln(\alpha D_{i-w})}{\ln(\alpha^{18}O_{i-w})} = \frac{0.019116}{0.003095} = 6.18$$

O'Neil (1968) and Suzuoki and Kumura (1973), measured two different sets of equilibrium fractionation factors between water and ice (Table 1). Suzuoki and Kumura (1973) found fractionation factors of $\alpha D_{i\text{-}w}$ = 0.0206 and $\alpha^{18}O_{i\text{-}w}$ = 0.0028, these fractionation factors produce a freezing slope between δD and $\delta^{18}O$ that equals 7.29.

Table 1. Values of fractionation factors for ^{18}O and D in water-ice reactions and equilibrium slope values (Lacelle, 2011)

	O'Neil (1968)			Suzuoki and Kumura (1973)		
	$\alpha_{i\text{-}w}$	$\ln(\alpha_{i\text{-}w})\cdot 1000$	$\varepsilon_{i\text{-}w}$	$\alpha_{i\text{-}w}$	$\ln(\alpha_{i\text{-}w})\cdot 1000$	$\varepsilon_{i\text{-}w}$
^{18}O	1.0031	3.095	3.100	1.0028	2.796	2.800
D	1.0193	19.116	19.300	1.0206	20.391	20.600
Slope (D-^{18}O)		6.18	6.23		7.29	7.36

Therefore, there are two freezing slope possible, 6.18 and 7.29, that can be obtained between δD and $\delta^{18}O$ during ideal Rayleigh-type fractionation. Isotope fractionation during freezing is dependant of many other variables such as the initial isotope composition of the water, freezing rate, thickness of boundary layer and isotope diffusion at the ice-water interface (Lacelle, 2011). The result is a theoretical freezing slope value that can be estimated using the following equation:

$$[11]\ S_{D-18O} = \frac{\ln(\alpha D_{FR}) + \alpha D_{\delta O}}{\ln(\alpha^{18}O_{FR}) + \alpha^{18}O_{\delta O}} \text{ (Lacelle, 2011)}$$

where: $\alpha_{\delta O}$ and α_{FR} are defined in equation 7 and 8, respectively.

For boundary layer thicknesses less than about 0.02 cm, increasing freezing rates results in increase in $S_{D\text{-}18O}$ values. Using the ice-water fractionation factors defined by O'Neil (1968), $S_{D\text{-}18O}$ values range from 5.4, for low initial δ value and freezing rate, to 6.18 at high initial δ and freezing values (Lacelle, 2011). If the Suzuoki and Kumura (1973) fractionation factors between ice and water are used, the values of $S_{D\text{-}18O}$ range from 6.6 to 7.29 (Lacelle, 2011). Therefore, freezing of liquid water reduces the slope between D and ^{18}O to values of ~5.4 to 7.3 (Figure 12) depending on initial $\delta^{18}O$ and freezing rate (Souchez and Jouzel, 1984; Lacelle, 2011).

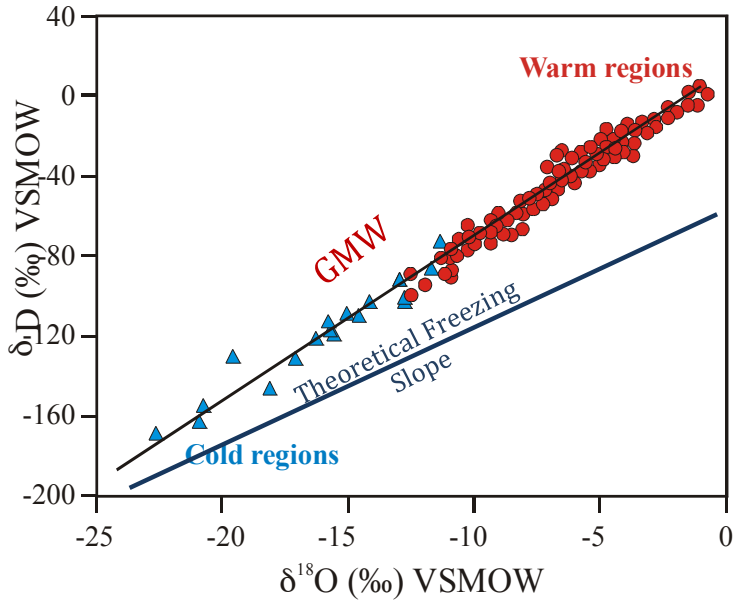

Figure 12. δD and $\delta^{18}O$ values for precipitation plotted along the GMWL and a theoretical freezing slope of < 7.3 (Lacelle et al., 2009)

1.3.3 Isotope fractionation during equilibrium vapour deposition

Unlike freezing of liquid water, there are limited studies on ice-vapour fractionation during the growth of ice. Fractionation in vapour deposited ice in soils occurs when water vapour diffuses into the soil and freezes. Heavier isotopes tend to condense first in the ice. Therefore, $\delta^{18}O$ and δD in vapour deposited ice are enriched by 14.7‰ and 127‰, respectively from their source of vapour, due to the equilibrium enrichment factors at 0°C between ice and vapour (Table 1 in Clark and Fritz, 1997). As vapour deposition continues, the isotope composition of the ice formed progressively becomes depleted as the isotope composition of the residual vapour trends toward lower values. In fact, results from ice-bearing permafrost core samples taken in upper University Valley in Antarctica, show that the first vapour deposited ice is enriched in $\delta^{18}O$ and δD relative to the moisture source and as we move deeper in the core the $\delta^{18}O$ and δD becomes lower (Lacelle et al., 2013; Fisher and Lacelle, 2014).

The theoretical slope between $\delta^{18}O$ and δD for vapour deposited ice in soils can be calculated using of the ratio of equilibrium fractionation factors between ice and vapour for D on ^{18}O. The fractionation factor for $10^3\ln(\alpha Di_{-v}) = 127$ at 0°C (Clark and Fritz, 1997) and for $10^3\ln(\alpha^{18}O_{i-v})$ is 14.7 at 0°C (Majoube, 1971). The result is a slope of 8.6 shown by equation 12.

$$[12]\ S_{D-18O} \approx \frac{10^3\ln(\alpha D_{i-v})}{10^3\ln(\alpha^{18}O_{i-v})} \approx \frac{127}{14.7} \approx 8.6$$

where $\alpha_{i\text{-}v}$ is the equilibrium isotope fractionation factor between ice and vapour for D and ^{18}O.

This predicted slope value is similar to the GMWL, however potential effects of initial composition of water vapour and diffusion rates are largely unknown. Results from ice-bearing permafrost cores in upper University Valley in Antarctica, show that vapour deposited ice plots along the GMWL (S≈8) line but is shifted below it due to lower δD values (Figure 13).

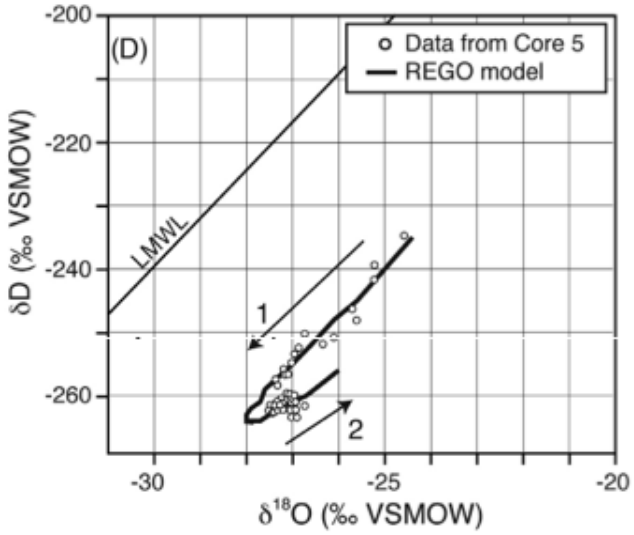

Figure 13. Pore water stable isotopes from core 5 taken from upper University Valley, Antarctica (Lacelle et al., 2013)

1.4 REGO model

Few numerical models were developed to study diffusion of vapour into soils and associated isotope fractionation. The thesis will use the REGO model to predict results using experimental temperature and humidity conditions as well as soil properties. REGO is a time varying one-dimension water vapour transport model through dry and icy soils that includes diffusion, advection and phase changes (Fisher, 2005; Fisher and Lacelle, 2014). REGO uses a standard diffusive water flux component that is dependent on the thermo-physical properties of the sediments and the direction of vapor-diffusion is dependent on vapor density differences in the soil column.

REGO was developed by Fisher (2005) to estimate the ice content formed by vapour diffusion/condensation in the Martian regolith where liquid water is absent. REGO was later supplemented with isotope fractionation capabilities, although ice-vapour fractionation factors remained poorly constrained below -30°C (Fisher and Lacelle, 2014). REGO uses as input parameters temperature and its cycles, the geothermal gradient, humidity and thermo-physical characteristics of the sediments (i.e., dry porosity, density, tortuosity, thermal diffusivity). The amount of ice emplaced in the soils is dependent on vapour diffusion rates, tensile stress, climate

parameters (i.e., mean annual air temperature and its amplitude, period of the temperature cycle, humidity in air and soils) and the thermo-physical characteristics of the sediments.

1.4.1 TMUT4

TMUT4 is a sub-routine in REGO that calculates the ice densities in a soil column from vapour diffusion and deposition (Fisher, 2005). The variables such as a geothermal gradient, thermal diffusivity, surface temperature, depth of the soil column, soil porosity, and period of diffusion were used to predict ground ice content in the soil. An example of the output of the model can be seen in Appendix A: Table A.1.

1.4.2 COISOTOP2

COISOTOP2 is a sub-routine that is capable of computing stable water isotopes values of the ice through ice soil column (Fisher and Lacelle, 2014). The input values of the source of moisture must be obtained and the thermal gradient of the soil column must be entered in the model. An example of the output of the model can be seen in Appendix A: Table A.2.

Chapter 2: Experimental growth of pore ice by vapour diffusion at stable ambient temperature

Summary

The objectives of this first experiment were to determine the ground ice content and stable water isotopes of the ice made by vapour deposition of two different sediments. This experiment was performed in an experimental chamber with cooling plates capable of creating a steep thermal gradient of -2.8°C/cm in a closed container. The experiment was performed using equipment capable of creating artificially frozen soils with precisely controlled parameters (e.g. temperature, vapour saturation) and two types of soil. Samples were left in the experimental chamber to let ice diffuse and crystalize into the sediments for a two-month growth period. The samples were afterwards extracted, analysed for their gravimetric water content and stable water isotope composition.

2.1 Equipment and material

This section describes the equipment and material used to grow ground ice by vapour diffusion in a soil column. The experiments were conducted in the CryoLab for Arctic, Antarctic and Planetary Studies (CLAAPS) at the Department of Geography, University of Ottawa.

2.1.1 Equipment

An environmental test chamber model RTC-16P made by Burnsco® Technologies Inc. was used to conduct the experiments (Figure 14A). This 16 ft^3 chamber is a refrigerating unit capable of reaching temperature between -70 to +177ºC with a precision of ±1ºC using two air compressors (2 Hp each) and one heater (4000 Watts) that cascade air into the chamber. The full specifications of the environmental chamber can be found in Table B1, Appendix B.

For the experiments, the soils samples were placed in steel soil caddies (h= 21.5 cm, r= 9 cm) (Figure 14B). Thermal insulation foil with a thickness of 0.5 cm was wrapped inside and outside the walls of the soil caddies to reduce the horizontal thermal gradient between the air

temperature in the chamber and that in the soil (i.e. edge effect). Inside the soil caddies are custom designed screen mesh (1 mm^2 grid) that can be placed on top of the soils at various heights that contain the crushed ice (Figure 14C).

Four stainless steel cooling plates with hollow interiors (h= 3 cm, r= 11 cm) (Figure 14D) were fabricated by the machine shop at the University of Ottawa. These cooling plates were connected in series using 0.25" metal pipes and Swagelok® copper connectors. The cooling plates were fed a heat transfer fluid (Syltherm XLT®) cooled by a FTS Systems Multicool® temperature conditioning bath (Figure 14E) that can reach temperature of -80ºC (± 0.1ºC). The Syltherm XLT® fluid is pumped from the low-temperature bath to the custom-made cooling plates by a Chemsteel® rotary gear pump from Oberdorfer® Pumps, which is capable of pumping fluids with a viscosity up to 100 SSU at a flow rate of 30 gpm (Figure 14F). The Multicool® temperature conditioning bath and pump are connected together with 1/4" Swagelok® FJ series convoluted metal hoses. The assembled setup can be seen in Figure 15.

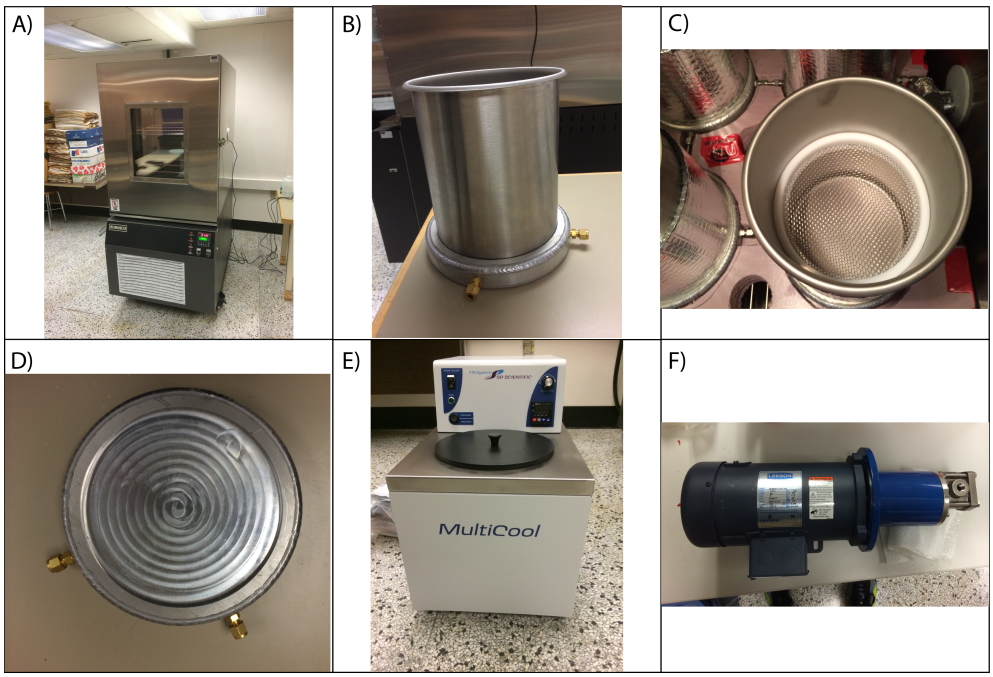

Figure 14. Equipment for the experiment: A) Burnsco® environmental test chamber, B) Stainless steel sample caddy on cooling plate, C) Stainless steel cooling plate with copper Swagelok® connectors D) Snow caddy inside the sample caddy, E) FTS Systems Multicool® temperature conditioning bath filled with Syltherm XLT® and F) Chemsteel® fluid pump

Figure 15. Assembled setup: Environmental chamber with the four cooling plates connected to the pump and the cold bath located in the Cryolab for Arctic, Antarctic and Planetary Studies.

2.1.2 Materials

For the experiments, two sediments matrices with very different physical properties were used: 1) soda lime glass beads and 2) JSC Mars-1 soil simulant. The source of water vapour was crushed ice placed on top of the sediments, simulating a snow-covered surface (i.e., $100\%_{ice}$). The physical and chemical properties of these materials are described below.

2.1.2.1 Glass beads

Soda lime glass beads were used since they provide accurate and replicable results due to their very uniform size/shape and inert chemical composition. The same glass beads were also used by Hudson et al. (2007, 2009) and their results could be compared. The glass beads are artificial sediments obtained from AGSCO Corporation and passed through size 30–40 sieves (coarse sand). Laser particle size analysis revealed that the average particle size was 533 ± 3 µm, no more than 10% of the beads were larger than 700 µm (coarse sand) and less than 20% were smaller than 400 µm (medium sand). All the grains were very well rounded and highly spherical (Figure 16A). The bulk density of the glass beads was measured to be 1.5 ± 0.1 g/cm^3 by weighing the sediments in a graduated glass cylinder. Deionized (DI) water was added to the soil in the graduated cylinder until they were saturated and the weight of water added was used to calculate the porosity of the glass beads, 33 ± 5%. As provided by the technical sheet, the

chemical composition of the beads is the following: SiO_2 (72.8%), Al_2O_3 (1.3%), CaO (8.0%), MgO (3.9%), Na_2O (13.3%), K_2O (0.3%), SO_3 (0.1%) and Fe_2O_3 and Fe_3O_4 (0.1%). For more information on the glass beads see Figure B1 in Appendix B.

2.1.2.2 JSC Mars-1 simulant

The JSC Mars-1 simulant was used for the experiment because it has been used by Hudson et al. (2007; 2009) in previous experiments on growth of ice by vapour diffusion and has different physical properties compared to the glass beads. The JSC Mars-1 simulant is a loose weathered soil that originates from a weathered palagonitic ash from Pu'u Nene cinder cone in Hawaii. Laser particle size analysis revealed that grain size ranges from 1000 µm (very coarse sand) to < 20 µm (silt) and averaging 285 ± 18 µm (medium sand). The bulk density of the JSC Mars-1 was measured to be 0.9 ± 0.1 g/cm^3 by weighing the soil in a glass graduated cylinder. DI water was added to the soil in the graduated cylinder until they were saturated and the weight of water added was used to infer the porosity. The porosity of the glass beads was calculated to 73 ± 5% due to its wide range particles and their sub-angular shape (Figure 16B). As specified in the technical sheet, the chemical composition of the JSC Mars-1 simulant is SiO_2 (43.7%), Al_2O_3 (23.4%), Fe_2O_3 (11.8%), CaO (6.2%), TiO_2 (3.8%), FeO (3.5%), MgO (3.4%), Na_2O (2.4%), P_2O_5 (0.9%) K_2O (0.6%) and MnO (0.3%). For more information, see the technical sheet produced by Allen et al. (1998). A comparison of the physical properties of the two sediments is shown in Table 2.

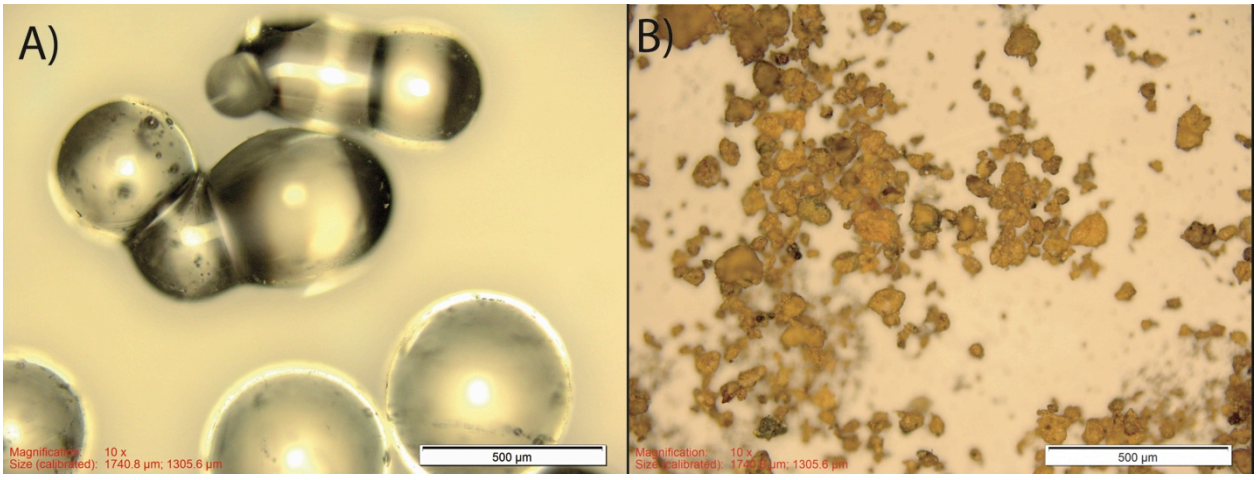

Figure 16. Microscopic pictures of the sediments used for experiments. A) Glass Beads B) JSC Mars-1. Images were taken with an Olympus BX41 binocular polarizing microscopes using a QImaging digital photomicrographic head.

Table 2. Physical properties of the two sediments

Parameter	Glass Beads	JSC Mars-1
Mean grain-size (μm)	533 ± 3	285 ± 18
Bulk density (g/cm^3)	1.5 ± 0.1	0.9 ± 0.1
Porosity (%)	33 ± 5	73 ± 5

2.1.2.3 Source of water vapour: crushed ice cubes

In a natural terrestrial setting, the source of water vapour for ground ice originates from the sublimation of snow. To replicate a snowpack above the sediments, crushed ice cubes of known grain size and δD-δ^{18}O composition were produced for the experiment. Ice cubes of 1 cm^3 were made in plastic trays using DI water placed in a freezer and afterwards crushed using a hammer on a metal plate that was earlier cooled in a freezer. The crushed ice had a wide range of fragment size that ranged from fine ice powder of a few mm^3 to 0.5 cm^3 chunks of ice. Crushing the ice cubes ensures an even δD-δ^{18}O composition and increases their surface to saturate the air with moisture. The crushed ice cubes were placed on top of the sediments, thus ensuring ground surface relative humidity of 100%$_{ice}$.

Four water samples each composed of five uncrushed ice cubes were let to melted in sealed Falcon® tubes at room temperature. The samples were brought to the G.G. Hatch Lab for δD-δ^{18}O analysis. Their δD values ranged from -82.2 to -83.1‰ and their δ^{18}O values range was -10.61 to -10.77‰, all within analytical precision (Table 3). Their mean values for δD is -82.5‰ and -10.7‰ for δ^{18}O.

Table 3. Stable water isotopes δD-δ^{18}O of crushed 1 cm^3 ice cubes

Sample ID	δD (‰VSMOW)	δ^{18}O (‰VSMOW)
PB-01	-82.2	-10.6
PB-02	-82.6	-10.6
PB-03	-83.1	-10.8
PB-04	-82.2	-10.7
Average	-82.5	-10.7

2.2 Experimental procedure and analyses

Before the start of the experiments, the two sediments (glass beads and JSC Mars-1 simulant) were oven-dried at 105ºC for 24 hours and let to cool at room temperature for 6 hours. Afterwards, the sediments were transferred into four sample caddies to a thickness of 12 cm. Two of the four caddies were filled with glass beads and the other two with the JSC Mars-1 soil simulant. Subsequently, 6 cm of crushed ice was added on top of the sediments. The sample caddies were covered using a plastic lid and sealed with marine grade silicone and Tuck® Tape to ensure that no moisture enters the caddies.

The four sample caddies were each placed on a cooling plate inside of the environmental test chamber that was earlier set to -5°C. Afterwards, the plates were cooled by pumping a heat transfer fluid, Syltherm XLT, chilled at -55°C by the cold bath. The fluid was pumped and circulated from the cold bath through Swagelok steel convoluted hoses to the plates. A sketch of the experiment setup can be seen in Figure 17. For a full explanation on the standard operating procedures of the experimental setup please see Appendix C.

The experimental set-up was left in the chamber for 62 days. After the 2-month growth period, the four soil caddies were removed from the chamber and a core was taken for each type of soil. All four soils contained ice, but were not ice-cemented. Only two of the four soils were samples, one for each type of soil. The soil was thus removed in 1 cm thick section using a small spoon. The soil samples were placed in sealed in polyurethane bags to thaw at room temperature. After thawing, each sample was shaken for a minute and transferred into sealed graduated 50 ml Falcon® conical centrifuge tubes for storage. Two sub-samples were then used to determine gravimetric water content and δD-δ^{18}O composition. The remaining crushed ice cubes now fused in one solid block on top of the soil, was cut into three ~2 cm thick sections using a handsaw and let to melt in polyurethane bags and analyzed for δD-δ^{18}O composition.

Gravimetric water content (GWC) is a method to assess the amount of water or moisture in a soil. The GWC was determined for each sample by taking a small ~50 ml subsample and placing it in an oven at 105°C for 24 hours. The moist and wet weights of the samples were determined. By definition, GWC is a weight ratio of pore water in a soil on its dry mass and can be calculated using the following equation by van Everdingen (1998):

$$[13]\ \text{GWC}\ (\%) = \left(\frac{\text{weight of moist soil (g)} - \text{weight of dry soil (g)}}{\text{weight of dry soil (g)}}\right) * 100$$

Given the low amount of water in the samples, pore water in the samples was extracted using the vacuum distillation method at the Advanced Research Complex (ARC), University of Ottawa. This extraction method consists creating a vacuum in glass and heating the sample to remove all pore water. A 50 ml Erlenmeyer was cleaned and bake at 105°C before each extraction. About 20-30 g of moist soil was placed in the Erlenmeyer and clamped on the extraction line. The Erlenmeyer flask was frozen using liquid nitrogen and a vacuum was created in the extraction line using a pump. The samples still under vacuum were heated using a customized heating plate at a starting temperature of 60°C and slowly increased up to 100°C to ensure the samples were completely dried. Pore water from the samples slowly evaporated and was transferred in the vacuumed line to a glass exetainer placed in liquid nitrogen. The distillation was stopped when the sediments looked completely dried (became lighter in colour) and no more moisture was accumulating in the exetainer. The distillation took between 1.5 to 2 hours depending on the amount of moisture in the soil.

Extracted pore water samples and melted crushed ice were analyzed for $^{18}O/^{16}O$ and for D/H composition at the G.G. Hatch Stable Isotope Laboratory in Department of Earth Sciences, University of Ottawa. The $^{18}O/^{16}O$ and D/H ratios were determined using a Los Gatos Research (LGR) high precision liquid water analyzer coupled to a CTC LC-PAL auto-sampler. Results are shown with the δ-notation ($\delta^{18}O$ and δD), where δ represents the parts per thousand differences between $^{18}O/^{16}O$ or D/H and reported to the Vienna Standard Mean Ocean Water (VSMOW). The analytical reproducibility for $\delta^{18}O$ and δD is ± 0.1‰ and ± 0.5‰, respectively.

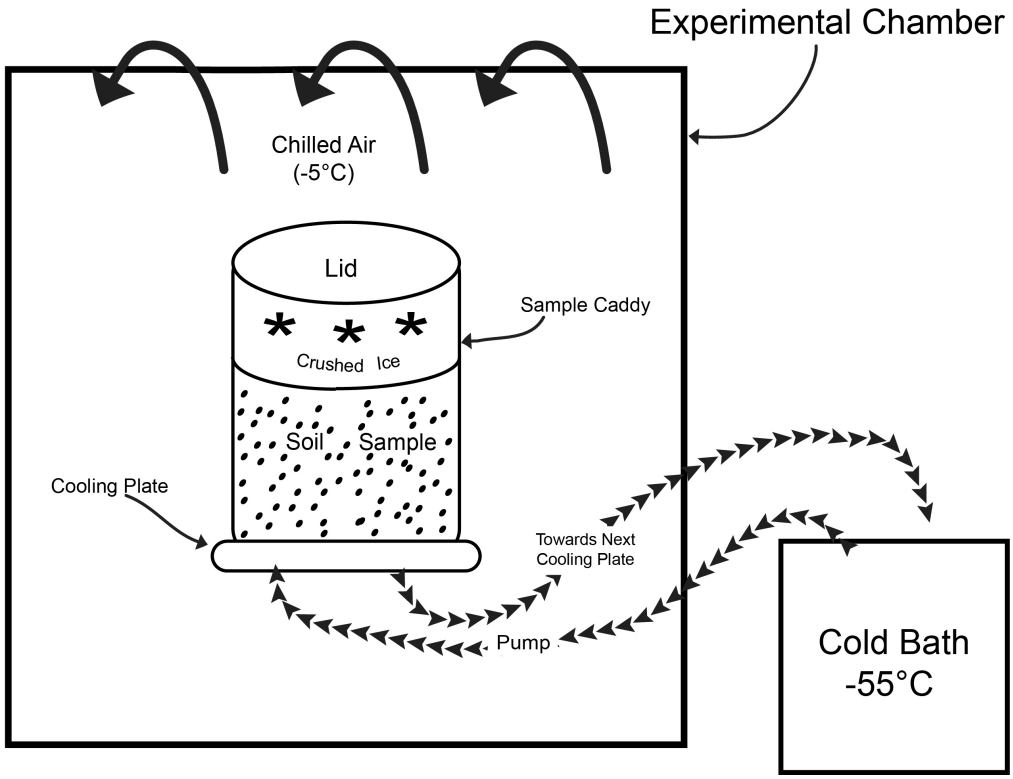

Figure 17. Schematic of the first experiment showing one of four soil caddies placed in the experimental chamber at a stable air temperature of -5°C and cold plate temperature of -55°C. Soil was placed at the bottom of the container with a thickness of 12 cm and 6 cm of crushed ice was placed above. Key components of the setup are shown: chamber, cold bath and sample caddy on its cooling plate (not to scale).

2.3 Results

2.3.1 Soil temperature variations in the sample caddies

Before attempting to produce ground ice by vapour diffusion, the temperature gradient and possible edge effect (temperature variations between the center and edge) inside the sample caddy was assessed using soil thermistors by Onset® Computer Corp model TMC6-HD (accuracy of ±0.25°C at 20ºC; ±0.5°C at 0ºC and resolution of 0.02°C at 20°C) connected to Onset® HOBO® data loggers.

The soil caddies were filled to 12 cm with glass beads and the JSC-1 simulants. No crushed ice was added on top of the soil to study the edge effects in the two soils. Two data loggers with each four thermistor strings were placed in the sample caddy at 2 cm vertical interval starting 1 cm above the bottom to produce a thermistor rod made of 6 sensors: one string was in the center

and the other one near the edge of the caddy. The sensors were held in place by holes drilled in a high-density foam blocks (Figure 18). The sample caddies were sealed with a lid and the containers were placed onto the cooling plates located inside the environmental chamber. Air temperature in the chamber was set to -5°C and the cooling plates were fed -55°C fluid from the cold bath.

After 12 hours, temperatures in the glass beads and JSC Mars-1 soil simulant had reached stability. For the glass beads, temperature at 1 cm depth was -17.7°C whereas it reached -49.5°C at 11 cm depth (vertical gradient of -3.2°C/cm; Figure 19). For the JSC Mars-1 soil simulant, temperature at 1 cm depth was -14.6°C whereas it reached -46.0°C at 11 cm depth (vertical gradient of -3.2°C/cm). The edge effect in the sample caddies is minimal given the temperature accuracy of ±0.5°C of the thermistors and that the temperature differences between the center and edge of the caddies is < 0.6°C for the glass beads and < 1.2°C for the JSC Mars-1 simulant.

Based on these vertical temperature gradient and equation [14], the calculated thermal diffusivity (k) for the glass beads and JSC Mars-1 simulant is 6.98 m^2/yr. This value is only an approximation due to errors of about 33% when calculating the derivative for the thermal conductivity and heat capacity.

$$[14]\ k = \frac{K}{\rho C}\ \text{(French, 1996)}$$

where K is the thermal conductivity of the soil which can be approximated by dT/dt using the slope of temperature change on time, ρ is the bulk soil density and C is the heat capacity that can be approximated with the vertical temperature gradient by d(dT/dz)/dz.

In a separate test, the thermal gradient in the soil caddies was assessed with 6 cm of crushed ice placed on top of the soils. The experiment was done in the same manner as in the first test. After 24 hours, the vertical thermal profile was calculated to -2.76°C/cm in both soil columns due to the insulating effect of the added crushed ice.

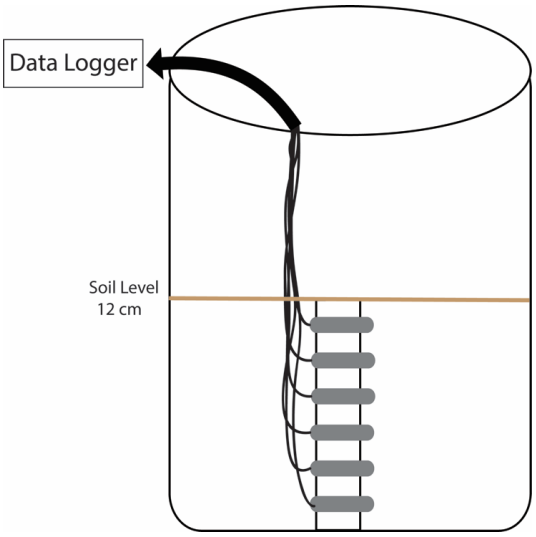

Figure 18. Sketch of the thermistor rod in the sample caddy. The sensors are placed every 2 cm starting at 1 cm above the bottom.

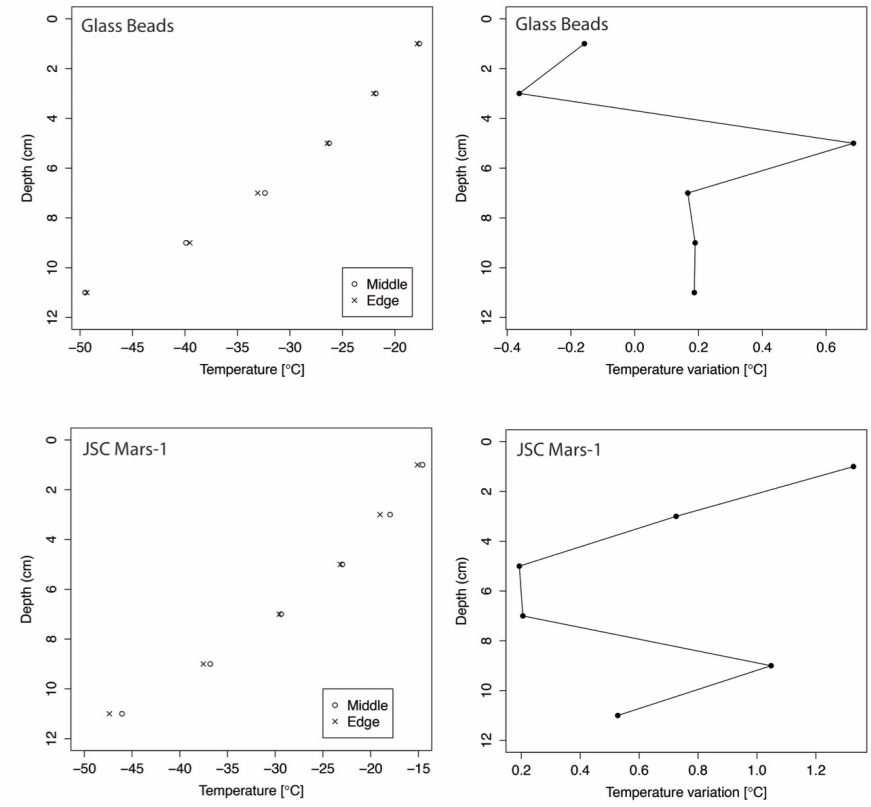

Figure 19. Temperature gradient between the edge and the center of the sample caddies filled with glass beads and JSC Mars-1 (Left). Temperature variation between the edge and the center of the sample caddies for the two types of soil (Right). Air temperature in the chamber was set to -5°C and the cooling plates were fed -55°C fluid.

2.3.2 Gravimetric water content and stable isotopes of water

After 62 days in the chamber, the four soil caddies were removed from the chamber and only one sample caddy for each type of soil was analysed for GWC and stable water isotopes. A layer of vapour deposited ice covered the exterior base of the cold plates and the sample caddy. The lid over the samples remained sealed and there were no signs of external moisture entering the sample caddies. Once the lid removed, the crushed ice on top of the soils had fused into one layer and still had its original thickness of 6 cm (Figure 20A). Below, the pure ice were small needle ice structures of a few mm long fused with a fine layer of soil attached to it. The remaining soil, although it contained ice, was not ice cemented. The soils were classified as structureless unconsolidated soil using the Murton and French's (1994) cryostructural classification. Two cone shaped features, 6 and 9 cm tall, made of pure ice and sediment was found on the bottom of the two soil caddy containing the glass beads (Figure 20B). This feature likely formed when ice on top of soil sample was slightly above 0°C for a brief period of time and a small portion of the ice melted. This feature was not observed in the JSC Mars-1 soil simulant.

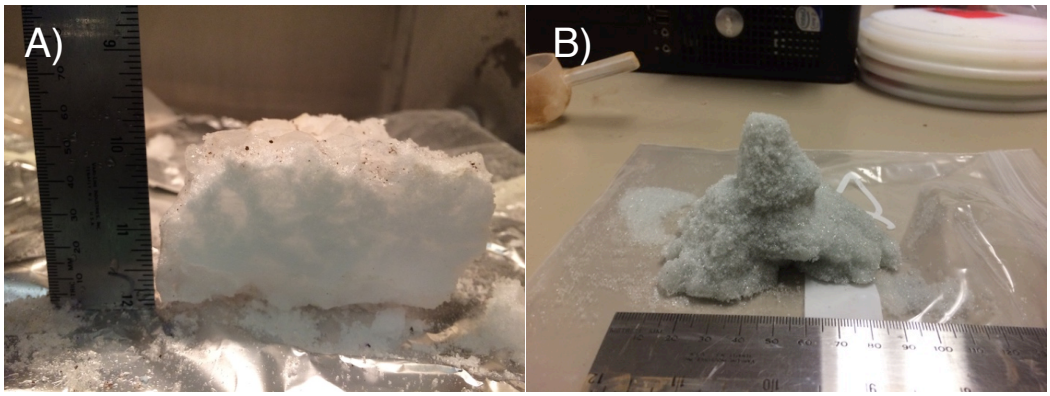

Figure 20. Photographs from the first experiment. A) Section of the headroom ice in one of the sample caddies. B) Cone shaped ice feature at the bottom of the glass beads soil sample.

The two soils showed similar GWC profile after a 62-day growth period, but with differing water content (Figure 21A). The glass beads reached a maximum GWC of 2.8% in the top 1 cm of the soil and the water content decreases gradually to a minimum of 0.1% at the bottom (12 cm). The JSC Mars-1 soil simulant had a much higher GWC in the top 1 cm (15.1%) then decreased to 0.8% at the bottom. On average, the GWC was 11x higher in the JSC Mars-1 soil and the difference was greatest (22x) at 2 cm depth.

The depth profile for both δD and δ^{18}O can be seen in Figure 21B-C. Compared to the start isotopic composition of the crushed ice (δD: -82.5‰ and δ^{18}O: -10.7‰), the residual crushed ice samples in both soils were enrichment in δ^{18}O by < 1.5‰ and depleted in δD by < -3.6‰. The difference in stable water isotopes of the residual crushed ice above both types of soils decreased with depth. The isotopic composition at the top of the residual crushed ice is slightly less depleted than the samples at the bottom of the ice. At the end of the experiment, stable water isotopes of the residual crushed ice above the JSC Mars-1 soil showed greater depletion in δ^{18}O and δD than the ice above the glass beads soils.

In both soil samples, only the first 3 cm of soil contained enough water for δD-δ^{18}O analysis. Between 0 to -2 cm in depth, the glass beads were more enriched in δD (9.1 to 3.2‰) and in δ^{18}O (4.2 to 2.1‰) than the original composition crushed ice. At -3 cm in depth, the glass beads became more depleted in δD depth by -3.0‰ and in δ^{18}O by -1.5 ‰.

The JSC Mars-1 pore water tends to have lower δD-δ^{18}O values compared to the glass beads by on average δD: -28.6‰ and δ^{18}O: -2.9‰. At 0 cm, the JSC Mars-1 soil was more enriched in δD by 26.9‰ and in δ^{18}O by 8.2‰ than the original composition crushed ice. At -2 cm the JSC Mars-1 sample was more depleted than be start composition by -49.5‰ in δD and -1.69‰ in δ^{18}O. As depth increased, pore ice in the glass beads and JSC Mras-1 soil further decrease in δD and δ^{18}O.

The co-isotope composition of the pore ice in both soils and their residual crushed ice are shown in

Figure 22. All the samples but one where below the GMWL. The crushed ice has undergone isotopic rearrangements in the two-month period from its initial isotopic values (δD: -82.5‰ and δ^{18}O: -10.7‰). The top portion of the residual crushed ice was more enriched in δ^{18}O and depleted in δD. The crushed ice has been enriched in δ^{18}O and slightly depleted in δD in all samples except for the JSC Mars-1 simulant at 6 cm. The pore ice samples of both soils have further distanced themselves from the initial isotope composition of the crushed ice.

The linear regression slope for the residual crushed ice samples for the glass beads is 3.9 (δD = 3.9 δ^{18}O – 45.4; R^2 = 0.27; p-value= 0.728) and 6.3 for the JSC Mars-1 soil (δD = 6.3 δ^{18}O –

24.4; R^2 = 0.99; p-value= 0.049). The value of the linear regression slope of the pore water for glass beads is 2.4 (δD = 2.4 δ^{18}O – 56.7; R^2 = 0.88; p-value= 0.064) due to the point above the GMWL and 8.1 for the JSC Mars-1 soil (δD = 8.1 δ^{18}O – 38.0; R^2 = 0.97; p-value= 0.1153). A point located at δ^{18}O: -2.5 ‰, δD: -55.6‰ on the JSC Mars-1 graph is probably an outlier due to a problem during the pore water extraction (incomplete water extraction). If this data point is removed and the data points of both soils are combined, the value of the linear regression becomes 6.8 (δD = 6.8 δ^{18}O - 24.7; R^2 = 0.38; p-value= 0.034).

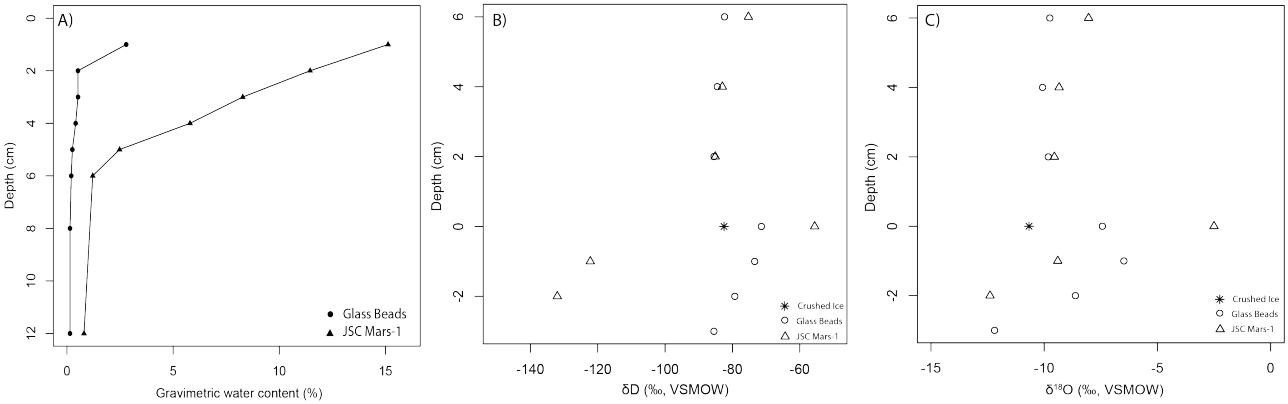

Figure 21. A) Gravimetric water, B) δD and C) δ^{18}O soil depth profiles after the two-month experiment. Note change in y-axis scale for GWC and δD-δ^{18}O.

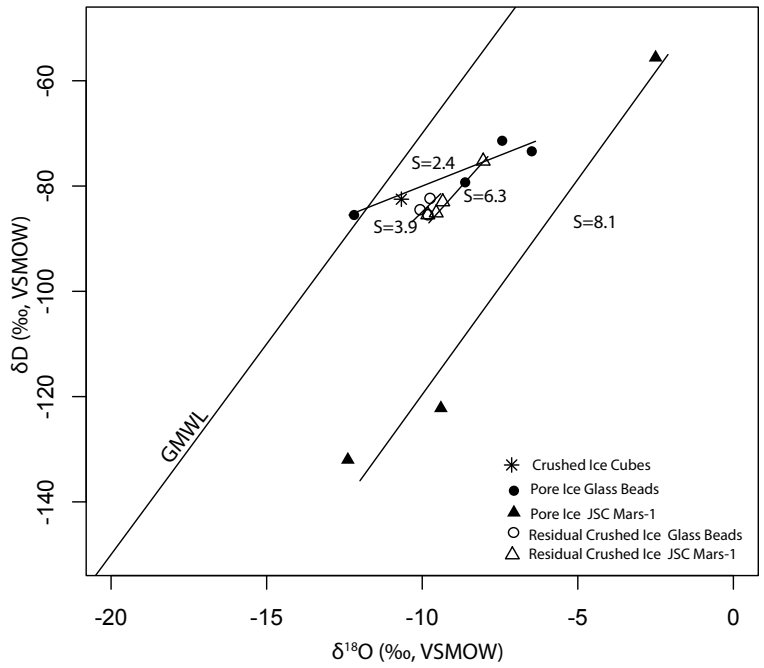

Figure 22. δD and δ^{18}O composition of initial crushed ice, residual crushed ice and pore ice in the glass beads and JSC Mars-1 soil simulant plotted along the GMWL.

2.4 Discussion

2.4.1 Gravimetric water content of vapour deposited ground ice

The JSC Mars-1 soil sample had on average 11x GWC than in the glass bead sample, however both soils showed a similar GWC profile with depth. In both soils, the uppermost 6 cm has the highest amount of GWC since it's closest to the source of moisture. Diffusion is a slow process that depends of the temperature gradient, concentration of moisture, porosity, connectivity and tortuosity of the pores (Hudson, 2008). Since both soils were subjected to the same thermal gradient and relative humidity, the remaining factors are soils properties with porosity being the greatest factor. Glass beads have a porosity of 33% which is > 2x porosity of the JSC Mars-1, 73%. In the case of vapour diffusion in soils, a higher porosity soil will reduce the Knudsen diffusion effect, thus increasing the effective diffusion (D_e, see equation 2) leading to higher vapour flux rate and hence higher ice content.

GWC was modeled using TMTUT4, a subsection of the REGO model (Fisher, 2005). The input parameters for the model can be seen in Table 4. The subsequent values were directly measured/controlled during the experiment and were inputted in the model. The period was set at 2 months, the mean surface temperature at -5°C, the geothermal gradient at -27600 Deg./100 m, the soil depth at 12 cm and initial porosity at 33% for the glass beads and at 73% for the JSC Mars-1 soil. Other input parameters not measured during the experiment were obtained from Fisher and Lacelle (2014) since they were found to be suitable averages for normal dry, non-icy, soils. These values included two thermal amplitudes of 1.00E-03°C and 1.30E-04°C, a short period of 2.74E-03 year, a minimal initial diffusivity of 630.00 m^2/year and a soil thermal diffusivity of 9.5 m^2/year. A stronger thermal diffusivity was used since the earlier calculated value of 6.9 m^2/year shown in section 2.3.1 had a high degree of uncertainty.

The model provides a descent fit for both soil types. The main difference between GWC measured and the values predicted by REGO is the as abrupt change in GWC at the depth of 2 cm for the glass beads and 6 cm in the JSC Mars-1 (Figure 23). The amount of GWC in the profiles are directly linked to the intensity of the geothermal gradient and period water vapour has to diffuse into the soil. Certain physical parameters such as porosity, grain contact, grain shape and sphericity influence the amount of ice one soil can contain. The dominant factor influencing soil ice content would be soil porosity since its the only variable that was changed in

the model to replicate the results for the two soil type. Soils with higher porosity such as the JSC Mars-1 soil will accumulate ice faster than a soil with less porosity.

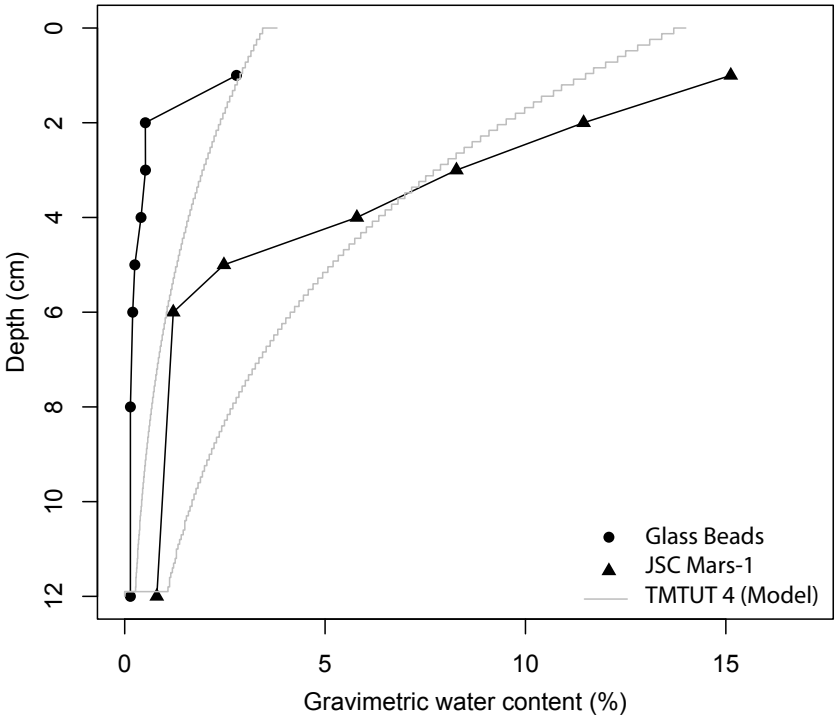

Figure 23. Gravimetric water content for the two soils in the first experiment compared to the TMUT4 model using a 12 cm soil column made of soil inside the experimental chamber. The growth period imputed in the model is 62 days with a thermal gradient of -2.76°C/cm and dry soil start.

Table 4. Parameters used for the TMTUT4 model for experiment 1

Parameter	Value
Period (Months)	2
Mean Temperature (°C)	-5
Amplitude 1 (°C)	1.00E-03
Short Period (Year)	2.74E-03
Soil Depth (m)	0.12
Steps (#)	100
Amplitude 2 (°C)	1.30E-04
Geothermal Gradient (Deg./100 m)	-27600
Thermal Diffusivity (m^2/yr)	9.50
Minimal Initial Diffusivity (m^2/yr)	630.00
Initial Porosity (%)	33% (Glass Beads) and 73% (JSC Mars-1)

To obtain higher ground ice content, the experiments would need to run for a much longer time. Even if the thermal gradient in the experiments was much stronger than in nature, time is the limiting factor when producing vapour deposited ice in perennially cryotic soils. According to the TMTUT4 model, it would take 8 months to fill the pores to their maximum in the first 1 cm of both soil types using a geothermal gradient of -2.76°C/cm and the GWC would be ~1% at 12 cm depth. To completely fill the 12 cm soils in the sample caddy with vapour deposited ice it would take ~32 years.

Vapour deposited ice has a characteristic concave downwards GWC profile since it is a function of the temperature on saturation vapour pressure. The saturation vapour pressure (ei) curve for ice can be seen in Figure 24 and was also suggested by Hudson et al., 2009 as the main justification for the shape of the curve. The concave downwards curve closely resembles the GWC profiles obtained experimentally and using the REGO model. The saturation vapour pressure curve was made using equation [15] with temperature (t) in °C and ei in hPa, (1 hPa= 100 Pa). The saturation vapour pressure of ice decreases exponentially when temperature decreases with depth.

$$[15]\ ei = 6.112\ e^{(22.46\ t/(272.62 + t))},\ (WMO, 2008)$$

where: t is in °C and ei in hPa.

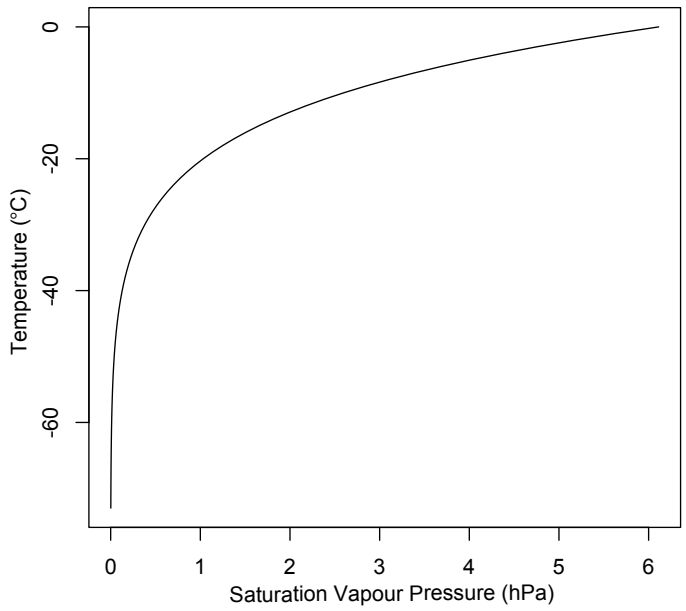

Figure 24. Saturation vapour pressure curve for ice using equation [15]

2.4.2 Stable water isotopes signatures of vapour deposited ground ice

The results of the experiment show that water isotopes in the residual crushed ice are more depleted in δD and enriched in δ^{18}O than in the soils by < -3.6‰ for δD and < 1.5‰ for δ^{18}O. Both soils were enriched in heavier water isotopes in its upper sections (0 - 2 cm) and more depleted in its lower section (< 2 cm) with respect to the start isotopic composition being the crushed ice cubes.

Overall, the depth profiles for δD and δ^{18}O creates a distinguishable, almost vertical, concave downwards shape in the residual crushed ice under sublimation. Isotopes of δD and δ^{18}O in the uppermost section of the residual crushed ice decrease in concentration with depth. The residual crushed ice will slowly become more enriched in heavier isotopes as more ice is sublimated just as thermokarst lakes become more enriched by evaporation (Turner et al., 2010).

Depth profiles for δD and δ^{18}O have a positive linear slope in the pore ice created by deposition. In the first cm of the soil, pore ice in all samples are enriched in δD and δ^{18}O from their start isotopic composition (crushed ice) and afterwards rapidly decrease linearly in concentration with depth. The concentration in stable water isotopes decrease more rapidly with depth in the soil since they likely follow a diffusion fractionation curve. The water isotopes made by vapour will be much lower in δD and δ^{18}O due to fractionation during phase change.

The δD-δ^{18}O co-isotope scatter plot shows that most of the samples are below the GMWL with an overall slope of 6.9 for all the samples. In theory this slope should be nearer to 8.6, equation [12], obtained by the equilibrium fractionation factors of δD on δ^{18}O between water vapour and ice. Additional pore water sample would be needed to verify the theoretical depositional slope. Pore ice in the soils is shifted below the GMWL is due to condensation. The shift occurs in a finite reservoir when vapour condensates into the soil which lead to isotope fractionation between vapour and ice.

The results of the first 3 cm of the pore water were modeled using COISOTOP2 model to evaluate the parameters needed to produce the results. The inputs of this first model are located in Table 5 and the results are in Figure 25. The temperature at which the phase change shifts from vapour to ice was set at -10°C (Fisher, 1991) and the relative humidity was assumed to be 100%. The start temperature of -10°C (top of the soil) and end temperature of -15°C (bottom of

the soil) was measured prior to the experiment using thermistors in the sample. The isotopic composition of the headroom ice was the same as the earlier measured crushed ice samples (δD: -82.5‰ and δ^{18}O: -10.7‰) and the water vapour isotopes were calculated to be δD: -187.6‰ and δ^{18}O: -23.3‰.

The output of the model has a positive slope of 8.15 and decrease linearly with depth. All pore water samples, with the exception of one, are below the model.

A second COISOTOP2 model was performed to investigate the δD-δ^{18}O composition of the full 12 cm core. The input values used are the same as indicated in Table 5 but the end temperature was changed to -55°C (the temperature at the bottom of the soil) instead of -15°C. The result of the model is shown in Figure 26 and demonstrate the isotopic values below 3 cm in depth for the two-month experiment.

The results in upper section of the core start by plotting on the GMWL but drift off to the left below δ^{18}O: -40‰ and δD: -400‰. This occurs when temperatures drop below -40°C and vapour-ice fractionation causes δ^{18}O to deplete faster than δD. The measured fractionation coefficients are not well measured below -40°C. As waters get ever more depleted in δD and δ^{18}O their values have to move towards the absolute minimum of -1000 ‰ for both δ^{18}O and δD (Fisher and Lacelle, 2014).

The experiment was performed, in a closed system where stable water isotopes could redistribute themselves in the soil through two processes: Graham's law of diffusion and by fractionation. Graham's law of diffusion stipulates that lighter molecules will diffuse faster than heavier molecules due to their kinetic energy. It takes more energy to displace the liter version of the isotopes (^{16}O and H) than its heavier isotope (^{18}O and D) because of their difference in molar mass. Oxygen 16 has a diffusion rate 1.061 times greater than oxygen 16 and hydrogen has a diffusion rate 1.414 times greater than deuterium. Therefore, ^{16}O and H will always diffuse faster than ^{18}O and D. A similar process occurs, through fractionation when the water molecules change phase. The heavier isotopes necessity more energy to change phases and tend to remain in their current state. When vapour deposits into solid ice, its heavier version (^{18}O and D) will preferentially stay in the air and more (^{16}O and H) will stay deposit into ice. Fraction will increase as vapour deposits further into the soil away from the source of vapour. By repeating

this process vapour will become more depleted in heavier isotopes near the bottom of the sediments.

The results obtained in this experiments are similar to those found by Lacelle et al. (2013. Their study located in University Valley, Antarctica found vapour diffused pore ice with slope values of 7.6 and 10.8 in two separate permafrost cores. Their results are more depleted in δD-δ^{18}O since the cores were taken from Antarctica where rainwater is already very depleted in heavier isotopes in this area.

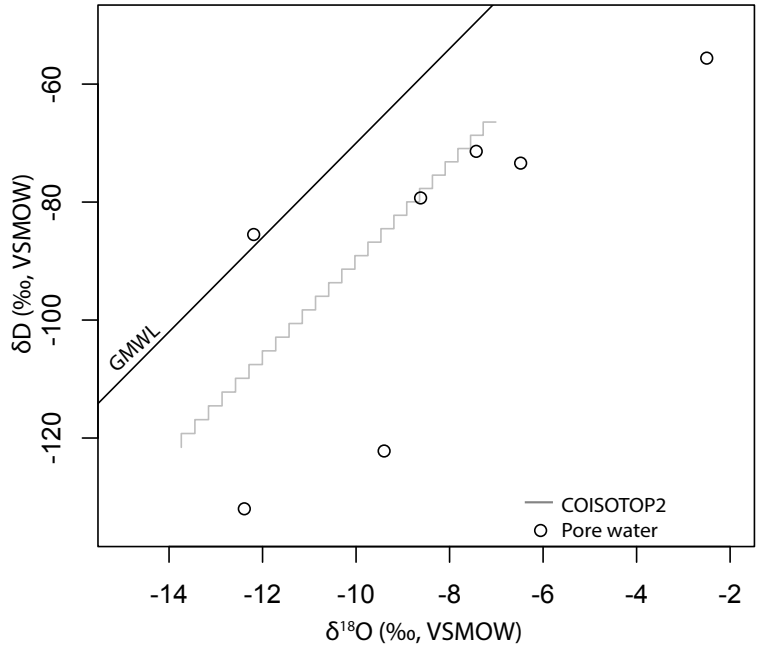

Figure 25. COISOTOP2 model of δD-δ^{18}O for the first 3 cm soil of both types of soil inside the experimental chamber. The growth period in the model is 62 days with a thermal gradient of -2.76°C/cm. The source of moisture is the crushed ice cubes with a starting isotopic value of δD: -82.5 ‰ and δ^{18}O: -10.7 ‰.

Table 5. Parameters used for the COISOTOP2 model in experiment 1

Parameter	Value
Shift Temperature (°C)	-10
Relative Humidity (%)	100
Start Temperature (°C)	-10
End Temperature (°C)	-15
Steps (#)	25
Headroom Ice δD (‰)	-82.5
Headroom Ice δ^{18}O (‰)	-10.7
Headroom Vapour δD (‰)	-187.6
Headroom Vapour δ^{18}O (‰)	-23.3

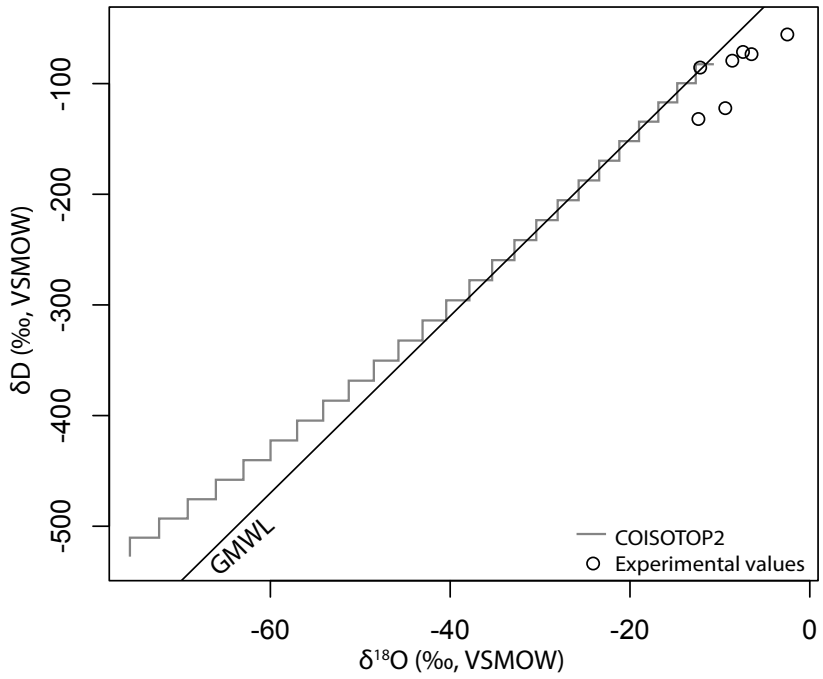

Figure 26. COISOTOP2 model for δD-δ^{18}O of the whole 12 cm sample in the first experiment under a geothermal gradient of -2.76°C using the stable isotopic values of the crushed ice cubes.

2.5 Conclusions

A first two-month experiment using two different types of soils with different porosities (33% and 73%) was performed in an experimental chamber capable of creating a thermal gradient of -2.76°C/cm in 12 cm of soil. The samples were analyzed for their GWC and for their stable water isotopes in both the above ice and in the soil. The experiment produced soils with GWC ranging from 15.1% (near surface) to 0.4% (at the bottom). The stable water isotopes of the source ice (δD: -82.5‰ and δ^{18}O: -10.67‰) placed on top of the soil pore ice were enrichment in δ^{18}O and depletion in δD. This was more noticeable in the JSC Mars-1 soil and varied slightly in depth (< 1.5‰ for δ^{18}O and < -3.6‰ for δD). Pore ice were enrichment in the first 0 to 2 cm in depth are enriched and depleted between 2 to 3 cm depth than the initial source of vapour. When plotted along the GMWL on a δD-δ^{18}O plot the values fall below the GMWL and follow it with a slope of 6.8.

Soil porosity significantly influenced GWC and the $\delta^{18}O$- δD composition in soils. On average, 11x more ice was deposited in the JSC Mars-1 soil simulant than in the glass beads soil. The difference is greatest at the surface and decreases greatly with depth. The JSC Mars-1 soil simulant has lower δD-$\delta^{18}O$ values than the glass beads on average by δD: -28.6‰ and $\delta^{18}O$: -2.9‰ lower.

Models further validate the results obtained in the experiment and helped visualize the isotopic composition below 3 cm depth where samples could not be extracted due to their low water content. The modelled isotopes passed $\delta^{18}O$: -40‰ and δD: -400‰ shift to the left of the GMWL as they become more depleted.

Chapter 3: Effects of magnesium perchlorate and a 3 cm air gap on the growth of pore ice by vapour diffusion

Summary

This second experiment focused on studying the effects of magnesium perchlorate in a soil column by determining the gravimetric water content in the soils and analyzing its pore water isotopes. In addition, a 3 cm air gap between the source vapour, crushed ice, and the soil was created to simulate the effects of an air pocket. The experiment was performed using the same method as in the first experiment to be able to compare the results and understand the effect of an air pocket. The diffusion period was again 62 days and the soils are the same as in the last chapter but finer sized ice (< 1 mm) was used to ensure air saturation. The crushed ice was inserted on top of the snow caddy located 3 cm above the soil. One sample for each type of soil was mixed with 0.1 vol.% magnesium perchlorate to investigate its effect on diffusion.

3.1 Equipment and material

The same two sediments (glass beads and JSC Mars-1) were used but the source of moisture came from crushed ice sieved at 1 mm. In addition, magnesium perchlorate was mixed into two of the four sediments samples, one for each type of soil, in a concentration of 0.1 vol. % to evaluate its effect on the pore ice content and stable water isotopes.

3.1.1 Crushed ice

Ice cubes (1 cm^3) were made in a plastic trays using DI water and crushed using a hammer in a cold room at -22°C. Afterwards, the ice was sieved through a 1 mm (Φ 0) mesh to retain only ice crystals smaller than 1 mm. This was done to have a homogenized porosity and increase the ice surface to ensure air saturation.

3.1.2 Magnesium perchlorate

The salt used in the experiment is magnesium perchlorate, $Mg(ClO_4)_2$, a powerful oxidation agent capable of reducing the eutectic point of water up to -67.15ºC (Clark and van Hart, 1981; Houtkooperand and Schulze-Makuch, 2010; Lenferink et al., 2013). When mixed with water,

magnesium perchlorate releases -568.90 kJ/mol through an exothermic reaction. This deliquescent salt should attract moisture and increase diffusion rates in the soil. Perchlorate is found in low concentrations in the McMurdo Dry Valleys ranging from 31 to 1100 µg/kg (Kounaves et al., 2010). Magnesium perchlorate was mixed into one sample for each of two types of soil in a concentration of 0.1 vol.% (5.33 g/sample), which is a much higher (> 2000x) concentration than found in the MDV.

3.2 Experimental procedure and analyses

The second series of experiment was performed in the same manner as in the first experiment in section 2.2. Two samples caddies were filled to a thickness of 12 cm with glass beads and another two with JSC Mars-1 soil. Both soils were placed in the oven at 105°C for 24 hours to remove any moisture. Magnesium perchlorate with a concentration of 0.1 vol. % (5.33 g/sample) was added in two of the sample caddies, one for each type of soil. The salt was stirred with the soil until it was uniformly distributed. Afterwards, the sample caddies with the soil were placed overnight in the environmental chamber set at -30°C. The next day, the snow caddies were placed 3 cm above the soil and filled with 3 cm of crushed ice. Thermal sensors were added into the two glass beads soil and set to log temperatures every 30 minutes to measure the temperature differences between the sample with and without salt. The sample caddies were covered with a lid and closed hermetically using marine grade silicone and Tuck® tape. Afterwards, the environmental chamber was set to -5°C and the cooling plates were fed -55°C fluid. The samples were left to diffuse in the experimental chamber for a duration of 2 months. A summary of the experimental design can be seen in Figure 27.

After a 62-day growth period, the four soil caddies were again non-consolidated and removed using a spoon at one cm thick increments. The samples were placed in sealed in polyurethane bags to thaw at room temperature. Each thawed samples were shaken for a minute and transferred into graduated 50 ml Falcon® conical centrifuge tubes for storage.

A subsample was analyzed for gravimetric water content and pore water was extracted from the remaining sample using a distillation method explained in section 2.2. The samples were prepared laboratory at the Advanced Research Complex (ARC), University of Ottawa.

The remaining crushed ice ~2 cm thick had fused in one solid block on top of each soil sample were placed into polyurethane bags and let to melt. Afterwards, the water samples were placed into 2 ml glass vials. The samples were sent for $^{18}O/^{16}O$ and for D/H analysis at the G.G. Hatch Stable Isotope Laboratory in Department of Earth Sciences, University of Ottawa, following methods described in section 2.2.

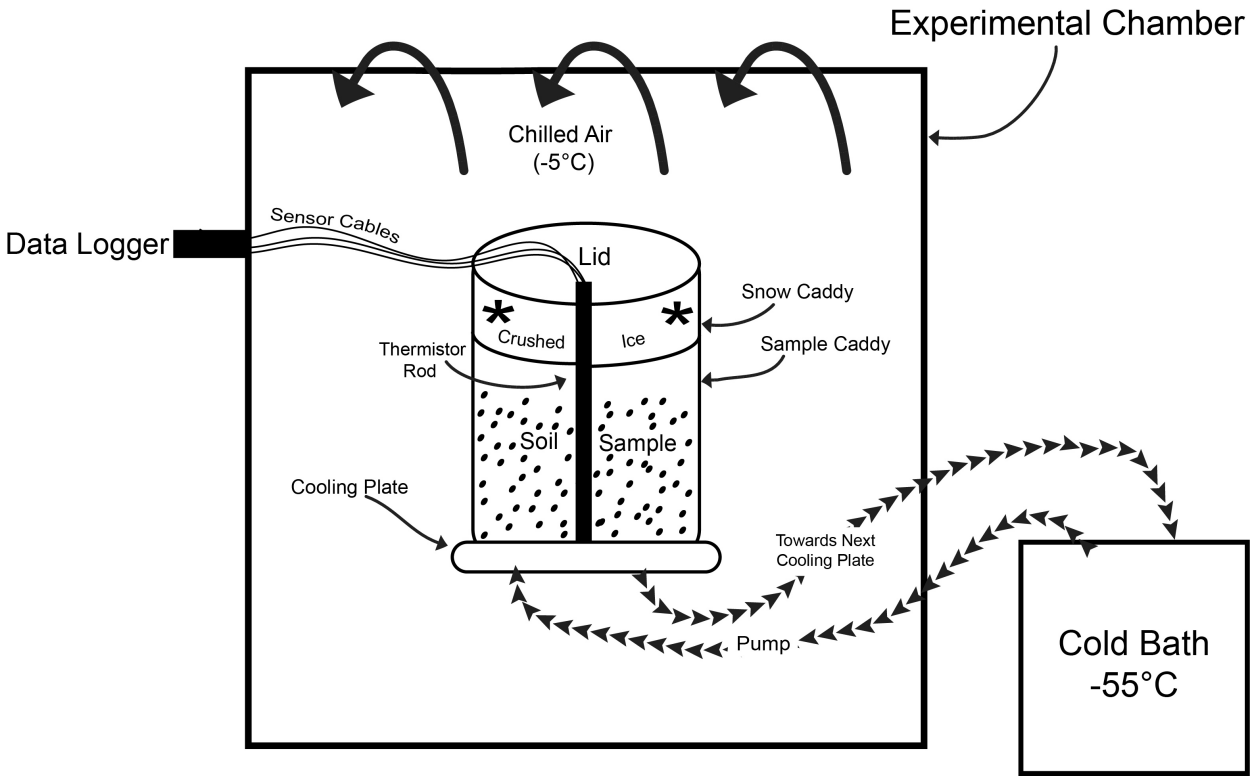

Figure 27. Schematic of the second experiment showing one of four soil caddies placed in the experimental chamber at -5°C. Soil was placed at the bottom of the container with a thickness of 12 cm and 3 cm thick layer of sieved crushed ice was placed 3 cm above the soil in a snow caddie. Key components of the setup are shown: chamber, cold bath, snow caddy 3 cm above soil, data logger and sample caddy on its cooling plate (not to scale).

3.3 Results

3.3.1. Soil temperature profiles

Thermistors rods were placed in two glass bead samples (one with magnesium perchlorate and one without). The average temperature readings for the glass bead samples is shown in Figure 28. The glass bead soil with the salt had a two-month average temperatures of -19.9°C at

1 cm depth and -43.5°C at 11 cm depth. The overall temperature gradient for this sample was -2.36°C/cm.

The glass bead sample without salt had slightly higher average temperatures of -18.4°C at 1 cm depth and -41.4°C at 11 cm depth. The average vertical thermal gradient in the unsalted glass beads soil was -2.30°C/cm. The sample with salt consistently had lower temperature values at the same depth as the other without salt. The temperature difference between both samples was on average 1.7 ±0.5°C. The temperature difference in the two samples could be due to uneven temperature distribution in the chamber due to the cascading air since the temperature difference in the air gap between the sample, the snow and the above ice is the same as in the soils. Ground temperatures between the glass beads sample with and without perchlorate were not influenced by the released of exothermic heat when vapour was absorbed by the salt. Therefore, the concentration of magnesium perchlorate in the soils was too low to influence temperatures in the soils.

Figure 29 shows the temporal variation in temperature at different depths in the soils. Overtime, the thermal gradient in the soil remained at -2.3°C/cm but due to ice accumulation on the equipment and pipes, the temperature of the heat transfer liquid (Syltherm® XLT) decrease by about 3°C and reached stability 10 days into the experiment. Ice that had accumulated on the outside the equipment due to their cold temperature was removed every week and additional fiberglass insulation was placed to stabilize the temperature. Since the thermal gradient the experiment remained constant at -2.3°C/cm this didn't affect the rate of diffusion. After stabilization thermistors recorded temperatures variations of less than ± 0.5°C. The temperature spike located on day 20 is due to a brief power outage and soil temperatures never went above 0°C.

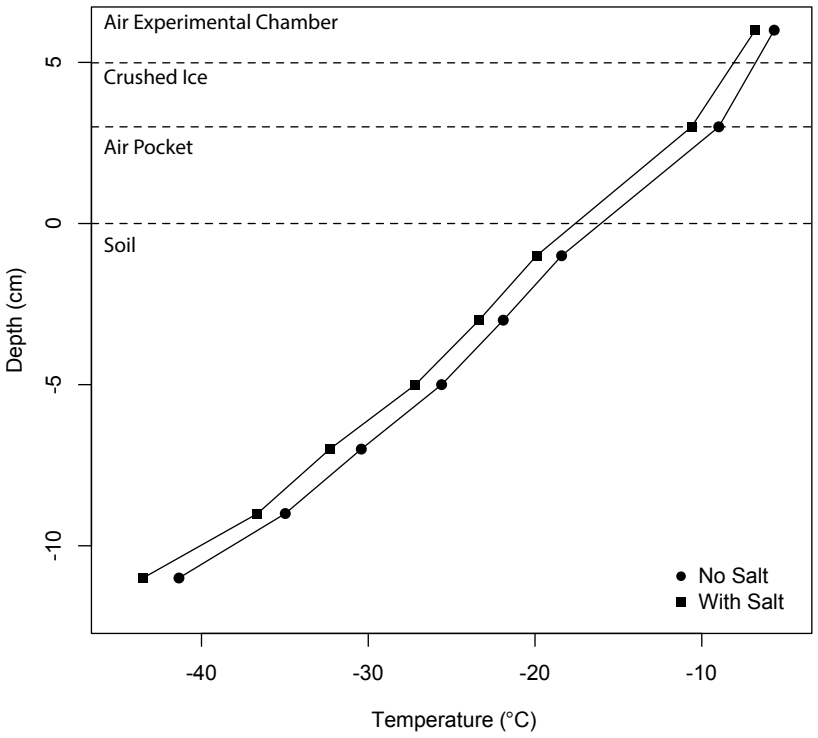

Figure 28. Temperature profile for two samples filled with glass beads of which one had 0.1 vol. % magnesium perchlorate mixed (salt). Data is the average temperature acquired every 30 min for the duration of the experiment (2 months).

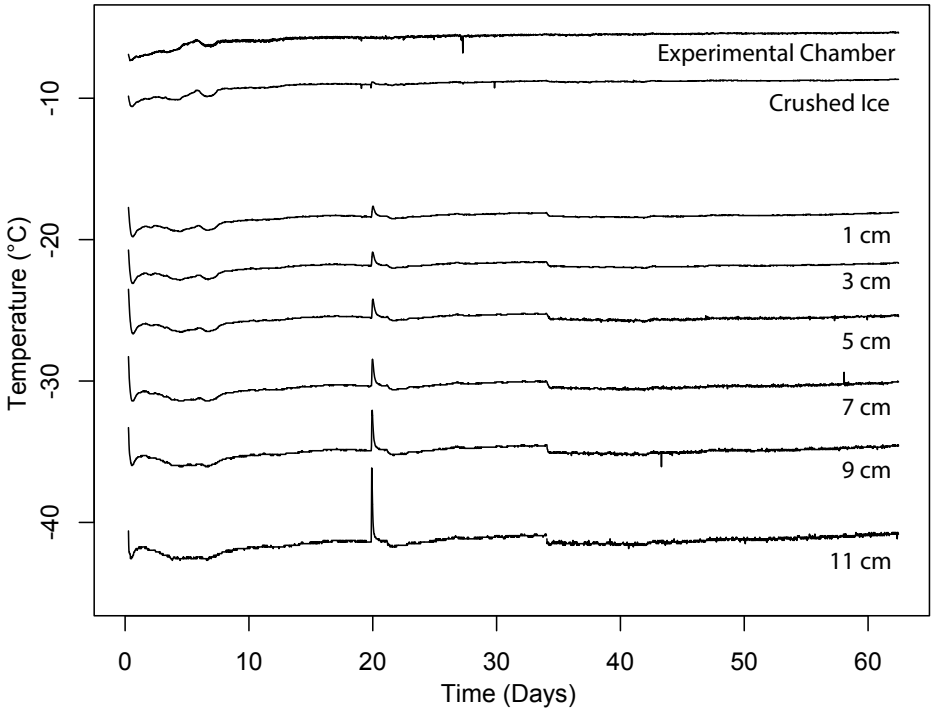

Figure 29. Temporal changes in temperature of the air in the chamber, the vapour source (ice) and sensors placed in the glass beads soil without salt between 1 to 11 cm during the 62-day experiment.

3.3.2 Gravimetric water content

After a two-month growth period, the sample caddies were removed from the chamber. The snow thickness had reduced to 2 cm and some of the snow that sublimated was deposited on top of the soil. The soils were classified as structureless unconsolidated soil using the Murton and French's (1994) cryostructural classification. The glass beads had more vapour deposited ice on top of the soil than the JSC Mars-1. At the surface of the soil, the glass beads had non-uniformed recrystallized ice about ~1 cm thick (Figure 30A) and the JSC Mars-1 had smaller ice patches < 1 cm thick (Figure 30B). The vapour sublimated from the source and followed to side of the caddy and deposited onto the freezing soil. The ice on top of the soil had hoar frost with long facets up to 1.5 cm in length on top of the glass beads. The JSC Mars-1 soil had much smaller hoar frost of a few mm in length.

GWC show very similar depth profiles for the samples containing with magnesium perchlorate and those without the salt; however, the JSC Mars-1 samples had a higher GWC (Figure 31). The glass beads (both samples containing salts and no salts) showed a higher GWC near the surface between 2.0 – 5.2 %, but it rapidly decreased below 1 % at 2 cm depth and continued to decrease near 0 % at the bottom of the core. The GWC at 1 cm depth in the JSC Mars-1 salt-free sample was 10.5% and 10.8% in the sample with magnesium perchlorate. The GWC then decreased to less than 2% at 6 cm depth and afterwards rapidly decreases towards 1 % at the bottom. Overall, the glass beads contained on average 7x less GWC than the JSC Mars-1 soil sample, a similar result to the series of experiments shown in Chapter 2.

Figure 30. Picture of vapour deposited hoar frost on top of the glass beads (A) and the JSC Mars-1 experimental soil (B)

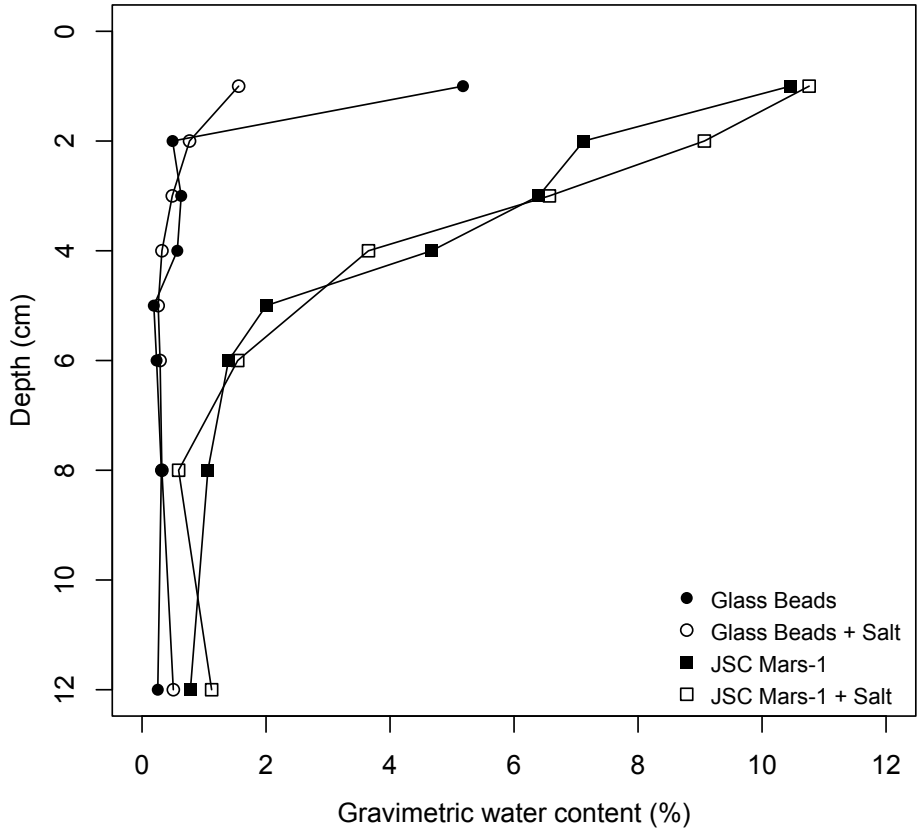

Figure 31. Gravimetric water content for the four samples during experiment 2. One sample of each soil type was mixed with 0.1 vol. % magnesium perchlorate (salt).

3.3.3 Stable water isotopes

Pore water isotopic composition of the first 1-2 cm in soils and their residual crushed ice is shown in Figure 32. The co-isotope plot for all soils in this experiment are both below and above the GMWL (Figure 32A). The ice samples taken above the soil for all samples (with the exception of the glass bead sample at -1 cm in depth) plot underneath the GMWL. The pore ice sample plot with a slope of 4.9 (δD=4.9 δ^{18}O - 37.0, R^2=0.81, p-value= < 0.01) and the residual crushed ice has a slope of 3.6 (δD=3.6 δ^{18}O – 46.5, R^2=0.99, p-value= < 0.01). Pore ice isotopes plot above the GMWL and cross it below δD: -90‰ and δ^{18}O: -12.0‰ in concentration. The more depleted samples plot slightly above the GMWL with a slope near 8.

The start isotopic composition of the crushed ice (δD: -82.5‰, δ^{18}O: -10.7‰) is used as a reference point shown by an asterisk in the plots. The remaining ice on the snow caddies of all

samples are enriched between 7.7 to 43.9 ‰ in δD and 2.1 to 10.4‰ in δ^{18}O. The snow caddy in the JSC Mars-1 samples has higher values in δD-δ^{18}O for the samples with salt.

Hoar frost at the surface of the soil (0 cm) were slightly enriched in the JSC Mars-1 samples and depleted in the glass beads samples when compared to the start ice composition. The hoar ice samples in JSC Mars-1 soil had a mean isotopic composition of -73.5‰ for δD and -5.9‰ for δ^{18}O. The hoar ice in the glass beads had a mean isotopic composition of -99.8‰ for δD and -15.4 ‰ for δ^{18}O.

Pore ice in the the glass bead soils are all depleted in δD and δ^{18}O with the exception of one sample located at -1 cm in depth in the unsalted sediments (Figure 32B-C). As depth increases samples become more depleted in δD and δ^{18}O. The glass bead samples had lower values in δD-δ^{18}O for the samples with salt. The average isotopic composition of the pore water samples from the glass beads with salt are δD: -116.7‰, δ^{18}O: -18.2‰ and the values of the only sample without salt is δD: -74.7‰, δ^{18}O: -8.5‰.

The isotopic composition of the pore water samples from the JSC Mars-1 soil are more depleted in heavier isotopes than the glass beads by on average -48‰ for δD and by -7‰ for δ^{18}O (Figure 32D-E). As depth increases samples become more depleted in δD and δ^{18}O. The average isotopic composition for the JSC Mars-1 soil with salt is δD: -159.7‰, δ^{18}O: -21.7‰ and without salt δD: -153.0‰, δ^{18}O: -24.9‰.

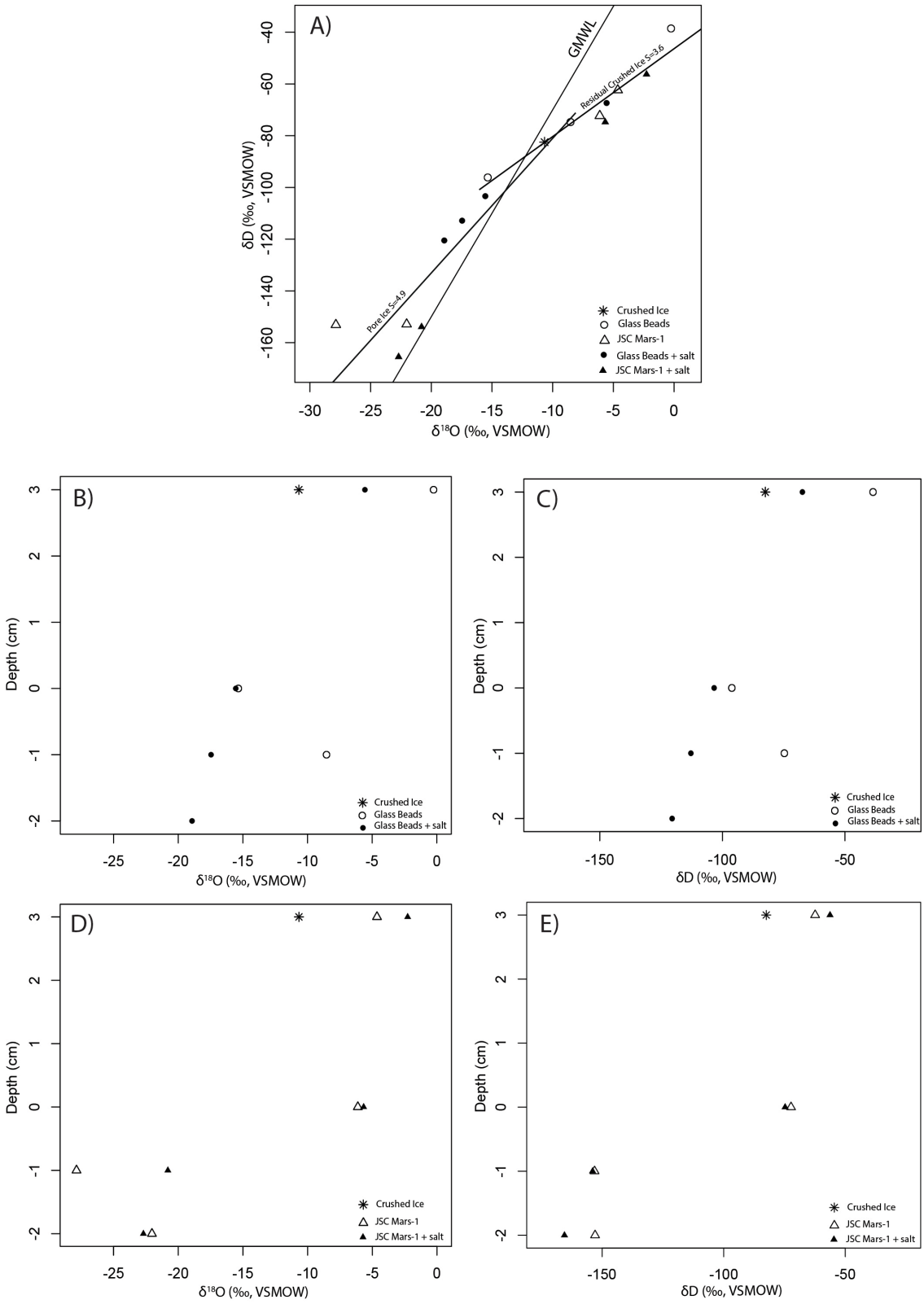

Figure 32. Stable water isotopes for the second experiment with the vapour source, crushed ice cubes, indicted by the asterisks. Co-isotope diagram (A). Variation in δ^{18}O(B) and in δD(C) with depth for glass beads. Variation in δ^{18}O(D) and in δD(E) with depth for JSC Mars-1.

3.4 Discussion

This section will focus on modeling and explaining the results obtained. In addition, results between the first experiment and this second experience will be compared to evaluate the effect of the air gap on the GWC and water isotopes.

3.4.1 Effect of magnesium perchlorate on GWC

The glass beads and JSC Mars-1 soils mixed with 0.1 vol.% magnesium perchlorate showed no observable variations in GWC with the salt-free soils. In theory, the GWC should be higher in the sample containing the salt since the magnesium perchlorate could attract more moisture into the soil since it is hygroscopic. The effect could have possibly been too small to be measurable or the quantity of magnesium perchlorate added to the soils was too small to have any effect on vapour diffusion rates. Therefore, the trapping process induced by the salt was less significate than the effect of vapour concentration in the air.

The TMTUT4 model using the input values in Table 6 was run to replicate the GWC results seen in the experiment. The subsequent values were directly measured/controlled during the experiment and were used as inputs in the model. The period was set at 2 months, the mean surface temperature at -5°C, the geothermal gradient at -23000 Deg./100 m, the soil depth at 12 cm and initial porosity at 33% for the glass beads and at 73% for the JSC Mars-1 soil. Other input parameters not measured during the experiment were obtained from Fisher and Lacelle (2014) since they were found to be suitable averages for normal dry, non-icy, soils. These values included two thermal amplitudes of 1.00E-03°C and 1.30E-04°C, a short period of 2.74E-03 year, a soil thermal diffusivity of 9.5 m^2/year and a minimal initial diffusivity of 630 m^2/yr. A stronger thermal diffusivity was used since the earlier calculated value of 6.9 m^2/year shown in section 2.3.1 had a high degree of uncertainty. This model doesn't take into consideration salts in soil or adsorption water.

The model, shown in Figure 33, provides a descent fit for both soil types but over estimates the GWC in the glass beads by about 0.5%. In the JSC Mars-1 soil the model overestimates its GWC up to the depth of 4 cm and underestimate by 4% the water content in the top portion of the soil.

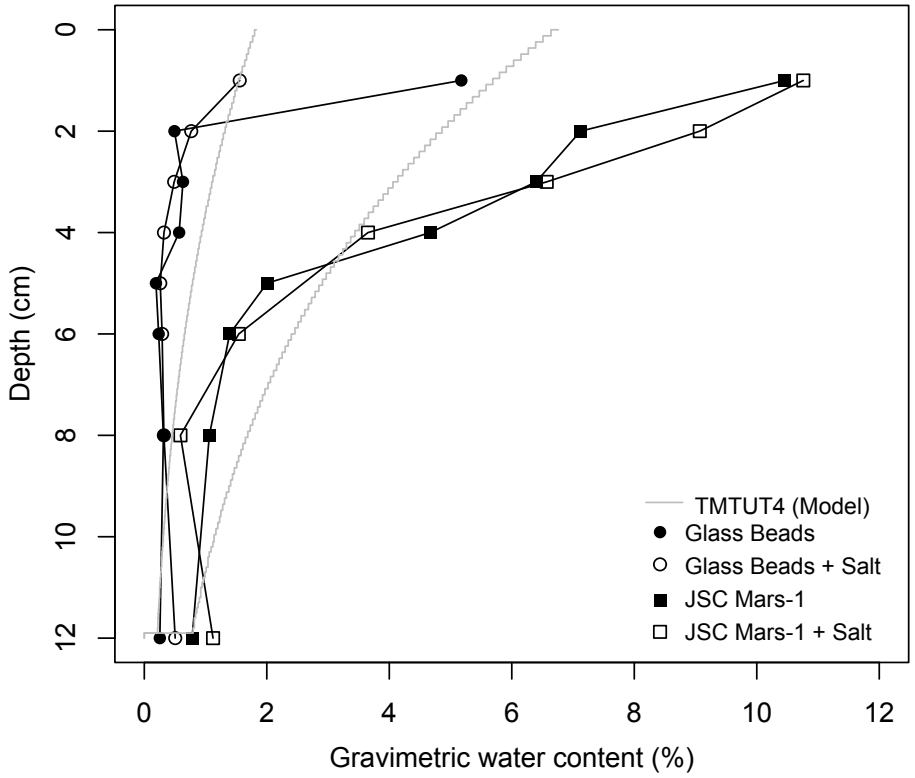

Figure 33. TMTUT4 model using the parameters in Table 6 compared to the experimental GWC values obtained in the second experiment

Table 6. Parameters used for the TMTUT4 model for experiment 2

Parameter	Value
Period (Months)	2
Mean Temperature (°C)	-5
Amplitude 1 (°C)	1.00E-03
Short Period (Year)	2.74E-03
Soil Depth (m)	0.12
Steps (#)	100
Amplitude 2 (°C):	1.30E-04
Geothermal Gradient (Deg./100m)	-23000
Thermal Diffusivity (m^2/yr)	9.50
Minimal Initial Diffusivity (m^2/yr)	630.00
Initial Porosity (%)	33% (Glass Beads) and 73% (JSC Mars-1)

3.4.2 Comparison of GWC with experiment 1

Figure 34 compares the GWC between the two soil types for both experiments. The GWC of the glass beads for the two experiments are almost identical with the exception of the first sample at 1 cm depth. In the JSC Mars-1, the GWC is higher in the top 5 cm of the first experiments and rapidly falls to becomes identical to the second experiment. The difference in GWC between

experiment 2 and 1 for the glass beads are of only 2.38 to -0.02% and becomes more pronounced in the JSC Mars-1 soil between 1.1 to -4.7% GWC. Overall, it appears the air space between the ice and the soil reduced the amount of ice in the soil compared to the first experiment.

The 3 cm air gap between the crushed ice and the soil had a more important impact on the finer grain sized soil. The air gap is a big change in porosity in the soil and moisture will tend to disperse in the open space instead of entering the soil. Therefore, the air gap did not create an evenly distributed relative humid in the air. The air closest to the snow caddy would be near 100% relative humidity and gradually decrease with depth towards top of the soil. Therefore, the relative humidity above the soil in the second experiment was lower than in the first experiment where ice was put directly above the soil.

Another factors that can explain the lower GWC obtained in the second experiment is porosity. The glass beads created a larger change in the porosity between the air (100%) and the soil (33%). The abrupt change in porosity created an area where ice could deposit instead of entering the soil. Evidence of this was shown in Figure 30 were ice covered the majority of the top of the glass beads sample and only about a quarter of the surface of the Mars-1 soil.

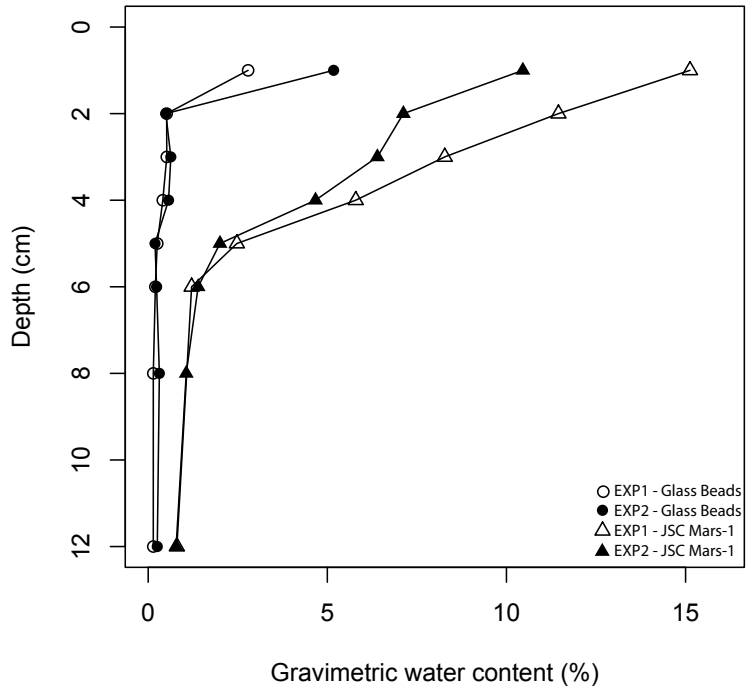

Figure 34. Gravimetric water content from the first and second experiments. Both glass beads and JSC Mars-1 soils are without salts.

3.4.3 Stable water isotopes comparison with experiment 1

The co-isotope plot for both experiments are shown in Figure 35 and show similar patterns in the two experiments. Both the first and second experiments match quite closely in the upper right of the plot which are mostly composed of residual ice samples and quickly diverge passed δD: -90‰ and δ^{18}O: -10‰, when samples are only made of pore ice. The key difference between both experiments is that pore ice measurements of δD-δ^{18}O plot in majority below the GMWL in the first experiment and over the GMWL in the second experiment. As seen in the earlier results, the effect of the salts in the second experiment had slightly further depleted δD and would not be responsible for the samples plotting above the GMWL. Therefore, the 3 cm air gap is likely the reason for such changes due to its unsaturated relative humidity above the soil.

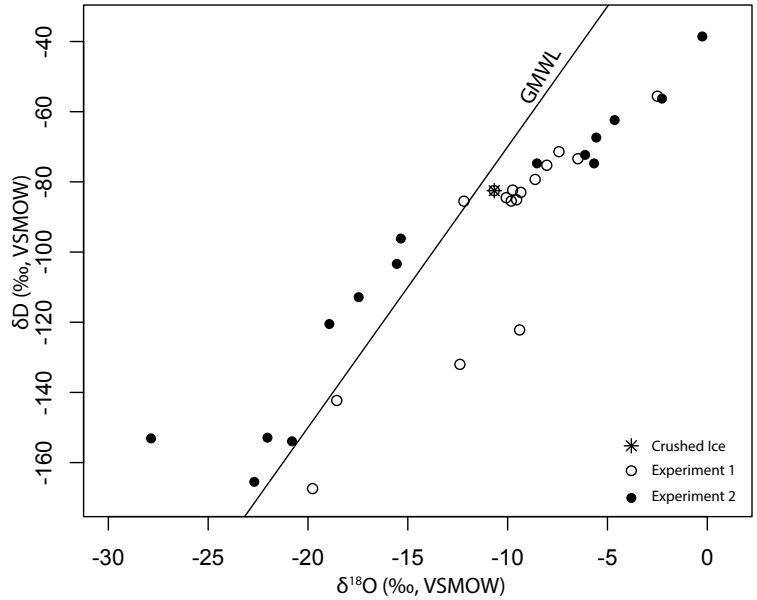

Figure 35. Co-isotope plot for experiment 1 and experiment 2. The start isotopic composition of the crushed ice is shown with an asterisk.

Two stable water isotope models for the pore ice of the second experiment was performed to replicate and explain the results. The first model can be seen in the left side of Figure 36. This COISOTOP2 model was run using the input parameters in Table 7 including the measured top soil temperature of -16°C and bottom temperature of -20°C in a 3 cm thick soil. The temperature at which the phase change shifts from vapour to ice was set at -10°C (Fisher, 1991) and the relative humidity was assumed to be 100%. The soil surface temperature (start temperature) and bottom temperature (end temperature) was measure to be -10°C and -15°C using thermistors in the sample. The initial water vapour isotopes were calculated to be δD: -215‰ and δ^{18}O: -28‰.

The modeled data plots under the GMWL with a slope near 8 but doesn't replicate the results seen. The model starts with a maximum isotopic composition of δD: -84.8‰ and δ^{18}O: -9.7‰ and linearly decreases to a minimum of δD: -147.5‰ and δ^{18}O: -17.3‰.

A second model was then run using a fictional start isotopic composition to try to recreate the measured data. The results of the model show in the right of Figure 36 were obtained using the same values in Table 7 but with a hypothetical initial water vapour concentration of δD: -230‰, δ^{18}O: -30‰ was changed to try to further deplete δD and δ^{18}O. The model is closer to the experimental values but still won't shift the values above the GMWL. The model starts with a maximum isotopic composition of δD: -104.6‰ and δ^{18}O: -12.7‰ and linearly decreases to a minimum of δD: -165.9‰ and δ^{18}O: -20.4‰.

To recreate values over the GMWL a re-sublimation of the source of moisture must occur and this isn't possible using only the COISOTOP2 model. The steps needed to create δD-δ^{18}O values above the GMWL is the following: 1) The initial crushed ice located on the snow caddy, 3 cm above the soil, sublimates; 2) Vapour made by that sublimation will migrate downwards and deposit on the surface of the soil; 3) The newly formed frost on top of the soil will re-sublimate and 4) Vapour from the re-sublimation will enter the soil and deposit into the pores. Through these processes vapour will be shifted above the GMWL and be more depleted in δD-δ^{18}O concentration than the first experiment.

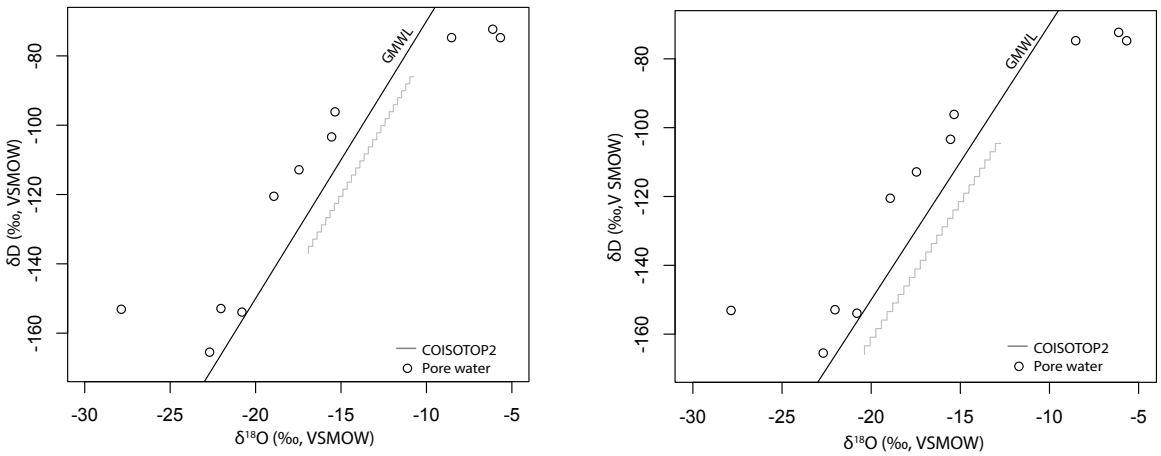

Figure 36. (Left) First COISOTOP2 model for experiment 2 using the input parameters specified in Table 7. (Right) Second COISOTOP2 model for experiment 2 with a hypothetical initial water vapour of δD: -230‰, δ^{18}O: -30‰. Pore water from all the samples in the second experiment were plotted.

Table 7. Input parameters for the first COISOTOP2 model for experiment 2

Parameter	Value
Shift Temperature (°C)	-10
Relative Humidity (%)	100
Start Temperature (°C)	-15
End Temperature (°C)	-20
Steps (#)	25
Headroom Ice δD (‰)	-215
Headroom Ice δ^{18}O (‰)	-28

3.5 Limitations of the experiments

These experiment were the first in this newly built experimental chamber and were perfected through trial and error. Sources of error for these experiments include temperature variations due to icing of the equipment, power outages and position of the samples in the chamber. Many of these parameters effected the stability of the temperature which the samples were subjected but didn't significantly vary the thermal gradient in the soil. Modifications and improvements are highlighted in the last chapter.

3.6 Conclusions

The second experiment produced pore ice from a vapour source made of crushed ice place 3 cm above the soil. Water vapour diffused into the soils for a duration of 2 months in the experimental chamber under a soil thermal gradient of -2.3°C/cm. The impacts of magnesium perchlorate and of a 3 cm air gap between the vapour source and soil has been investigated experimentally. The outcome of the experience shows that a concentration of 0.1 vol.% magnesium perchlorate had no influence on the GWC and helped further deplete δD by -0.8 and -38.1‰. The air gap created a large change in porosity and ice accumulated in that space. GWC was lower in this second experiment due to the unsaturated air gap. The stable water isotopes of the pore ice in the second experiment plotted above the GMWL due to a re-sublimation of the ice.

Chapter 4: Distribution and origin of ground ice in a seasonally frozen beach at Petrie Island, Ottawa (ON)

Introduction

To validate the isotopic signatures and ground ice distribution seen in the previous experiments a 52 cm core sample was taken from Petrie Island in Ottawa on March 3rd 2015 prior to spring thaw. The goal was to investigate the origin of its ground ice to gain insight on ice made by vapour deposition. The ice-cemented core was analyzed for gravimetric water content and stable water isotopes (δD-δ^{18}O).

The 2014-15 winter in Ottawa has been quite cold with an average daily air temperature from December 1st 2014 to March 3rd 2015 of -10.7°C. The site location chosen was on an exposed windy beach located beside the Ottawa River since it offered the best chances in holding vapour diffused ice. Beach sand is the best soil analogue to the McMurdo Dry Valleys, Antarctica since it's made of almost dry medium size sand and is uncovered by vegetation. Therefore, this area during winter offered the best chance of finding vapour diffused ground ice in proximity of Ottawa (ON).

4.1 Study Area

4.1.2 Site location

Petrie Island is located along the Ottawa River 20 km Est of downtown Ottawa, ON (Figure 37). The Ottawa region is characterized by cold humid winter and warm summers (Peel et al., 2007). The mean annual temperature in Ottawa is 10.9°C, with January being the coldest month (average high of -6.1°C and low of -15.3°C) and July being the warmest month (average high of 26.5°C and low of 15.4°C). The total annual precipitation is less than 950 mm with nearly a quarter falling as snow (Environment Canada, 2007). The large beach area on Petrie Island is made in majority of sand and finer material. The soils in the area freezes in winter to depths of ~1 m.

Figure 37. Coring site location on Petrie Island, Ottawa (ON) (Google Earth, 2015)

4.2 Winter 2014-2015 climate in Ottawa

The 2014-15 winter in Ottawa has been quite cold. Climate data was obtained from the weather station located at the Canada's Agriculture and Food Museum (45.38°N, 75.72°W) managed by Environment Canada (2015). In relation to the coring of date of March 3rd 2015, daily winter air temperature can be seen in Figure 38. The average daily air temperature from December 1st 2014 to March 3rd 2015 was -10.7°C, the minimum was -22.9°C and the maximum was 4.5°C. From January 20th to March 3rd, the daily maximum temperature never went above 0°C and the average temperature was -15.1°C. The total precipitation in between January 1st and February 1st was 89 mm of rain and 120 cm of snow. Thus, the ground protected by a thin layer of compacted snow < 10 cm did not melt prior to coring.

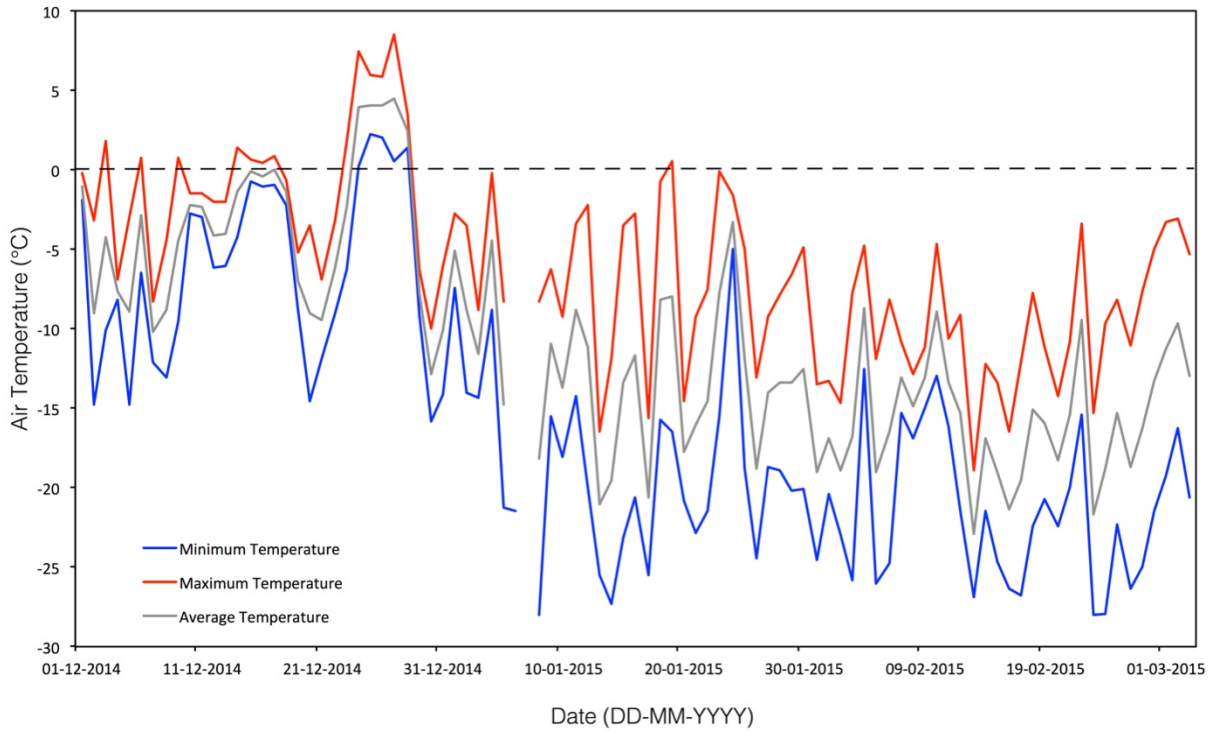

Figure 38. Air temperature in Ottawa (ON) from December 1st 2014 to March 3rd 2015. (Data: Environment Canada, 2015) The core sample were taken on March 3rd 2015.

4.3 Methodology

4.3.1 Field sampling

The ice-cemented beach was sampled on March 3rd 2015 at Petrie Island using a Cold Region Research Engineering Laboratory (CRREL) barrel, made of a hollow stainless steel barrel with welded double helix flight configuration and tungsten-carbide teeth. The core extracted was 52 cm in length, 7.5 cm in width and was overlain by an uneven 5-10 cm thick layer of hard packed snow (Figure 39). The frozen core was sectioned in 2-3 cm thick pucks in the CryoLab for Arctic, Antarctic and Planetary Studies (CLAAPS) at University of Ottawa and transferred in polyethylene bags for thawing. The thawed samples were afterwards transferred in sealed 50 ml conical centrifuge tubes for storage until analysis.

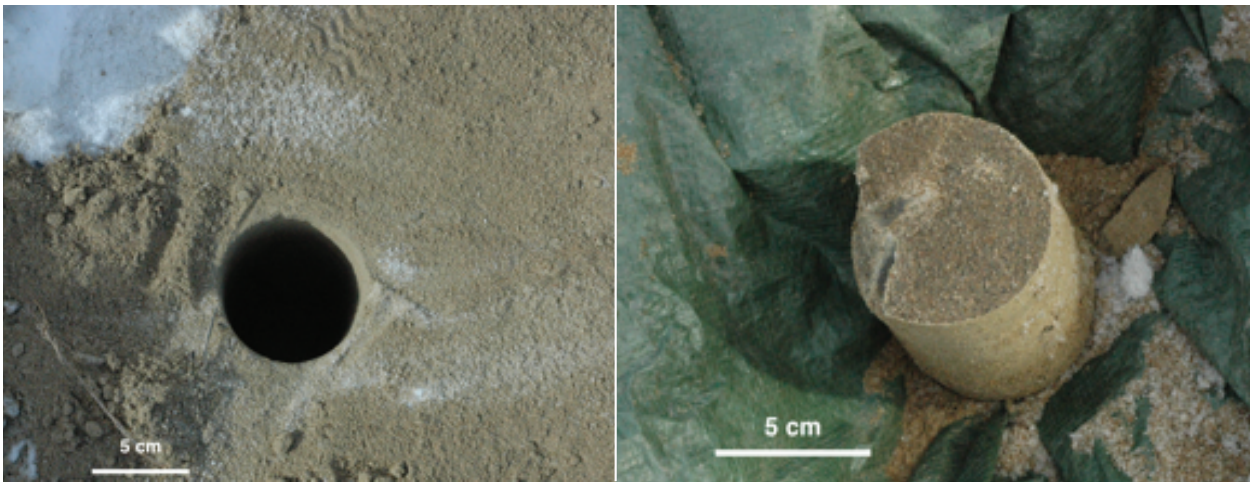

Figure 39. (Left) Picture of the core hole and (Right) section of the 52 cm core sample taken at Petrie Island, Ottawa, ON

4.3.2. Local meteoric water line for Ottawa

Data was taken from the Global Network of Isotopes in Precipitation (GNIP) database from the International Atomic Energy Agency website (IAEA/WMO, 2015) to reconstruct the local meteoric water line (LMWL) for Ottawa. The water isotope for Ottawa data was collected by the Environmental Isotope Laboratory (University of Waterloo) for the past 25 years and the last complete year (2011) was taken to create the LMWL for Ottawa.

4.3.3 Laboratory analysis

Samples were subdivided to measure their gravimetric water content and for pore water extraction. The gravimetric water content of the samples was determined using the van Everdingen (1998) equation and the same methods explained earlier in section 2.2. The remaining dried soils were weighed and their volume measured using a glass graduated cylinder to determine its bulk density. Afterwards, DI water was added in to a graduated cylinder until the soils reached saturation and were weighed to determine the soil's porosity. Soil samples were examined under a microscope to determine its grain size distribution.

Water from the samples was extracted using a vacuum distillation method at the Advanced Research Complex, University of Ottawa. This extraction method consists in creating a vacuum in glass pipes and heating the sample to remove all pore water. For a full explanation of the procedure see section 2.2. Extracted pore water was sent for $^{18}O/^{16}O$ and D/H analysis at the G.G. Hatch Stable Isotope Laboratory in Department of Earth Sciences, University of Ottawa. The

$^{18}O/^{16}O$ and D/H ratios were determined using a Los Gatos Research (LGR) high precision liquid water analyzer coupled to a CTC LC-PAL auto-sampler. Results are shown with the δ-notation ($\delta^{18}O$ and δD), where δ represents the parts per thousand differences between $^{18}O/^{16}O$ or D/H and reported to the Vienna Standard Mean Ocean Water (VSMOW). The analytical reproducibility for $\delta^{18}O$ and δD is ± 0.1‰ and ± 0.5‰, respectively.

4.4 Results

4.4.1 Regional meteoric δD-δ^{18}O values for Ottawa

The local meteoric stable isotopes (δD-$\delta^{18}O$) values for Ottawa vary throughout the year due to changing atmospheric temperatures. The LMWL for Ottawa can be seen in Figure 40, it has a slope of 8.1 and an intercept of 12.0 ($\delta D = 8.1\delta^{18}O + 12.0$, r^2=0.98, p-value= < 0.05). The isotopic values are the lowest in January ($\delta^{18}O$: -21.58‰, δD: -159.05‰) and highest in May ($\delta^{18}O$: -4.82‰, δD: -26.46‰). The average isotopic values for rain was $\delta^{18}O$: -7.99‰, δD: -52.17‰ and for snow $\delta^{18}O$: -16.72‰, δD: -123.19‰.

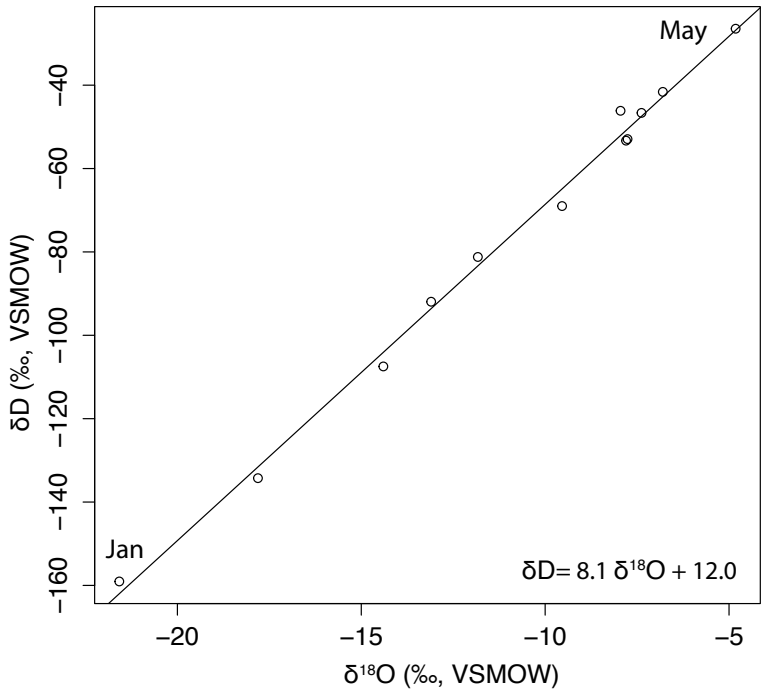

Figure 40. Local meteoric water line of Ottawa (ON) for 2011
(Data from IAEA/WMO, 2015)

4.4.2 Physical properties, gravimetric water content and stable isotopes of water

The stratigraphy at the coring site consisted of 5-10 cm of snow above a 1 cm layer of dry and loose sand protecting the underlying ice-cemented sediments. The sediments on the beach is made in majority of medium size sand with some silt particles with a bulk density of 1.65 g/cm^3 and a low porosity of 29.3%. The ice-cemented sand had a structureless cryostructure throughout the entire core length according to the Murton and French's (1994) cryostructural classification.

Figure 41A shows a the GWC profile in the core. The GWC in the core varied between 3.6 to 16.7%. From 0 to 30 cm depth, the GWC decrease from 12 to 3.6% and had an average GWC of 6.94% with a standard deviation of 3.2%. Below that depth, the GWC rapidly increases to 16.7% until 33 cm and remains near 15% GWC for the remaining of the core. The bottom portion of the core (30-52 cm) has an average GWC of 14.52% with a standard deviation of 2.4%.

The δD profile in Figure 41B shows deuterium down to -107.6‰ in the upper section of the core and increase with depth up to a maximum of -78.7‰. Figure 41C shows the δ^{18}O profile in the core. The δ^{18}O values vary between -11.15‰ and -14.8‰. In the top 30 cm of the core, δ^{18}O and δD values averaged -13.2‰ SD: 0.7‰ and -98.2‰ SD: 4.8‰ and beneath that depth averaged -12.4‰ SD: 0.9‰ and -89.4‰ SD: 7.8‰, respectively.

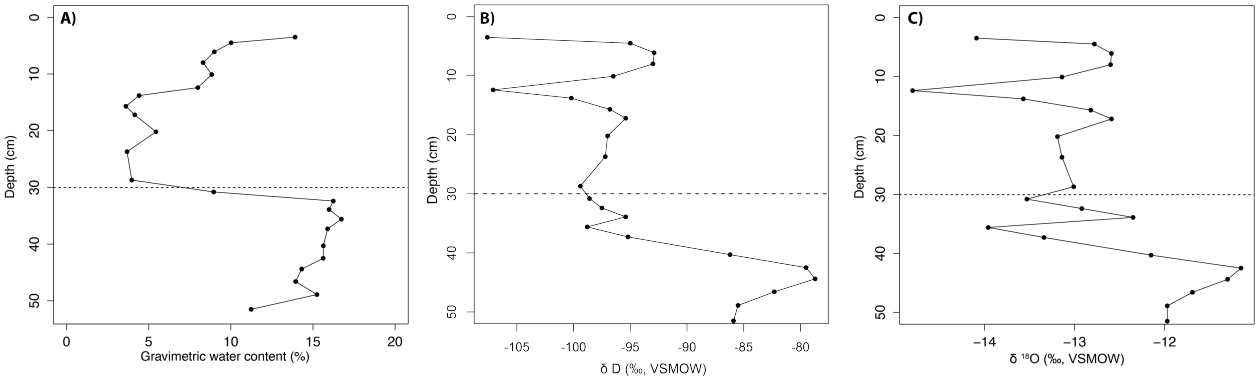

Figure 41. A) Gravimetric water content, B) δD depth profile and C) δ^{18}O depth profile for the core taken from Petrie Island, Ottawa (ON). The dotted line represents the depth that separates the two types of frozen ground.

In a δD-δ^{18}O diagram, most of the sample plot near the GMWL (Figure 42). The δD and δ^{18}O between 0-30 cm depth plot more often below the line and the remaining portion of the core

plot on or very close to the GMWL. The uppermost section of the core (0-29 cm) has a slope of 6.7 with the following equation $\delta D = 6.7\delta^{18}O - 9.7$ ($r^2 = 0.88$, p-value= < 0.05) and the lower section (30 - 52 cm) has a slope of 7.9 with the following equation $\delta D = 7.9\delta^{18}O + 8.3$ ($r^2 = 0.88$, p-value= < 0.05).

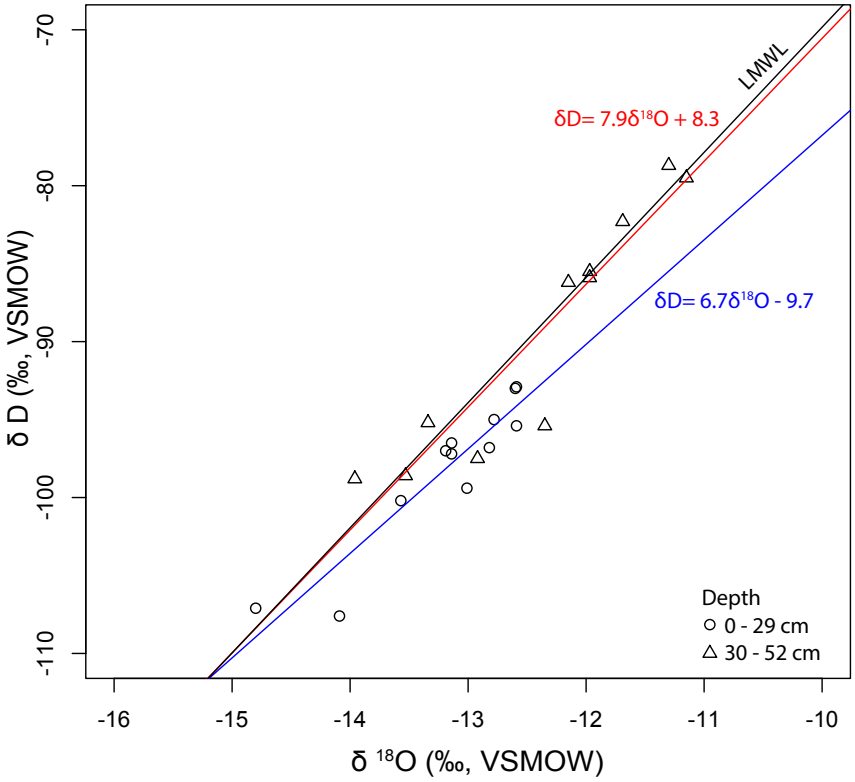

Figure 42. Co-isotope plot for the core taken at Petrie Island, Ottawa (ON). Regression lines for 0-29 cm: $\delta D = 6.7\delta^{18}O - 9.7$ ($r^2 = 0.88$, p-value= < 0.05) and 30-52 cm: $\delta D = 7.9\delta^{18}O + 8.3$ ($r^2 = 0.88$, p-value= < 0.05). LMWL: $\delta D = 8.1\delta^{18}O + 12.0$

4.5 Discussion

The origin of the pore ice in the core comes from a variety of sources. It is therefore important to identify all the possible sources of moisture. It is possible to identify an origin of the pore ice by identifying the sources of moisture by analyzing stable water isotopic signatures.

4.5.1 Origin of the pore ice

For ice to aggrade in the seasonally frozen grounds a source of moisture must be present. Petrie Island is on a man made beach environment with four main sources of moisture in the winter: i) interstitial pore moisture, ii) water table, iii) overlying snow and iv) rain.

The sand isn't dry in the beginning of winter and interstitial pore moisture is present due to rain during the fall season. The water table on the coring site would be near 0.5 to 1 m below the surface since the site was only 20 m away from the Ottawa River. Moisture from the water table would move upwards into the soil and increase its water content. Precipitations in the form of snow can accumulate on top of the soil and can either sublimate or melt into soil. Rain can cause the snow to melt and enter into the soil.

Isotopic values obtained in the seasonally frozen soil were plotted alongside Ottawa's rain and snow averages to determine the sources of moisture of the samples (Figure 43). The uppermost layer of pore ice resembles mostly mean isotopic snow values and the lower layer of ice between 30 to 52 cm resemble more the mean isotopic rain values. Due to their similar isotopic composition it possible they would be the major source of water by which the pore ice in the two sections are formed. Therefore, the lower section of the core would be made in majority by rain water infiltrated by water coming from the Ottawa River.

Furthermore, the δD-$\delta^{18}O$ slope in the uppermost layer is 6.7 ($\delta D = 6.7\delta^{18}O - 9.7$ ($r^2 = 0.88$, p-value= < 0.05) and is within the maximum theoretical freezing slope of 7.3 (Lacelle, 2011). This would indicate that the majority of the water was created by freezing of the pore water in a finite reservoir. The lower section of the core has a slope of 7.9 with the following equation $\delta D = 7.9\delta^{18}O + 8.3$ ($r^2 = 0.88$, p-value= < 0.05) and would be typical of an open system. Ice creating by freezing water with slopes > 7 has been documented in literature. Mackay (1990) found a co-isotope slope of 7.2 for ice in an intrusive pingo with the initial source of water was ground-water below a drained lake. Ingólfsson and Lokrantz (2003), found massive ground ice with a co-isotope slope of 7.5 suggesting a glacial origin. Therefore, it is reasonable to consider the lower section of the core (30-52 cm) is below the ground water table, a large open system, and no fractionation occurred.

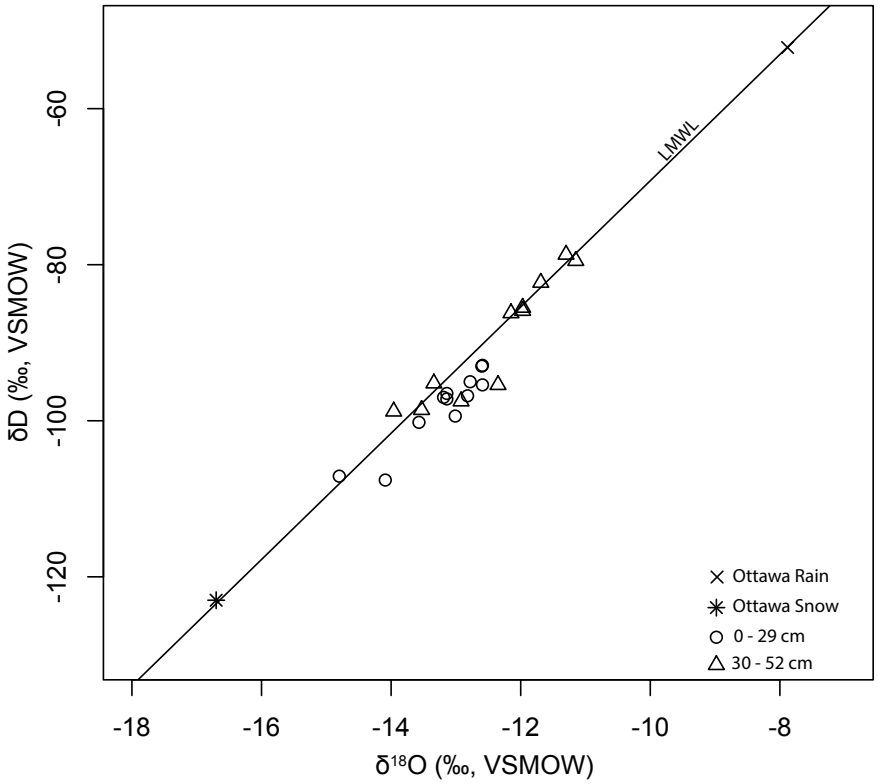

Figure 43. Stable water isotopes of Petrie Island core with Ottawa's rain and snow average values. LMWL: $\delta D = 8.1\delta^{18}O + 12.0$

Stable water isotopes models using COISOTOP2 for a core made purely by vapour deposition using the input values in Table 8 is shown in Figure 44. The mean winter air temperature of -10°C was used as an input in the model with a thermal gradient of 4°C/cm. The start isotopic composition chosen for the model is the Ottawa River average values $\delta^{18}O$: -10.7‰ and δD: -81.2‰ (Telmer and Veizer, 2000) since in seasonally frozen ground the vapour flux would be from the bottom towards to surface of the soil and not from the above snowpack as would have been indicated by the resembling snow values for Ottawa. The water vapour isotopes for the Ottawa River were calculated to be δD: -174‰ and $\delta^{18}O$: -2.22‰. The temperature at which the phase change shifts from vapour to ice was set at -10°C (Fisher, 1991) and the relative humidity was assumed to be 100%.

The model plots below the LMWL with a slope of 8.6 ($\delta D = 8.6\delta^{18}O + 10.39$, $r^2=1$, p-value < 0.05). The $\delta^{18}O$-δD values found in the core would rather indicate the soil isn't completely made of vapour ice since the concentration in $\delta^{18}O$ and δD from the model are much lower. It is

possible that only a fraction of the pore water in the soil was made by deposition since the upper-most section of the model is near the pore water sample. This would validate that the pore water is made of a mixture of interstitial water accumulated prior to freezing and vapour diffusion ice.

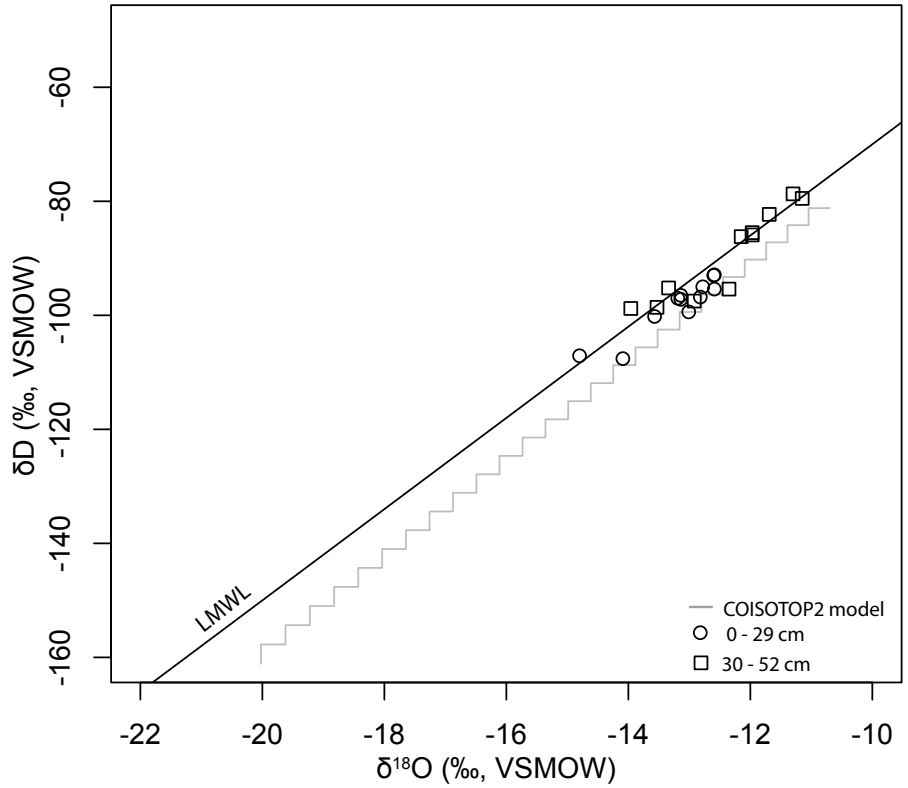

Figure 44. Stable water isotopes model using COISOTOP2 for seasonally frozen core made purely by vapour deposition compared to the core taken at Petrie Island, Ottawa. LMWL: $\delta D = 8.1\delta^{18}O + 12.0$

Table 8. Input parameters in COISOTOP2 model for the Petrie Island Core

Parameter	Value
Shift Temperature (°C)	-10
Relative Humidity (%)	100
Start Temperature (°C)	0
End Temperature (°C)	-10
Steps (#)	25
River water δD (‰)	-81.2
River water δ^{18}O (‰)	-10.7
Source Vapour δD (‰)	-174.0
Source Vapour δ^{18}O (‰)	-22.2

4.5.2 Growth of pore ice

To further understand how vapour ice can be formed in a seasonally frozen grounds a vapour ice growth model, TMTUT4, was run using input parameters in Table 9. These parameters include a soil surface temperature of -10°C (mean winter air temperature for Ottawa). A dry soil column of 30 cm with a thermal gradient of 0.30°C/cm. This means that in a soil column of 30 cm would have a top temperature of -10°C and a bottom temperature of 0°C. The period was set at 3 months, initial porosity of 29.3% for the beach soil. Other input parameters not measured were obtained from Fisher and Lacelle (2014) since they were found to be suitable averages for normal non-icy soils. These values included two thermal amplitudes of 1.00E-03°C and 1.30E-04°C, a short period of 2.74E-03 year, a soil thermal diffusivity of 9.5 m^2/year and a minimal initial diffusivity of 630.00 m^2/yr.

Table 9. Parameters used for the TMTUT4 model for the core taken at Petrie Island

Parameter	Value
Period (Months)	3
Mean Temperature (°C)	-10
Amplitude 1 (°C)	1.00E-03
Short Period (Year)	2.74E-03
Soil Depth (m)	0.30
Steps (#)	100
Amplitude 2 (°C):	1.30E-04
Geothermal Gradient (Deg./100m)	3000
Thermal Diffusivity (m^2/yr)	9.50
Minimal Initial Diffusivity (m^2/yr)	630.00
Initial Porosity (%)	29.3

The results indicated that less than 0.09% GWC (Figure 45) would have been made purely by vapour diffusion and would have an almost linear relationship between GWC and depth. This isn't indicative of vapour diffused ice and would not have been detected in the soil. Therefore, the soil most likely contained some water prior to freezing and are not only made by vapour.

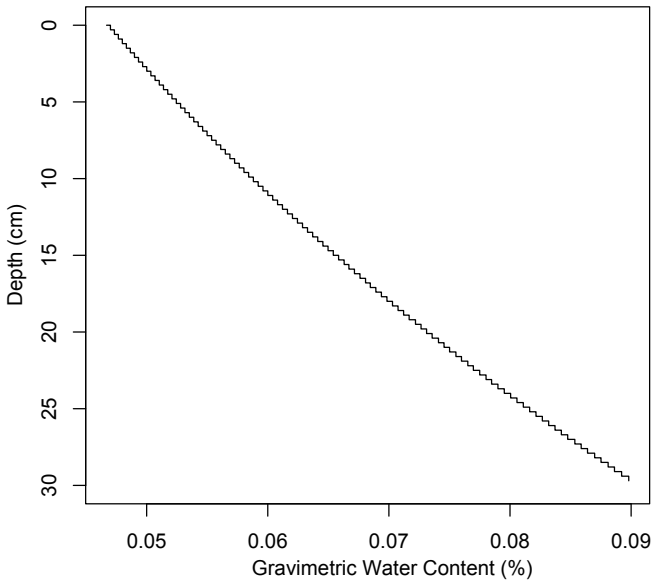

Figure 45. TMTUT4 model of Gravimetric water content for the upper portion (0-29 cm) of the core taken at Petrie Island, Ottawa (ON)

To increase the soil ice content a stronger thermal gradient is needed since the time period can't be extended. The soil was most likely moist to start and a freezing front smaller 30 cm could slowly advance from top down. A progressive freezing front would create a stronger thermal gradient in the soil and increase vapour ice production. This seasonal transient ice table could start at the top of the soil and move downwards. The freezing front can be sustained in the soil column due to the latent heat released due to condensing and freezing of water. Therefore, it is possible to create a strong thermal gradient in a smaller soil column.

A TMTUT4 model was run for a freezing front with a thickness of 2.5 cm with a top temperature of -10°C and bottom temperature of 0°C. The model was run using the same parameters specified earlier in Table 10 but this time the geothermal gradient was set to 4°C/cm. Results indicate that this model would be able to create GWC from 6.7 to 12.9% in a period of 3 months. Another model was performed for a thicker freezing front of 5 cm and using the same parameters specified in Table 10 and changing the geothermal gradient to 2°C/cm. The models show that the GWC in the soil after 3 months would between 1.68 to 3.2%. Therefore, it is possible that a portion of the upper section (0 – 29 cm) would be created by vapour diffusion/deposition and the remaining water would come from the in place interstitial pore moisture accumulated prior to freezing. This scenario with the 5 cm freezing front would be the

best fit to explain that part of the ice in the core would be due to vapour and more than half of the ice would have been made by freezing of interstitial pore water by a advancing freezing front.

Beyond 30 cm in depth, the soil is near saturation and has no pore space for vapour to diffuse into. When the freezing front approaches the 30 cm depth interstitial pore water freezes with a homogenized GWC of 14.5%, which is significantly lower than the upper portion with an average of only 6.9%.

4.6 Conclusion

Pore ice from soils taken at Petrie Island, Ottawa (ON) is made from various sources of water and can be distinguished using stable water isotopes to understand their complex evolution. In summary, unfrozen pore water from rain events in the fall would progressively freeze when a shallow 2.5 cm to 5 cm freezing front enters the soil and create the majority of the GWC of the soil. Afterwards, vapour and melt water from the overlying snowpack can enter the soil. This explains why the section is slightly more depleted in δD and is dryer than the lower section. Below 30 cm, the pores are nearly completely filled by in situ ground water and do not allow vapour ice to form.

Chapter 5: Review of growth of vapour deposited ice and associated δD-δ^{18}O trends

Summary

Ice originating from vapour deposition can be created in five distinct environments: in the atmosphere, at the surface, in caves, in seasonally frozen grounds and in permafrost. Theoretically, stable water isotopes of vapour deposited ice plot along the GMWL with a slope of ~8.6 and are often shifted below and even sometimes above the GMWL. This distinct isotopic signature of vapour derived ice can be used to differentiate vapour made by vapour from ice made by freezing. Ice samples that plot with a slope of < 7.3 would originate from freezing of liquid water and slopes > 7.3 would indicated ice formed by vapour. Another possible indication of vapour deposited ice in soils is a pore ice content profile with a concave downwards shape.

5.1 Ice content and profile of vapour deposited ice in cryotic soils

Pore ice content profiles made by vapour deposition have a typical concave downward shaped GWC profile associated to them as seen in the past two experiments and in the uppermost portion (0-29 cm) of the soil at Petrie Island, Ottawa (ON). The top section of the soil will have the most amount of ice and decreases exponentially with depth as seen in the first experiment (Figure 46). Afterwards, the ice content will slowly decrease or stabilize at a certain ice content due to changes in vapour saturation in the soil. As seen in section 2.4.1 the concave downwards shape is attributed to the amount of moisture in soils. The saturation vapour pressure (ei) curve in Equation [15] shows an exponential relation between vapour and temperature. Air at lower temperature can't contain as much moisture as warmer air.

In a natural setting, it is possible that the upper-most portion of the soil be nearly dry. This has been observed in perennially cryotic zone in the MDV (Figure 46). The first few cm of soil is classified as dry permafrost containing less than 3 wt. % ice content and protects the ice-table.

Compared to the experiments, places such as the perennially cryotic zones of the MDV had lots of time to form ice by vapour and therefore would contains more ice. The time it takes to fill

the pores depend on the physical and thermal properties of the soil such as their thermal diffusivity, thermal conductivity, heat capacity, and porosity. These soil properties will dictate how well energy from the air can influence the soil below and the strength of the thermal gradient. The higher the thermal gradient the more ice will aggrade in a shorter time period.

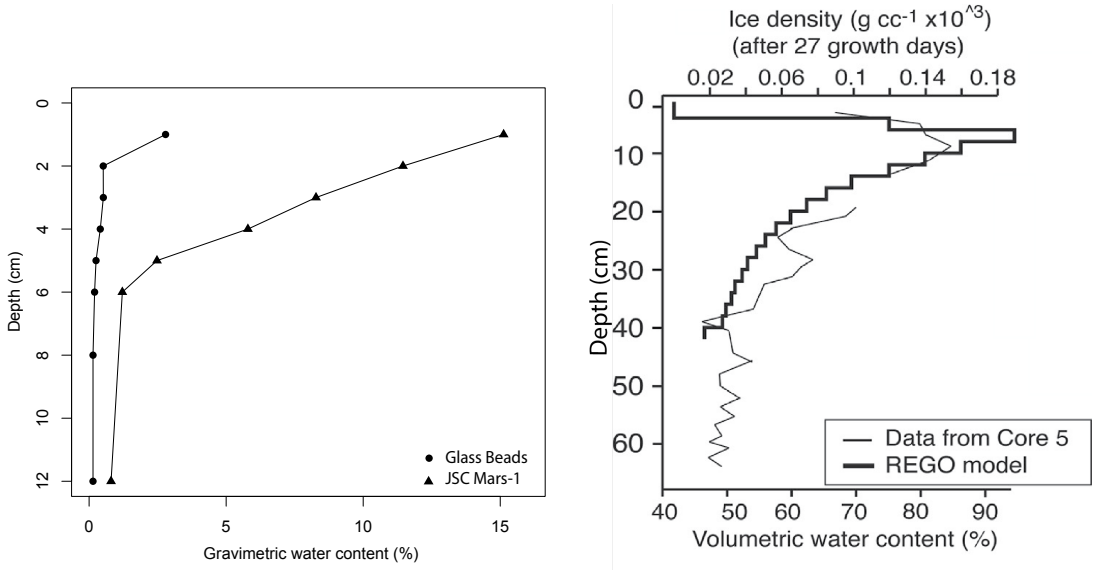

Figure 46. (Left) Gravimetric water content from the first experiment. (Right) volumetric water content from a core taken in the perennially cryotic zone of University Valley, Antarctica (Lacelle et al., 2013).

Similar results have been found by experiments made by Hudson et al. (2009) under Martian temperature (193 to 268K) and pressure (600 Pa). Pore ice densities for their experiments are shown in Figure 47. The experiments conducted over a period of > 72 hrs in length have similar patterns to the ones found by this thesis. Pore ice densities are high at the top of the sediments, quickly decrease up to a depth of ~0.04 m from the base and slowly converged near 0 kg/m^3 at the bottom. Hudson et al., (2009) found that low humidity or short-duration (< 72 hrs) experiments produce an ice table depth beneath an ice-free layer. Longer duration (> 72 hrs) experiments and higher vapor densities, produced stable surface ice similar to the one in this thesis. They concluded that ice contents in the soil formed by vapour deposition have a concave downwards shape due to the saturation vapour pressure. They also found that the ice table has a sharp interface located underneath a small layer of dry sediments and that diffusion rate decrease with time due to ice crystals growth in the available pore space.

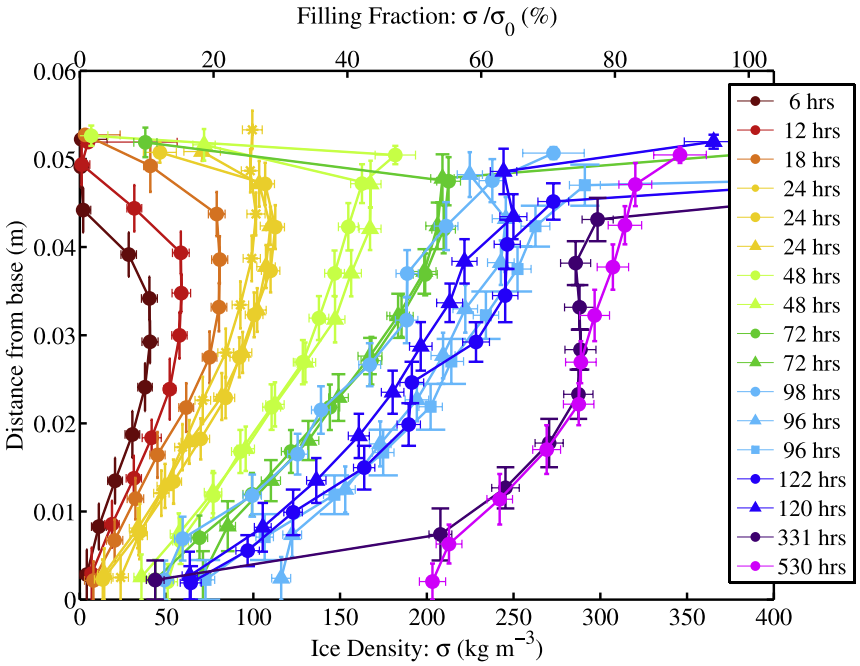

Figure 47. Ice density of vapour deposited pore ice in a 5 cm soil column for various length of time (6 hrs to 530 hrs). The ice was developed during a series of experiments performed under Martian conditions by Hudson et al., 2009.

5.2 δD-δ^{18}O profiles and trends of vapour deposited ice in cryotic soils

A residual snowpack over soil in a closed system will have a stable isotopes depth profiles with an almost vertical concave downwards shape. The δD and δ^{18}O depth profiles for the underlying soil pore ice below the residual snowpack will have linear shape (Figure 48). The snowpack would be enriched in heavier water isotopes at its surface and decrease in composition with depth due to sublimation. The upper portion of the soil can be slightly more enriched in its upper portion and quickly deplete in δD and δ^{18}O with depth. In soils, isotopes rapidly fractionate with depth due to phase changes from vapour to ice. As the ice forms further into the soil it has a lower concentration in δD and δ^{18}O, and this produces a linear relationship with depth. Further depletion with depth will occur until vapour interact with a lower source of ice (Lacelle et al., 2013). The lower source ice can diffuse in the above vapour deposited ice and modify its isotopic composition.

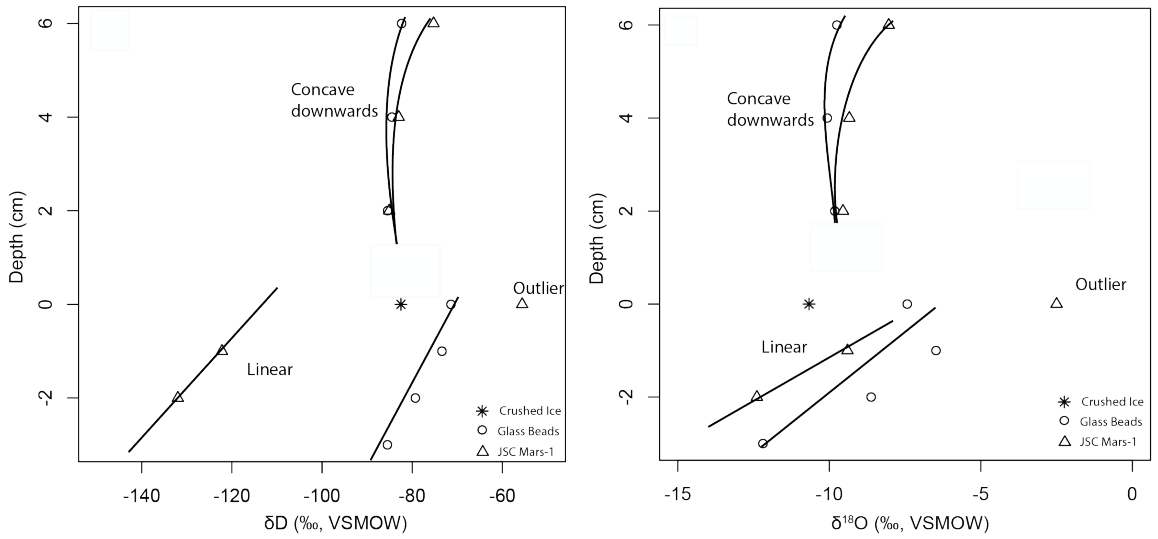

Figure 48. (Left) δD and (Right) δ^{18}O soil depth profiles for the first experiment after the two-month growth period.

Various types of ice formed by vapour have been plotted along the GMWL in Figure 49 and their slope values can be seen in Table 10. The samples come from pore ice in the first and second experiment, from seasonally frozen grounds located at Petrie Island in Ottawa (ON) and from permafrost found in University Valley, Antarctica (Lacelle et al., 2013). Unpublished pipkrake samples taken near Gatineau (QC) were obtained from Clark et al. (unpublished data). Snow values for DEC-FEB 2011 in Ottawa were obtained from (IAEA/WMO, 2015). Massive ice blockages from two cave in northern Yukon were obtained from Lauriol and Clark (1993). Cave hoar frost samples were taken by Lacelle et al. (2009) and Yonge et al. (1999).

Pore ice samples have a wider distribution range than the other types of ice and plot further from the GMWL with a similar slope. Samples from the first and second experiment performed for this thesis have a slope of 6.8 (r^2= 0.38, p-value= 0.034) and 4.6 (r^2= 0.87, p-value= < 0.01), respectively. Samples from the upper portion of Petrie Island plot with a slope of 6.7 (r^2= 0.88, p-value= < 0.01) since its pore ice originate from both liquid and vapour water. The core from a seasonally cryotic soil in the MDV has an overall slope of 10.9 (r^2= 0.83, p-value= < 0.01) but can be further divided into three sections with distinct slopes. The upper portion (first 6 cm) of the core with a slope of -0.2 (r^2= 0.004), the middle portion (6 – 32 cm) has a slope of 7.6 (r^2= 0.88) and the lower section (< 32 cm) has a slope of -0.05 (r^2= 0.002). The slope in the upper

portion and is near 0 since would be due to adsorption and the lower portion have a slope near null since the ice reached the set lower boundary value by diffusion (Lacelle al., 2013).

Pipkrakes samples plot both above and below the GMWL with a slope of 1.1 (r^2= 0.17, p-value= < 0.01) and vary more in δD than in δ^{18}O. These could be explained by calculation the the ratio of the diffusion fractionation factors ($\alpha_{Diffusion}D/\alpha_{Diffusion}{}^{18}O$ = 1.0166/1.0323 = 0.98) if completely made by vapour (Clark and Fritz, 1997).

Ottawa snow sample fall as expected on the GMWL and vary depending on air temperatures. Massive ice blockages plot above and below the GMWL with a slope of 7.2 (r^2= 0.99, p-value= 0.033) which are made by vapour entering the cave in summer and depositing on the freezing cave walls. Hoar ice in caves plot above and below the GMWL depending on the source of moisture with a slope of 8.5 (r^2= 0.90, p-value= < 0.01).

In summary, ice made by vapour will have a slope near 8 and the majority of the time plot below the GMWL but can be shifted above if the vapour source comes frost re-evaporation. This can occur in cave environments or in an air pocket where air is re-evaporated. A summary plot of the theoretical freezing and deposition line along side the GMWL can be seen in Figure 50. An evaporation-condensation line was added to illustrate the possibility of water re-evaporation which would give values above the GMWL.

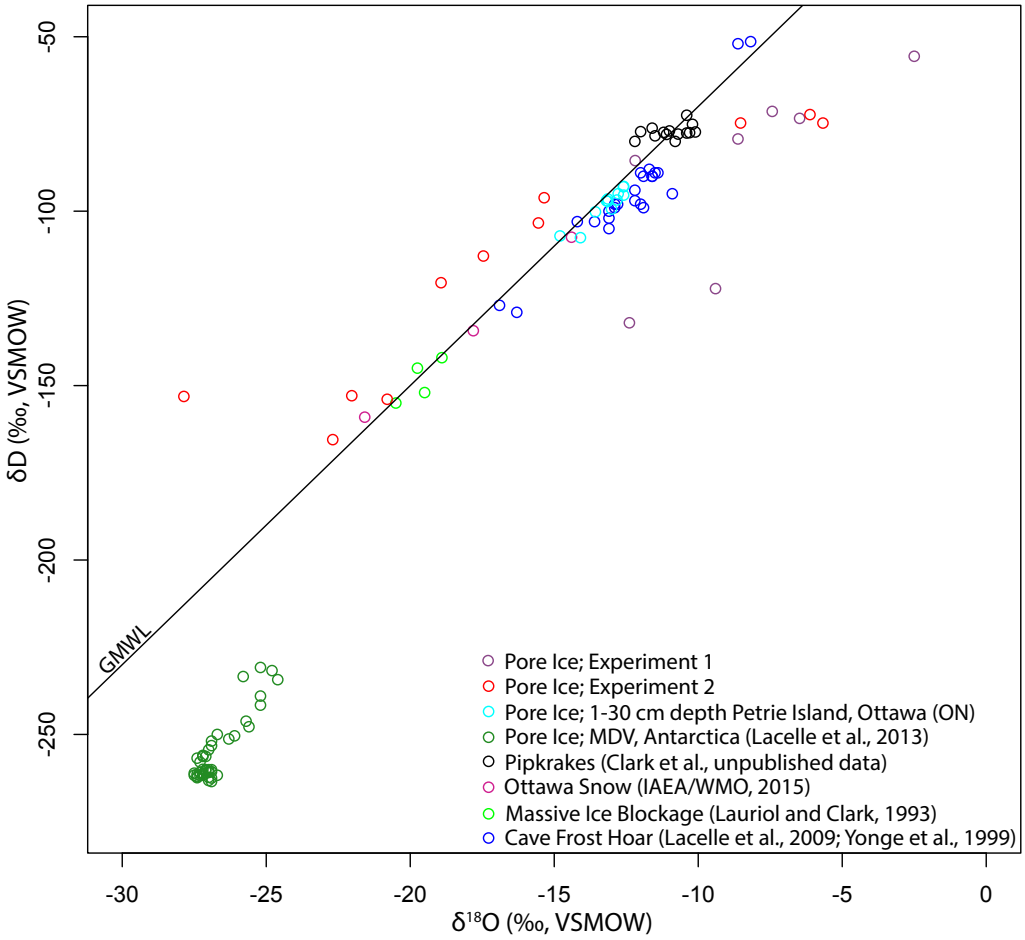

Figure 49. Summary plot of different types of ice made by vapour deposition placed alongside the GMWL. Pore ice samples shown are for from the first experiment, the second experiment, Petrie Island, Ottawa (ON) and from University Valley, Antarctica (Lacelle et al., 2013). Pipkrake data was obtained from Clark et al. (unpublished data). Snow values for DEC-FEB 2011 in Ottawa were obtained from (IAEA/WMO, 2015). Massive ice blockages from two cave in northern Yukon were obtained from Lauriol and Clark (1993). Cave hoar frost samples were taken by Lacelle et al. (2009) and Yonge et al. (1999).

Table 10. Slope of different types of ice made by vapour

Samples	Slope	r^2	p-value
Pore Ice; Experiment 1	6.8	0.38	0.034
Pore Ice; Experiment 2	4.9	0.81	< 0.01
Pore Ice; 1-30 cm depth Petrie Island, Ottawa (ON)	6.7	0.88	< 0.01
Pore Ice; MDV, Antarctica (Lacelle et al., 2013)	10.9	0.83	< 0.01
Pipkrakes (Clark et al., unpublished data)	1.1	0.17	0.147
Ottawa Snow (IAEA/WMO, 2015)	7.2	0.99	0.033
Massive Ice Blockage (Lauriol and Clark, 1993)	7.2	0.63	0.203
Cave Hoar frost (Lacelle et al., 2009; Yonge et al., 1999)	8.5	0.90	< 0.01

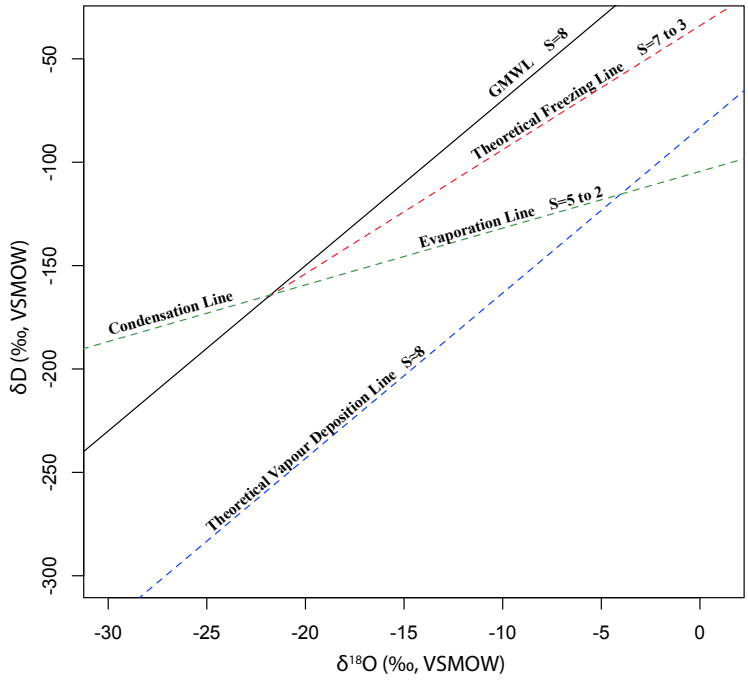

Figure 50. Theoretical depositional and freezing line for water. Freezing occurs at a slope between 7 and 3. Vapour ice will deposit on a surface with a slope near 8. Evaporation and condensation line was placed to illustrate how values could be located above the GMWL.

5.3 Designing the perfect experiment

The next experiments should focus on creating more ground ice to ensure more samples at lower depths can be analyzed. To create more ice in the least amount of time, the source of moisture needs to be placed directly over the sediments. The soil should be made of a finer sand sized glass beads of ~0.25 mm to increase porosity but not too small that it creates problems during pore water extraction. Furthermore, it would be more efficient to set the environmental chamber to 0°C instead of -5°C to create a steeper temperature gradient in the soil. With this modification, the thermal gradient in the soil would increase to -3.1°C/cm. Using the smaller glass beads and this stronger thermal gradient it would take 4 months to produce enough ice to analyze the δD-δ^{18}O content of the full 12 cm thick sample. A sample with magnesium perchlorate at 0.2 vol.% and another at 0.5 vol.% would be useful to see at which point perchlorate has an effect on diffusion rates in the soil. Other modifications such adding more insulation on cooling plates inside the chamber and a dehumidifier would help reduce icing on the equipment.

Appendix A

Examples of numerical model outputs:

TMTUT4 MODEL

INPUT VALUES

PERIOD (Year): 0.170

MEAN TEMP (K): 268.00

AMPLITUDE 1 (K): 1.00E-03

SHORT PERIOD (Year): 2.74E-03

AMPLITUDE 2 (K): 1.30E-04

GEOTHERMAL GRAD. (DEG/100M): -32000.00

DIFUST THERMAL (M^2/a): 9.50

INITIAL DISFUSMIN (M^2/a): 630.00

START POROSITY: 0.33

Table A.1. Output Values for TMTUT4 Model

DEPTH (M)	AVEGRAD (DEG/M)	AVEGRAD-VAP (KG/M^4)	DICE/RUN (KG/M^3)	DIFFUSM (M^2/a)	POROSITY (%)
0.00E+00	-3.20E+02	-8.48E-02	7.01E+01	6.30E+02	2.53E-01
1.20E-03	-3.20E+02	-8.24E-02	6.84E+01	6.30E+02	2.55E-01
2.40E-03	-3.20E+02	-8.01E-02	6.67E+01	6.30E+02	2.57E-01
3.60E-03	-3.20E+02	-7.78E-02	6.50E+01	6.30E+02	2.59E-01
4.80E-03	-3.20E+02	-7.56E-02	6.33E+01	6.30E+02	2.61E-01
6.00E-03	-3.20E+02	-7.35E-02	6.17E+01	6.30E+02	2.63E-01
7.20E-03	-3.20E+02	-7.14E-02	6.01E+01	6.30E+02	2.64E-01
8.40E-03	-3.20E+02	-6.94E-02	5.86E+01	6.30E+02	2.66E-01
9.60E-03	-3.20E+02	-6.74E-02	5.71E+01	6.30E+02	2.68E-01
1.08E-02	-3.20E+02	-6.54E-02	5.56E+01	6.30E+02	2.69E-01
1.20E-02	-3.20E+02	-6.35E-02	5.42E+01	6.30E+02	2.71E-01
1.32E-02	-3.20E+02	-6.17E-02	5.28E+01	6.30E+02	2.72E-01
1.44E-02	-3.20E+02	-5.99E-02	5.14E+01	6.30E+02	2.74E-01
1.56E-02	-3.20E+02	-5.82E-02	5.01E+01	6.30E+02	2.75E-01
1.68E-02	-3.20E+02	-5.65E-02	4.87E+01	6.30E+02	2.77E-01
1.80E-02	-3.20E+02	-5.48E-02	4.75E+01	6.30E+02	2.78E-01
1.92E-02	-3.20E+02	-5.32E-02	4.62E+01	6.30E+02	2.80E-01
2.04E-02	-3.20E+02	-5.16E-02	4.50E+01	6.30E+02	2.81E-01
2.16E-02	-3.20E+02	-5.01E-02	4.38E+01	6.30E+02	2.82E-01
2.28E-02	-3.20E+02	-4.86E-02	4.26E+01	6.30E+02	2.84E-01
2.40E-02	-3.20E+02	-4.72E-02	4.15E+01	6.30E+02	2.85E-01
2.52E-02	-3.20E+02	-4.58E-02	4.04E+01	6.30E+02	2.86E-01

2.64E-02	-3.20E+02	-4.44E-02	3.93E+01	6.30E+02	2.87E-01
2.76E-02	-3.20E+02	-4.30E-02	3.82E+01	6.30E+02	2.88E-01
2.88E-02	-3.20E+02	-4.18E-02	3.72E+01	6.30E+02	2.89E-01
3.00E-02	-3.20E+02	-4.05E-02	3.62E+01	6.30E+02	2.91E-01
3.12E-02	-3.20E+02	-3.93E-02	3.52E+01	6.30E+02	2.92E-01
3.24E-02	-3.20E+02	-3.81E-02	3.42E+01	6.30E+02	2.93E-01
3.36E-02	-3.20E+02	-3.69E-02	3.33E+01	6.30E+02	2.94E-01
3.48E-02	-3.20E+02	-3.58E-02	3.24E+01	6.30E+02	2.95E-01
3.60E-02	-3.20E+02	-3.47E-02	3.15E+01	6.30E+02	2.96E-01
3.72E-02	-3.20E+02	-3.36E-02	3.06E+01	6.30E+02	2.97E-01
3.84E-02	-3.20E+02	-3.26E-02	2.98E+01	6.30E+02	2.98E-01
3.96E-02	-3.20E+02	-3.16E-02	2.89E+01	6.30E+02	2.98E-01
4.08E-02	-3.20E+02	-3.06E-02	2.81E+01	6.30E+02	2.99E-01
4.20E-02	-3.20E+02	-2.96E-02	2.73E+01	6.30E+02	3.00E-01
4.32E-02	-3.20E+02	-2.87E-02	2.66E+01	6.30E+02	3.01E-01
4.44E-02	-3.20E+02	-2.78E-02	2.58E+01	6.30E+02	3.02E-01
4.56E-02	-3.20E+02	-2.69E-02	2.51E+01	6.30E+02	3.03E-01
4.68E-02	-3.20E+02	-2.61E-02	2.44E+01	6.30E+02	3.03E-01
4.80E-02	-3.20E+02	-2.52E-02	2.37E+01	6.30E+02	3.04E-01
4.92E-02	-3.20E+02	-2.44E-02	2.30E+01	6.30E+02	3.05E-01
5.04E-02	-3.20E+02	-2.37E-02	2.23E+01	6.30E+02	3.06E-01
5.16E-02	-3.20E+02	-2.29E-02	2.17E+01	6.30E+02	3.06E-01
5.28E-02	-3.20E+02	-2.22E-02	2.10E+01	6.30E+02	3.07E-01
5.40E-02	-3.20E+02	-2.14E-02	2.04E+01	6.30E+02	3.08E-01
5.52E-02	-3.20E+02	-2.08E-02	1.98E+01	6.30E+02	3.08E-01
5.64E-02	-3.20E+02	-2.01E-02	1.93E+01	6.30E+02	3.09E-01
5.76E-02	-3.20E+02	-1.94E-02	1.87E+01	6.30E+02	3.10E-01
5.88E-02	-3.20E+02	-1.88E-02	1.81E+01	6.30E+02	3.10E-01
6.00E-02	-3.20E+02	-1.82E-02	1.76E+01	6.30E+02	3.11E-01
6.12E-02	-3.20E+02	-1.76E-02	1.71E+01	6.30E+02	3.11E-01
6.24E-02	-3.20E+02	-1.70E-02	1.66E+01	6.30E+02	3.12E-01
6.36E-02	-3.20E+02	-1.64E-02	1.61E+01	6.30E+02	3.13E-01
6.48E-02	-3.20E+02	-1.59E-02	1.56E+01	6.30E+02	3.13E-01
6.60E-02	-3.20E+02	-1.54E-02	1.51E+01	6.30E+02	3.14E-01
6.72E-02	-3.20E+02	-1.49E-02	1.47E+01	6.30E+02	3.14E-01
6.84E-02	-3.20E+02	-1.44E-02	1.42E+01	6.30E+02	3.15E-01
6.96E-02	-3.20E+02	-1.39E-02	1.38E+01	6.30E+02	3.15E-01
7.08E-02	-3.20E+02	-1.34E-02	1.34E+01	6.30E+02	3.15E-01
7.20E-02	-3.20E+02	-1.29E-02	1.30E+01	6.30E+02	3.16E-01
7.32E-02	-3.20E+02	-1.25E-02	1.26E+01	6.30E+02	3.16E-01
7.44E-02	-3.20E+02	-1.21E-02	1.22E+01	6.30E+02	3.17E-01
7.56E-02	-3.20E+02	-1.17E-02	1.18E+01	6.30E+02	3.17E-01

7.68E-02	-3.20E+02	-1.13E-02	1.14E+01	6.30E+02	3.18E-01
7.80E-02	-3.20E+02	-1.09E-02	1.11E+01	6.30E+02	3.18E-01
7.92E-02	-3.20E+02	-1.05E-02	1.07E+01	6.30E+02	3.18E-01
8.04E-02	-3.20E+02	-1.01E-02	1.04E+01	6.30E+02	3.19E-01
8.16E-02	-3.20E+02	-9.79E-03	1.01E+01	6.30E+02	3.19E-01
8.28E-02	-3.20E+02	-9.45E-03	9.73E+00	6.30E+02	3.19E-01
8.40E-02	-3.20E+02	-9.12E-03	9.43E+00	6.30E+02	3.20E-01
8.52E-02	-3.20E+02	-8.80E-03	9.13E+00	6.30E+02	3.20E-01
8.64E-02	-3.20E+02	-8.49E-03	8.83E+00	6.30E+02	3.20E-01
8.76E-02	-3.20E+02	-8.19E-03	8.55E+00	6.30E+02	3.21E-01
8.88E-02	-3.20E+02	-7.90E-03	8.27E+00	6.30E+02	3.21E-01
9.00E-02	-3.20E+02	-7.61E-03	8.01E+00	6.30E+02	3.21E-01
9.12E-02	-3.20E+02	-7.34E-03	7.75E+00	6.30E+02	3.22E-01
9.24E-02	-3.20E+02	-7.08E-03	7.49E+00	6.30E+02	3.22E-01
9.36E-02	-3.20E+02	-6.82E-03	7.25E+00	6.30E+02	3.22E-01
9.48E-02	-3.20E+02	-6.58E-03	7.01E+00	6.30E+02	3.22E-01
9.60E-02	-3.20E+02	-6.34E-03	6.78E+00	6.30E+02	3.23E-01
9.72E-02	-3.20E+02	-6.11E-03	6.56E+00	6.30E+02	3.23E-01
9.84E-02	-3.20E+02	-5.89E-03	6.34E+00	6.30E+02	3.23E-01
9.96E-02	-3.20E+02	-5.67E-03	6.13E+00	6.30E+02	3.23E-01
1.01E-01	-3.20E+02	-5.46E-03	5.92E+00	6.30E+02	3.24E-01
1.02E-01	-3.20E+02	-5.26E-03	5.73E+00	6.30E+02	3.24E-01
1.03E-01	-3.20E+02	-5.07E-03	5.53E+00	6.30E+02	3.24E-01
1.04E-01	-3.20E+02	-4.88E-03	5.35E+00	6.30E+02	3.24E-01
1.06E-01	-3.20E+02	-4.70E-03	5.17E+00	6.30E+02	3.24E-01
1.07E-01	-3.20E+02	-4.52E-03	4.99E+00	6.30E+02	3.25E-01
1.08E-01	-3.20E+02	-4.35E-03	4.82E+00	6.30E+02	3.25E-01
1.09E-01	-3.20E+02	-4.19E-03	4.65E+00	6.30E+02	3.25E-01
1.10E-01	-3.20E+02	-4.03E-03	4.49E+00	6.30E+02	3.25E-01
1.12E-01	-3.20E+02	-3.88E-03	4.34E+00	6.30E+02	3.25E-01
1.13E-01	-3.20E+02	-3.73E-03	4.19E+00	6.30E+02	3.25E-01
1.14E-01	-3.20E+02	-3.59E-03	4.04E+00	6.30E+02	3.26E-01
1.15E-01	-3.20E+02	-3.45E-03	3.90E+00	6.30E+02	3.26E-01
1.16E-01	-3.20E+02	-3.32E-03	3.77E+00	6.30E+02	3.26E-01
1.18E-01	-3.20E+02	-3.19E-03	3.63E+00	6.30E+02	3.26E-01
1.19E-01	-3.20E+02	-3.07E-03	3.51E+00	6.30E+02	3.26E-01
1.20E-01	-3.20E+02	-2.95E-03	0.00E+00	6.30E+02	3.30E-01

COISOTOP2 MODEL

INPUT VALUES

SHIFT TEMP (°C): -10.00

RELATIVE HUMIDITY WITH ICE (%): 1.00

START TEMP (°C), END TEMP (°C) and STEPS (#): -5.00, -55.00, 25

START HEADROOM ICE SURFACE DEL 18O (‰): -10.64

START HEADROOM ICE SURFACE DEL D (‰): -82.19

START HEADROOM VAPOUR SURFACE DEL 18O (‰): -22.64

START HEADROOM VAPOUR SURFACE DEL D (‰): -180.89

Table A.2. Output Values for COISOTOP2 Model

TEMP (K)	DEL 18O (‰)	DEL D (‰)	d (‰)
268.16	-10.65	-82.2	3
266.16	-12.551	-99.084	1.326
264.16	-14.516	-116.422	-0.291
262.16	-16.547	-134.207	-1.829
260.16	-18.646	-152.427	-3.261
258.16	-20.814	-171.07	-4.559
256.16	-23.217	-192.906	-7.169
254.16	-26.264	-215.635	-5.52
252.16	-29.414	-238.691	-3.38
250.16	-32.668	-262.037	-0.692
248.16	-36.029	-285.637	2.599
246.16	-39.5	-309.45	6.553
244.16	-43.084	-333.436	11.232
242.16	-46.781	-357.553	16.698
240.16	-50.597	-381.756	23.017
238.16	-54.532	-406.001	30.254
236.16	-58.59	-430.241	38.478
234.16	-62.773	-454.43	47.758
232.16	-67.085	-478.519	58.163
230.16	-71.528	-502.461	69.764
228.16	-76.105	-526.206	82.635
226.16	-80.819	-549.708	96.843
224.16	-85.673	-572.917	112.464
222.16	-90.669	-595.786	129.567
220.16	-95.811	-618.268	148.224
218.16	-101.103	-640.317	168.503

Appendix B

Table B1. Burnsco Tech. Experimental Chamber Specifications

Specification	Measurement
Model	RTC-16P
Volume	16 FT^3
Inner Dimensions (WxDxH)	26” x 30” x 36”
Outer Dimensions (WxDxH)	35” x 56” x 74”
Temperature Range	-65ºC to + 177ºC
Tolerance at the sensor (ºC)	+1.0ºC
Heating Change Rate	-40ºC to 85ºC within 45 min
Cooling Change Rate	85ºC to -40ºC within 50 min
Live Load Capability	900 Watts @ -40ºC
Controller	Setpoint/Programmable PID
Refrigeration System	Cascade, Air 2@ 2Hp
Air Heaters	1 x 4000 Watts
Fan Motor	1 x ¼ Hp
Supply Voltage	208 - 230 V/1Ø/60 Hz or, 208-230V/3Ø/ 60Hz
Full Load Amps	45 or 32
Heat Rejection @ 20ºC Ambient (BTHU)	31,844
Drain	½”
Weight (lbs)	1600

AGSCO CORPORATION

TECHNICAL DATA

GLASS BEADS

TYPICAL CHEMICAL COMPOSITION

SILICA	(SiO_2)	72.8%
ALUMINA	(Al_2O_3)	1.3
CALCIUM OXIDE	(CaO)	8.0
MAGNESIUM OXIDE	(MgO)	3.9
SODIUM OXIDE	(Na_2O)	13.3
POTASSIUM OXIDE	(K_2O)	0.3
SULFATE	(SO_3)	0.1
FERROUS & FERRIC OXIDE	(Fe_2O_3 & Fe_3O_4)	0.1

TYPICAL PHYSICAL PROPERTIES

SIZE RANGE	Typically 80% by weight in range on smaller US Sieve.
SILICA CONTENT	Minimum 67% to assure chemical stability.
SPECIFIC GRAVITY	2.45 - 2.55 g/cm^3.
HARDNESS	DPH 50g load - 540 kg/m^2 (Rockwell 48-50C). Mohs - 5.5
COLOR	Clear or crystal, free from surface films.
STANDARD PACKAGING	Fifty pound multi-wall bags with polyethylene barrier. All sizes listed below US Sieve #100 contain flow aid additive.
AVAILABLE SIZES	20/30, 30/40, 40/50, 50/70, 60/100, 70/140, 100/170, 120/200, 140/270, 170/325, 270 & Finer.

Specifications Available: Mil G9954A, AMS2431, MS0097 V6, D00468, and many others. Call AGSCO for details.

160 West Hintz Road
Wheeling, Ilinois 60090
P: 847-520-4455 • F: 847-520-4970

60 Chapin Road, PO Box 669
Pine Brook, New Jersey 07058
P:973-244-0005 • F:973-244-0091

Figure B1. Glass beads technical data (AGSCO, 2015)

Appendix C

Standard Operating Procedures for the Experimental Chamber

1) Check Syltherm XLT liquid levels, they should at least be enough to cover 1 inch above the output. Point of interest: Syltherm XLT is flammable keep away from ignition sources.

2) Clean the 2 strainers in FTS Systems Multicool cooling bath of any debris.

3) Turn on the pump and turn the flow speed dial to 30. Check for any leaks in the system.

4) Turn the flow speed dial to 70 and let it run overnight. This will allow the fluid to mix with any water.

5) The next morning, turn on the cooling bath and set the unit to the desired temperature using the up/down arrows. Keep pump speed to 70. DO NOT inject very cool fluid directly into the pipes. This will create sudden stress of the welds and pipes. The system needs to slowly decrease in temperature.

6) Seal firmly the lid of the cooling bath using straps or objects to apply pressure. This will limit the amount of moisture entering into the liquid. If moisture enters into the liquid ice can form. Ice will block pipes and can decrease efficiency of the Syltherm.

7) Insulate the lid with pink fiberglass layers and any exposed areas to limit ice accumulation.

8) Once the temperature of the fluid has decreased to -10°C turn on the Burnsco environmental test chamber to the desired temperature (see Watlow user's manual). This will help the cooling bath reach a stable temperature.

9) Listen to the sound inside the chamber. You should hear a good gushing sound. If you hear a hissing sound or no flow at all, IMMEDIATELY turn off the pump! Refer to troubleshooting for help.

9) Decrease the pumps flow speed to 40 in order to reach lowest temperatures < -50°C.

10) Make sure there isn't any cool spots outside the piping and carry-on with your experiment.

11) Change any wet and iced insulation on motor/pipes/cooling bath every ~2 weeks. Ice can aggrade inside the environmental chamber but make sure it doesn't cause any heaving of the pipes.

Troubleshooting:

Problem: The liquid doesn't flow very fast even if the pump speed is high.

Solution: IMMEDIATELY turn off the pump! Ice has been building up in the pipes. Check for heaving on the cooling plates since pressure may break it open. Wait until everything is above 0°C and check for further damages.

Problem: Cold bath doesn't go lower than its set value.

Solution: The unit can't keep up. Slow down the pump speed and make sure the cooling/heating button on the unit is on the cooling. Typically, the unit can reach temperatures of -60°C if everything is well insulated.

Problem: Temperatures are increasing slightly over time

Solution: This is normal the system becomes less efficient as ice aggrades inside and outside the chamber. Change insulation if saturated with ice. The insulation needs to be changed every ~2 weeks.

Problem: The pump makes clunk-clunk-clunk noises.

Solution: Poor alignment inside the pump. Check if the pump is due for service and ask the lab supervisor for help.

For further help, please refer the user's manual of the individual equipment in the black binder.

Bibliography

Allen, C.C., Morris, R.V., Lindstrom, D.J., Lindstrom, M.M. and Lockwood, J.P., 1998. JSC MARS-1: Martian Regolith Simulant. Lunar and Planetary Science. XXVIII. Available Online: http://www.orbitec.com/store/JSC_Mars_1_Characterization.pdf. Accessed July 18, 2014.

AGSCO, 2014. Data sheet: Glass Beads. Available online: http://catalog.agsco.com/item/all-categories/industrial-minerals/pn-1059. Accessed July 18, 2014.

Bentley, W., 1907. Studies of frost and ice crystals. Monthly Weather Review, 35, 397-403.

Birkeland, K.W., Johnson, R.F. and Schmidt, D.S., 1998. Near-Surface Faceted Crystals Formed by Diurnal Recrystallization: A Case Study of Weak Layer Formation in the Mountain Snowpack and Its Contribution to Snow Avalanches. Arctic and Alpine Research, 30, 2, 200-204.

Bockheim, J.G. and McLeod, M., 2008. Soil distribution in the McMurdo Dry Valleys, Antarctica. Geoderma, 144, 43-49.

Branson, J., Lawler, D.M. and Glen, J.W., 1996. Sediment inclusion events during needle ice growth: A laboratory investigation of the role of soil moisture and temperature fluctuations. Water Resources Research, 32, 2, 459-466.

Burton, J.A., Prim, R.C., Slichter, W.P., 1953. The distribution of solute in crystal growth from the melt. Theoretical. Journal of Chemical Physics, 21, 1987–1991.

Clark, B., and van Hart, D., 1981. The salts of Mars. Icarus, 45, 370-378.

Clark, I.D, Lauriol, B., Lacelle, D., Flemming, C., Trimper, S. and Khader, O., Unpublished data. Stable water isotopes of pipkrakes near Gatineau, QC.

Clark, I.D. and Fritz, P., 1997. Environmental Isotopes in Hydrogeology. Lewis Publisher, U.S.A., 328.

Craig, H., 1961. Isotopic variations in meteoric waters. Science, 133, 3465, 1702-1703.

Doran, PT., McKay, C.P., Clow, G.D., Dana, G.L., Fountain, A.G., Nylen, T., Lyons, W.B., 2002. Valley floor climate observations from the McMurdo Dry Valleys, Antarctica 1986- 2000. Journal of Geophysical Research, 107, 4774–4784.

Environment Canada, 2015. Historical Climate Data. Available online: http://climate.weather.gc.ca/index_e.html. Accessed on the January 13, 2015.

Espinosa, R.M., Franke, L. and Deckelmann, G., 2008. Phase changes of salts in porous materials: Crystallization, hydration and deliquescence. Construction and Building Materials, 22, 1758-1773.

Fisher, D.A., 2005. A process to make massive ice in the martian regolith using long-term diffusion and thermal cracking. Icarus, 179, 387-397.

Fisher, D.A., 1991. Remarks on the deuterium excess in precipitation in cold regions. Tellus, 438, 401–407.

Fisher, D.A. and Lacelle, D., 2014. A model for co-isotopic signatures of evolving ground ice in the cold and dry environments of Earth and Mars. Icarus, 243, 454-470.

Fisher, D. A., Lacelle, D., Pollard, W., Davila, A. and McKay, C. P., In review. Ground surface temperature and humidity, soil airflow and the geothermal gradient determine the ice table depth in University Valley, McMurdo Dry Valleys of Antarctica. Journal of Geophysical Research.

Fountain, A.G., Nylen, T.H., Monaghan, A., Basagic, H., Bromwich, D., 2009. Snow in the McMurdo Dry Valleys. Antarctica. International Journal of Climatology, 30, 633–642.

French, H. H., 1996. The Periglacial Environment, Second ed. Longman Limited, Essex, England, 341.

Gibbs, 2014. Needle Ice. Weather, 69, 3.

Google Earth 7.1, 2015. Satellite image of Petrie Island, Ottawa, ON. 45°30’07”N, 75°29’47”W. Available online: http://www.google.com/earth/index.html. Visited on the February 10, 2015.

Harris, S.A., 1979. Ice Caves and Permafrost Zones in Southwest Alberta. Erdkunde, 33, 1, 61-70.

Ho, C.K. and Webb, S.W. (eds.), 2006. Gas Transport in Porous Media. Springer, Dordrecht, The Netherlands, 440.

Hobbs, P.V., 1974. Ice Physics. Oxford University Press, Oxford, England, 856.

Houtkooper, J.M. and Schulze-Makuch, D., 2010. The Possible Role of Perchlorates for Martian Life. Journal of Cosmology, 5, 930-938.

Hudson, T.L., 2008. [Ph.D. Thesis] Growth, Diffusion, and Loss of Subsurface Ice on Mars: Experiments and Models. California Institute of Technology, Pasadena, California.

Hudson, T.L., Aharonson, O., Schorghofer, N., 2009. Laboratory experiments and models of diffusive emplacement of ground ice on Mars. Journal of Geophysical Research, 114, E01002.

Hudson, T.L., Aharonson, O., Schorghofer, N., Farmer, C.B., Hecht, M.H. and Bridges, N.T., 2007. Water vapour diffusion in Mars subsurface environments. Journal of Geophysical Research, 112, E05016.

IAEA/WMO, 2015. Global Network of Isotopes in Precipitation. The GNIP Database. Available online: http://www.iaea.org/water. Accessed October 2, 2015.

Ingólfsson, Ó. and Lokrantz, H., 2003. Massive ground ice body of glacial origin at Yugorski Peninsula, Arctic Russia. Permafrost and Periglacial Processes, 14, 199-215.

Jouzel, J., Souchez, R.A., 1982. Melting and refreezing at the glacier sole and the isotopic composition of the ice. Journal of Glaciology, 28, 35–42.

Kounaves, S.P., Stroble, S.T., Anderson, R.M., Moore, Q., Catling, D.C., Douglas, S., McKay, C.P., Ming, D.W., Smith, P.H., Tamppari, L.K. and Zent, A.P., 2010. Discovery of Natural Perchlorate in the Antarctic Dry Valleys and Its Global Implications. Environmental Science and Technology, 44, 7, 2360-2364.

Kowalewski, D.E., Marchant, D.R., Swanger, K.M. and Head, J.W. III, 2011. Modeling vapor diffusion within cold and dry supraglacial tills of Antarctica: Implications for the preservation of ancient ice. Geomorphology, 126, 159-173.

Kuzmin, R.O., 2005. Ground Ice in the Martian Regolith. Adv. Astrobiol. Biogeophys., 155-189.

Lacelle, D., 2011. On the $\delta^{18}O$, δD and D-excess relations in meteoric precipitation and during equilibrium freezing: theoretical approach and field examples. Permafrost and Periglacial Processes, 22, 13-25.

Lacelle, D., Davila, A.F., Fisher, D.A., Pollard, W.H., DeWitt, R., Heldmann, J.L., Marinova, M.M., McKay, C.P., 2013. Excess ground ice of condensation-diffusion origin in University Valley, McMurdo Dry Valleys of Antarctica: evidence from isotope geochemistry and numerical modeling. Geochimica and Cosmochimica Acta, 120, 280–297.

Lacelle, D., Lapalme, C., Davila, A.F., Pollard, W., Marinova, M., Heldmann, J. and McKay, C.P., 2015. Solar radiation and air ground temperature relations in cold and hyper-arid Quartermain Mountains, McMurdo Dry Valleys of Antarctica. PPP, DOI: http://dx.doi.org/10.1002/ppp.1859.

Lacelle, D., Lauriol, B. and Clark, I.D., 2004. Seasonal isotopic imprint in moonmilk from Caverne de l'Ours (Quebec, Canada): implications for climatic reconstruction. Can. J. Earth Sci., 41, 1411–1423.

Lacelle, D., Lauriol, B. and Clark, ID., 2009. Formation of seasonal ice bodies and associated cryogenic carbonates in Caverne de l'Ours, Québec, Canada: Kinetic isotope effects and pseudo-biogenic crystal structures. Journal of Cave and Karst Studies, 71, 48-62.

Lauriol, B. and Bertrand, P., 2014. Eaux, Glaces et Cavernes. Éditions MultiMondes, Québec, QC, Canada. 144 p.

Lauriol, B., Carrier, L. and Thibaudeau, P., 1988. Topoclimatic Zones and Ice Dynamics in the Caves of Northern Yukon, Canada. Arctic, 41, 3, 215-220.

Lauriol, B. and Clark, I.D., 1993. An approach to determine the origin and age of massive ice blockages in two arctic caves. Arctic and Periglacial Processes, 4, 77-85.

Lawler, D.M., 1993. Needle ice processes and sediment mobilization on a river banks: The River Ilston, West Glamorgan, UK. J. Hydrol., 150, 81-114.

Lawrie, R., 2012. Photographs of frost and ice patterns. Weather, 67, 12, 325.

Lenferink, H.J., Durham, W.B., Stern, L.A. and Pathare, A.V., 2013. Weakening of ice by magnesium perchlorate hydrate. Icarus, 225, 2, 940-948.

Lock, G.S.H., 1990. The Growth and Decay of Ice. Cambridge University Press, Cambridge, NY, USA, 434.

Mackay, J.R., 1990. Seasonal growth bands in pingo ice. Canadian Journal of Earth Sciences, 27, 115-1125.

Mackay, J.R., 1972. The World of Underground Ice. Annals of the Association of American Geographers, 62, 1, 1-22.

Mackay, J.R. and Mathews, W.H., 1974. Needle Ice Striped Ground. Arctic and Alpine Research, 6, 1, 79-84.

Magono, C. and Lee. C.W., 1966. Meteorological Classification of Natural Snow Crystals. Journal of the Faculty of Science, Hokkaidô University, Japan, 7, 2, 4, 331- 335.

Majoube, M., 1971. Fractionnement en oxygene-18 et en deuterium entre l'eau et sa vapeur. J. Chim. Phys., 197, 1423-1436.

Mason, B.J., Bryant, G.W. and Van Den Heuval, A.P., 1963. The growth habits and surface structures of ice crystals. Phil. Mag. 8, 505-526.

McClung, D. and Schaerer, P.A., 2006. The Avalanche Handbook. Third Edition. The Mountaineers Books, Seattle, WA, USA, 342.

Mellon, M. and Jakosky, B., 1993. Geographic Variations in the Thermal and Diffusive Stability of Ground Ice on Mars. Journal of Physical Research, 98, E2, 3345-3364.

Murton, J.B. and French, H.W., 1994. Cryostructures in permafrost, tuktoyaktuk coastlands, western Arctic, Canada. Canadian Journal of Earth Sciences, 31, 737-747.

Nel, W. and Boelhouwers J., 2014. First observations of needle ice formation in sub-Antarctic. Antarctic Science, 26, 3, 327-328.

O'Neil, J.R., 1968. Hydrogen and oxygen isotope fractionation between ice and water. Journal of Physical Chemistry, 72, 3683– 3684.

Peel, M.C., Finlayson, B.L. and McMahon, T.A., 2007. Updated world map of the Köppen-Geiger climate classification. Hydrology and earth system sciences discussions, 4, 2, 439-473.

Petrenko, V.F. and Whitworth, R.F., 2002. Physics of Ice: Oxford University Press, Oxford Scholarship Available Online: http://www.oxfordscholarship.com/view/10.1093/acprof:oso/9780198518945.001.0001/acprof-9780198518945. Accessed February 5, 2015.

Reid, R., Prausnitz, J. and Poling, B., 1987. The Properties of Gases and Liquids, 4th ed., McGraw-Hill, New York, NY, 803.

Shumskii, P.A., 1964. Principles of Structural Glaciology. Dover Publications, Inc., New York, NY, 497.

Snyder, R.L., Melo-Abreu, J.P., 2005, Frost protection: fundamentals, practice and economics. Rome: FAO. Available online: http://hdl.handle.net/10400.5/4727. Accessed November 20th, 2015.

Souchez, R.A. and Jouzel, J., 1984. On the isotopic composition in δD and δ^{18}O of water and ice during freezing. Journal of Glaciology, 30, 369-372.

Statistics Canada, 2007. Weather conditions in Capital and Major Cities (Precipitation). Statistics Canada. Available online: http://www.statcan.gc.ca/tables-tableaux/sum-som/l01/cst01/phys08a-eng.htm. Accessed March 15, 2015.

Suzuoki, T., Kumura, T., 1973. D/H and 18O/16O fractionation in ice-water systems. Mass Spectroscopy, 21, 229–233.

Telmer, K. and Veizer, J., 2000. Isotopic constraints on the transpiration, evaporation, energy, and gross primary production budgets of a large boreal watershed: Ottawa River basin, Canada. Global Biogeochemical Cycles, 14, 1, 149-165.

Turner, K.W., Wolfe, B.B. and Edwards, T.W.D., 2010. Characterizing the role of hydrological processes on lake water balances in the Old Crow Flats, Yukon Territory, Canada, using water isotope tracers. Journal of Hydrology, 386, 103-117.

van Everdingen, R.O., 1998. Multi-language Glossary of Permafrost and Related ground-ice Terms. National Snow and Ice Data Center/World Data Center for Glaciology, Boulder, CO.

WMO (World Meteorological Organization), 2008. Guide to Meteorological Instruments and Methods of Observation, Appendix 4B, WMO-No. 8 (CIMO Guide), Geneva.

Yonge, C.J. and MacDonald, W.D., 1999. The potential of perennial cave ice in isotope palaeoclimatology. Boreas, 28, 357-362.